CATHODOLUMINESCENCE AND FLUID INCLUSION CHARACTERISTICS OF HYDROTHERMAL QUARTZ FROM PORPHYRY DEPOSITS

by

Mitchell M. Bennett

A thesis submitted to the Faculty and Board of Trustees of the Colorado School of Mines in partial fulfillment of the requirements for the degree of Master of Science (Geology).

Golden, Colorado

Date _____

Signed: _____

Mitchell Bennett

Signed: _____

Dr. Thomas Monecke

Thesis Advisor

Signed: _____

Dr. Nigel Kelly

Thesis Co-Advisor

Golden, Colorado

Date _____

Signed: _____

Dr. Paul Santi

Professor and Head

Department of Geology and Geological Engineering

ABSTRACT

Porphyry deposits are one of the world's most important repositories of copper, gold, and molybdenum. Integrated fluid inclusion petrography and cathodoluminescence microscopy showed that stockwork veins in porphyry deposits are composed of multiple quartz generations. Early quartz showing a bright blue luminescence precipitated from a high-temperature fluid causing potassic alteration of the surrounding rock. The nature of the fluid inclusion assemblages entrapped in the quartz correlates with the depth of vein formation. Intermediate density fluid inclusions occur in deep deposits such as Butte in Montana while brine and vapor inclusions are abundant in deposits formed at intermediate depths, including Bingham Canyon in Utah and Far Southeast in the Philippines. Vapor inclusions dominate in the shallow deposits of the Maricunga belt in Chile. In mineralized veins, the early quartz is overprinted by quartz that precipitated at distinctly lower temperatures. The textural relationships between the different quartz generations are complex as formation of each generation of quartz was accompanied by alteration of the preexisting quartz. Alteration processes range from modification and quenching of the cathodoluminescence signal of the preexisting quartz to changes in the trace element content and whole-sale structural reorganization. In all deposits studied, late quartz showing a red-brown luminescence is texturally associated with the ore minerals. Based on the fluid inclusion evidence, ore deposition must have occurred over a temperature interval centered on the critical point of water. At Bingham Canyon, the ore-forming fluid was a hypersaline liquid while sulfide precipitation took place from a low-salinity liquid causing chlorite-sericite or sericite-pyrite alteration of the wall rocks in other deposits. The study shows that the identified characteristics of porphyry quartz are unique, allowing transported porphyry grains to be identified in stream sediments. Based on two case studies, it is demonstrated that quartz can be used as a pathfinder mineral in porphyry exploration.

TABLE OF CONTENTS

LIST OF FIGURES

LIST OF TABLES

LIST OF ABBREVIATIONS

BLEG	Bulk leach extractable gold
CL	Cathodoluminescence
EMP	Electron microprobe
g/cc	Grams per cubic centimeter
g/t	Grams per metric ton
LA-ICP-MS	Laser ablation-inductively coupled plasma-mass spectrometry
Ma	Million years ago
Mt	Million metric tons
SEM	Scanning electron microscope
WDS	Wavelength-dispersive spectroscopy
vol.%	Volume percent
wt.%	Weight percent

ACKNOWLEDGEMENTS

I am truly indebted and thankful to Thomas Monecke for his expertise in the complex subtlety of cathodoluminescence microscopy, for inspiring my fascination with economic geology, and for his ongoing support in completing this research. Special thanks go to Jim Reynolds for many critical discussions on fluid inclusions and for his patient instruction in the art of fluid inclusion petrography. Nigel Kelly also deserves thanks for guiding my research into the dynamics of quartz recrystallization and dissolution-reprecipitation and for his invaluable experience with density separation using heavy liquids. I also owe my sincerest thanks Antonio Arribas for conceiving the idea of applying fluid inclusion and CL petrography to coarse BLEG sands as an exploration tool, and for his generous contributions that made this research possible.

Sincere thanks go to John Muntean, Patrick Redmond, and Brian Rusk for contributing archival samples and for their insight into vein-scale processes of the deposits they have studied for so many years. I also owe a debt of gratitude to Heather Lowers for her discussion and comments and for numerous sessions on the electron microprobe at the U.S. Geological Survey in Denver. It is my great pleasure to thank Jens Götze of the Institute of Mineralogy at the Technische Universität Bergakademie Freiberg in Germany for his correspondence and for the spectroscopic analysis of the different generations of FSE vein quartz. The staff of the QEMSCAN Facility in the Department of Geology and Geological Engineering at Colorado School of Mines are also deserving of thanks for their helpfulness and tolerance for my invasion of their lab space; thanks to Carla Sanchez and Matt Dye for their contributions to the BLEG grain mount sample preparation procedure, and to Katharina Pfaff for her assistance and expertise in automated mineralogical analysis and the quantification of grain size distributions. I also thank Michael Schmid of the Institute for Theoretical Physics at the Technische Universität Wien in Austria for contributing his adjustable watershed plugin for ImageJ. The automated counting method used herein would not have been possible without his input. I am also indebted to John Skok for the timely and expert preparation of numerous thin sections over the course of this research, several of which were rush jobs that he graciously

pushed through the work queue. It is my pleasure to thank Mark Lindsay, Daven Mashburn, and the rest of the Newmont Haiti and PNG exploration teams for kindly providing BLEG trace metal values, location data, and sand samples for the project.

Financial support for the research was provided by Newmont through the Centre of Earth Resources Science and Engineering at the Colorado School of Mines. Steve Enders and Perry Eaton are thanked for facilitating the research. I also acknowledge a graduate fellowship by the Society of Economic Geologists Foundation. Additional support was provided by the Steven Mooney Fellowship at the Department of Geology and Geological Engineering at Colorado School of Mines.

Lastly, I owe my deepest gratitude to Megan Miclette for her unwavering support and patience over the course of this research. I also thank my parents for their support throughout my many years of education.

CHAPTER 1
INTRODUCTION

1.1 Porphyry Environment

Porphyry deposits are currently the world's largest source of Cu ore, and frequently contain recoverable concentrations of Ag, Au, Mo, and minor amounts of Pd, Te, Se, Bi, Zn, Sn, W, and Pb. Deposits of this type supply approximately 75% of the world's Cu, 50% of the Mo, 20% of the Au, and most of the Re (Sillitoe, 2010). Porphyry deposits form in suprasubduction and post-subduction environments via the intrusion of oxidized, felsic to intermediate calc-alkaline magmas enriched in chalcophile metals and volatile species including H_2O, S, and Cl (Richards, 2009). Magmas generated in these environments intrude into the upper crust along structural weaknesses to form porphyritic stocks from <1 to 10 km depth (Muntean and Einaudi, 2001; Sillitoe and Hedenquist, 2003).

The ore zones of porphyry deposits typically occupy cupola-shaped regions that are spatially centered on the porphyritic stocks. Sulfide and oxide ore minerals occur in three predominant styles, and may be disseminated in the wall rock along thin veinlets (Titley, 1982), concentrated in lodes and veins (Einaudi, 1977, 1982), or present as components of clasts and/or cements in breccias (Sillitoe et al., 1984; Skewes and Stern, 1996). On average, elements of economic interest are enriched 100- to 1000-times in the mineralized rocks compared to unmineralized rocks of similar composition (Seedorff et al., 2005). High-grade ore in porphyry deposits is hosted in stockwork zones of hydrothermal quartz veins that cut the host intrusion and surrounding country rocks.

1.2 Hydrothermal Alteration and Vein Types

Formation of the various styles of mineralization in porphyry intrusions is associated with widespread alteration of the host intrusion. Hydrothermal alteration occurs at sub-solidus conditions in response to the interaction of the porphyry with magmatic-

hydrothermal fluids migrating upward through the previously solidified portion of the intrusion and the entrainment of external meteoric water into the magmatic-hydrothermal system (Seedorff et al., 2005). Alteration results in the formation of characteristic mineral associations in veins and wall-rock selvages that formed under geochemically similar conditions. These include the intrusion-centered potassic (K-silicate) and chlorite-sericitic or sericite-pyrite alteration facies, which grade into a propylitic alteration facies with increased distance from the centre of the intrusion (Seedorff et al., 2005).

A generalized correlation can be made between the formation of the alteration facies and declining temperatures of the magmatic-hydrothermal system following emplacement of the porphyritic intrusion. The potassic alteration facies is characterized by alteration of hornblende to fine-grained (shreddy) biotite and of plagioclase to K-feldspar, but may also include tourmaline, calcite, fluorite, anhydrite, apatite, and/or quartz (Seedorff et al., 2005). Temperature estimates from mineral stability constraints and fluid inclusion studies (see below) suggest that the potassic alteration facies forms at conditions in excess of ~400^{o}C in most deposits. The potassic alteration facies usually occurs tightly around and within the intrusive stock, and is commonly overprinted by the later chlorite-sericitic or sericite-pyrite alteration facies around and above the pluton. The sericite-rich alteration facies develop at temperatures below ~4000^{o}C, and are characterized by alteration of K-feldspar to white mica (muscovite at high temperature or illite at lower temperatures) and quartz, but may also include chlorite, fluorite, and/or apatite (Seedorff et al., 2005). The timing of the formation of hypogene sulfide minerals, mostly bornite, digenite, chalcopyrite, pyrite, and molybdenite, with respect to these two styles of alteration has been a matter of considerable debate over the past decades (cf. Hedenquist et al., 1998).

The potassic and chlorite-sericite or sericite-pyrite facies grade into the propylitic alteration facies with increased distance from the centre of the intrusion. The propylitic alteration facies is generally developed on a regional scale, and is the lowest temperature alteration style in porphyry deposits. It is characterized by alteration of feldspars to albite, white mica, and montmorillonite, and of mafic minerals to chlorite and epidote (Seedorff

et al., 2005). Propylitic-altered rocks may contain calcite, ankerite, and/or relict apatite, but ore minerals are scarce (Seedorff et al., 2005).

Vein morphology, crosscutting relationships, mineral content, orientation, and the mineralogy of alteration halos have traditionally been used to differentiate vein types in porphyry systems. In most, but not all porphyry deposits, progressively younger veins are formed at decreasing temperatures, determined from temperature estimates based on mineral assemblages, fluid inclusions (see below), and sulfur isotope fractionation trends (Seedorff et al., 2005). Vein types common in porphyry deposits include A-, D-, and so-called banded veins.

A-veins, first described by Gustafson and Hunt (1975) at El Salvador in Chile, consist of 50-90 vol.% “sugary” granular quartz, K-feldspar, anhydrite, bornite, and chalcopyrite, with rare biotite, apatite, and rutile. They are broadly contemporaneous with potassic alteration and typically lack centerlines or banding (Seedorff et al., 2005). A-veins show a variety of morphologies, ranging from irregular and discontinuous to straight walled. This suggests that these veins form at high temperatures at ductile to brittle conditions over a spectrum of strain rates (Fournier, 1999).

In many deposits, A-veins are crosscut by later D-veins, also originally described from El Salvador (Gustafson and Hunt, 1975). D-veins are composed of pyrite and quartz, with sericitic alteration halos that contain sericite with variable chlorite, pyrite, quartz, anhydrite, and rutile. Other sulfide minerals may coexist with pyrite in veins, and show systematic variance with depth from pyrite, bornite, and enargite at shallow levels to pyrite and chalcopyrite, pyrite-only, and finally to pyrite and tennantite at progressively deeper levels (Gustafson and Hunt, 1975). D-veins are usually straight-walled and continuous, suggesting formation in brittle rock at temperatures below ~400°C (Fournier, 1999).

In some porphyry deposits, such as those of the Maricunga belt in Chile (Muntean and Einaudi, 2000, 2001), banded veins have been recognized. The banded appearance of

these veins originates from the presence of abundant vapor inclusions and microscopic magnetite grains that form dark, botryoidal bands that are continuous across quartz crystals. Banded veins typically lack alteration selvages, and are not correlated with a specific alteration facies.

1.3 Link to the Epithermal Environment

It is now widely accepted that there is a genetic link between porphyry deposits at depth and certain epithermal precious metal deposits forming in the shallow crustal environment. Fluid inclusion, age dating and isotopic investigations at the Far Southeast Cu-Au porphyry and adjacent Lepanto high-sulfidation epithermal deposit, Philippines, have been instrumental in establishing fluid evolution in porphyry deposits and their link to the epithermal environment (Arribas et al., 1995; Hedenquist et al., 1998). Recent investigations of lithocap alunite mineral composition within the Mankayan mining district also suggest that there is a measureable compositional zonation between the Far Southeast and Lepanto deposits, further reinforcing the conclusion that the two deposits are genetically related (Chang et al., 2011).

1.4 Fluid Inclusion Inventory of Vein Quartz

The physiochemical evolution of the hydrothermal fluids forming porphyry deposits and related epithermal mineralization at shallower crustal levels is recorded in the different stockwork vein types and their relative timing of formation with respect to the cooling of the porphyritic intrusion. As hydrothermal quartz is the most abundant gangue mineral in the stockwork veins, fluid inclusion and trace element studies on this mineral are key in understanding the fluid evolution of the magmatic-hydrothermal system (Hedenquist et al., 1998; Muntean and Einaudi, 2000, 2001; Rusk and Reed, 2002; Redmond et al., 2004; Rusk et al., 2006, 2008a; Redmond and Einaudi, 2010).

The fluid inclusion inventory of vein quartz is petrographically distinct at different levels in porphyry deposits. At greater depth, as exemplified at Butte (Rusk and Reed,

2002; Rusk et al., 2006) and the deepest levels of Bingham (Redmond et al., 2004; Redmond and Einaudi, 2010), the magmatic-hydrothermal fluids have not undergone phase separation and occur as vapor-like single-phase fluids (cf. Driesner and Heinrich, 2007). The entrapped inclusions are simple two-phase inclusions (liquid H_2O and vapor H_2O), with big vapor bubbles. These inclusions are referred to as intermediate density fluid inclusions (cf. Redmond et al., 2004; Landtwing et al., 2005, 2010).

As the magmatic-hydrothermal fluids rise to shallower crustal levels and undergo decompression, the fluids enter the two-phase field of the H_2O-NaCl model system and split into a hypersaline liquid and a corresponding low-salinity vapor phase through condensation (cf. Driesner and Heinrich, 2007). Inclusions that trap the hypersaline liquid contain halite crystals under standard conditions. They are referred to as brine inclusions. The corresponding vapor phase formed during phase separation at depth ascends rapidly due to its buoyancy and may condense into shallow meteoric water, generating an extremely acidic solution that can form a leach cap in the near-surface environment (Stoffregen, 1987; Hedenquist et al., 1998; Hedenquist and Taran, 2013). Vapor trapped in vein quartz forms vapor inclusions that can be readily recognized as such at standard conditions. The petrographically linked occurrence of brine and vapor inclusions is very common in early A-veins associated with K-silicate alteration halos in porphyry deposits worldwide.

In very shallow porphyry intrusions, as exemplified by those of the Maricunga belt in Chile (Muntean and Einaudi, 2000, 2001), the magmatic-hydrothermal fluids occur in the vapor plus salt stability field of the H_2O-NaCl system (cf. Driesner and Heinrich, 2007). Under these low pressure conditions, banded quartz veins can form that mostly contain vapor inclusions.

1.5 Cathodoluminescence of Vein Quartz

While the different fluid inclusions types can be readily identified petrographically, different quartz types contained within a single quartz vein cannot be distinguished

using conventional optical microscopy. Recent detailed investigations have shown that stockwork veins are commonly composed of multiple quartz types, implying that the evolution of the magmatic-hydrothermal system is more complex than suggested by the study of vein types in hand specimen (Rusk and Reed, 2002; Redmond et al., 2004; Landtwing and Pettke, 2005; Rusk et al., 2006, 2008a; Klemm et al., 2007, 2008; Pudack et al., 2009; Landtwing et al., 2010; Müller et al., 2010; Redmond and Einaudi, 2010).

CL microscopy represents one of the most effective analytical tools to distinguish different types of quartz in the stockwork veins as the CL properties of quartz relate to the genetic conditions of quartz growth (and alteration). The observed luminescence of quartz results from the combined effects that composition, crystal structure and strain or damage of the structure have on electron beam interactions. The emission spectrum of quartz is a direct manifestation of the real structure of the crystal (Marfunin, 1979; Götze et al., 2001).

Hydrothermal quartz in porphyry deposits displays a wide variety of CL textures and shows more secondary textures than quartz found in most other deposit types (Rusk, 2012). These CL textures reflect the superposition of various events throughout the evolution of the magmatic-hydrothermal system. Utilization of CL allows interpretation of complex growth textures in optically similar quartz, and permit different episodes of quartz growth to be tied into the overall paragenesis.

Recent studies of porphyry quartz from Bingham Canyon in Utah using SEM-CL have highlighted complexities of vein formation in porphyry deposits (Redmond et al., 2004; Landtwing and Pettke, 2005; Landtwing et al., 2010; Redmond and Einaudi, 2010). These studies found that stockwork veins typically contained early granular quartz crystals showing bright luminescence with strong oscillatory growth zoning, in addition to late weak- to non-luminescent quartz lacking well-defined growth zoning. Bright luminescing quartz contained abundant brine and coexisting vapor inclusions, whereas weakly luminescent quartz contained rare lower-salinity liquid inclusions with significantly lower homogenization temperatures and fewer vapor inclusions. Late quartz is present in

embayments along crystal margins and in cracks which cut growth zones in early quartz, and is interpreted to have formed via dissolution and reprecipitation of early quartz. Similar textures and characteristic luminescence have been observed in porphyry-style deposits at Butte in Montana (Rusk and Reed, 2002; Rusk et al., 2006); Nevados de Famatina in Argentina (Pudack et al., 2009); Grasberg in Indonesia (Rusk et al., 2008b); Oyu Tolgoi and Zesen Uul in Mongolia (Müller et al., 2010); and Pebble in Alaska (Marsh, 2012).

In all cases studies so far, the ore minerals appear to postdate the late weak- to non-luminescing quartz, implying that ore formation is late in the paragenesis. With the exception of Bingham Canyon in Utah, mineralization does not appear to be associated with the development of potassic alteration. The results of the CL observations require development of a new model of porphyry deposit formation that takes a more complex evolution of the magmatic-hydrothermal system into account (cf. Heinrich et al., 2005; Williams-Jones and Heinrich, 2005).

1.6 Research Aims

The research conducted as part of the present thesis aims to contribute to the development of a refined deposit model of porphyry formation through a comparison of the fluid inclusion and CL characteristics of quartz contained in stockwork veins from several porphyry deposits worldwide. The research places emphasis on the study of the textural context of fluid inclusions using optical CL microscopy (cf. Neuser, 1995; Götze et al., 2001) to reconstruct changes in the physicochemical conditions of quartz growth during the formation of complex multi-phase quartz veins.

While fluid inclusion and CL techniques are clearly instrumental in building and advancing our understanding of the processes that lead to ore formation in the porphyry environment, these techniques are not widely used in mineral exploration. The present thesis also shows that these techniques can be combined effectively in an exploration scenario.

The thesis explores the hypothesis that quartz grains derived from porphyry veins can be confidently identified in fluvial deposits based on their unique fluid inclusion and CL properties. If methods could be developed to rapidly screen the sand-sized fraction of fluvial deposits for these types of quartz, the presence or absence of porphyry quartz in stream sediments could be used to vector towards a porphyry source. As stream sediment geochemical surveys are routinely conducted in mineral exploration for porphyries, important additional exploration criteria derived from the study of quartz could potentially be generated at comparably low cost.

1.7 Thesis Layout

The research detailed in this thesis is presented as three contributions, each of which is followed by a discussion of experimental results. The chapters are written as manuscripts and will be submitted to peer-reviewed international science journals.

In the first part of the thesis, observations from combined fluid inclusion and optical CL investigations of A-veins from the Far Southeast Cu-(Au) porphyry deposit in the Philippines are discussed. Quartz types initially defined by Hedenquist et al. (1998) are studied through fluid inclusion petrography and CL microscopy. This is followed by CL spectral investigations and EMP trace element mapping of the different quartz types. The section concludes with a discussion of quartz types identified at the deposit in terms of their fluid inclusion, CL, and trace element characteristics, with special focus on how these properties of quartz can be modified by hydrothermal alteration following initial crystal growth.

The second part of the thesis details the fluid inclusion and CL investigation of archival samples of vein material from well-documented porphyry deposits emplaced at different crustal depths. Quartz veins from several deposits were examined to build a comprehensive understanding of the fluid inclusion and CL characteristics of hydrothermal quartz formed at different crustal levels, and to identify characteristics that might be ubiquitous across porphyry-type deposits. Samples from the Butte Cu-Mo porphyry in

Montana (Rusk and Reed, 2002; Rusk et al., 2006, 2008a,b); the Bingham Canyon Cu-Mo-(Au) porphyry in Utah (Redmond et al., 2004; Landtwing and Pettke, 2005; Landtwing et al., 2010; Redmond and Einaudi, 2010); and the Au-(Cu) and Au porphyry deposits from the Maricunga belt in Chile (Muntean and Einaudi, 2000, 2001) were studied by fluid inclusion petrography and optical CL microscopy. The section concludes with a comparison of quartz types between the different deposits and demonstrates that certain CL textures are characteristic of hydrothermal quartz from porphyry deposits.

The third section details the application of fluid inclusion and CL characteristics of porphyry quartz established during the previous sections to sand samples from prospective exploration targets. Stream-sediment samples provided by Newmont from Vert de Gris in Haiti and Hide's Creek in Papua New Guinea were examined for the same fluid inclusion and CL characteristics observed in the porphyry samples. This allows for positive identification of porphyry quartz grains in the fluvial setting. Two dispersion studies are presented that determine the dilution of hydrothermal quartz eroded from known porphyry source relative to other minerals. Time- and cost-efficient methods for isolating quartz from background minerals in sands and techniques for rapidly quantifying porphyry-derived quartz grains are examined in this section.

The thesis concludes with a synthesis of the findings from the three parts. In addition, suggestions for future research are made.

CHAPTER 2
HYDROTHERMAL ALTERATION OF QUARTZ AND INHERITANCE OF FLUID INCLUSION ASSEMBLAGES: A CASE STUDY ON VEIN QUARTZ FROM THE FAR SOUTHEAST PORPHYRY CU-AU DEPOSIT, PHILIPPINES

2.1 Introduction

Porphyry copper deposits are currently the world's largest source of copper, with precious metals commonly being recovered as by-products. Hypogene ores in these deposits are comprised of large, low-grade stockwork and disseminated sulfide zones that occur within shallowly emplaced (<1 to 10 km) plutonic stocks or within the surrounding country rocks (Lowell and Guilbert, 1970; Gustafson and Hunt, 1975; Titley and Beane, 1981; Seedorff et al., 2005). The stockwork zones in these deposits are composed of quartz veins of variable morphologies, orientations, macroscopic textures, vein fillings, and associated alteration halos (Gustafson and Hunt, 1975; Clark, 1993; Gustafson and Quiroga, 1995; Arancibia and Clark, 1996; Muntean and Einaudi, 2000).

A comprehensive study on the Far Southeast porphyry deposit in the Mankayan mining district of northern Luzon, Philippines, by Hedenquist et al. (1998) provided an important foundation for the current understanding of the development of stockwork zones in porphyry deposits and the link between the porphyry and epithermal environments. Based on careful age dating, petrographic, and fluid inclusion investigations, these authors demonstrated that porphyry quartz veins record a complex history of fluid flow events, explaining the formation of different styles of mineralization and alteration at different times during the evolution of the magmatic-hydrothermal system.

The present study provides new evidence constraining the processes involved in the formation of porphyry veins at the Far Southeast porphyry deposit. A combination of analytical techniques is used to characterize the different generations of quartz present in the stockwork veins, including optical microscopy, fluid inclusion petrography, cathodoluminescence microscopy and spectroscopy, as well as electron microprobe mapping and

spot analysis. The findings of this study have far-reaching implications to the interpretation of fluid inclusion data in porphyry systems and also contribute to a better understanding of the paragenetic relationships in mineralized magmatic-hydrothermal systems.

2.2 Geologic Setting

The Far Southeast porphyry Cu-Au deposit is located within the Mankayan mining district, which forms part of a 150-km-long belt of porphyry and epithermal deposits in the Central Cordillera of the northern Luzon, Philippines (Fig. 2-1).

The Mankayan district comprises a basement of Late Cretaceous to Middle Miocene volcanic to epiclastic rocks. The Late Cretaceous to Paleogene Lepanto metavolcanic rocks form the lowermost stratigraphic unit. They comprise metamorphosed submarine andesitic-basaltic flows and pillow lavas that crop out in the western part of the district. The Lepanto metavolcanic rocks are unconformably overlain by the Apaoan sedimentary rocks that primarily consist of epiclastic siltstones and sandstones. The Late Oligocene to Middle Miocene Balili volcaniclastic rocks, which are composed of andesitic breccias and tuffs, polymictic conglomerates, wackes, and shales, represent the youngest stratigraphic unit of the basement (Concepcíon and Cinco, 1989; Garcia, 1991; Hedenquist et al., 1998; Imai, 2000; Claveria, 2001). A large Miocene intrusion, the Bagon tonalite, is hosted by the basement rocks and is now exposed at the western margin of the Mankayan district (Fig. 2-1).

The Late Cretaceous to Middle Miocene basement of the Mankayan district is blanketed by the Early Pleistocene Imbanguila hornblende-bearing dacite, comprising both pyroclastic deposits and porphyritic lavas. The Imbanguila hornblende dacite is overlain by the chemically similar Bato hornblende-biotite dacite, which is composed of porphyritic lava domes and pyroclastic flow units. Formation of the Imbanguila hornblende dacite predated mineralization at Far Southeast and Lepanto while deposition of the Bato hornblende-biotite dacite postdated the hydrothermal activity (Garcia, 1991; Arribas et al., 1995; Hedenquist et al., 1998; Imai, 2000; Claveria, 2001). The Lapangan tuff

represents the youngest volcanic deposit in the district, forming a thin and discontinuous cover of poorly consolidated dacitic air-fall tuff (Chang et al., 2011).

The top of the high-grade Cu-Au ore zones of the Far Southeast porphyry deposit is located at an elevation of 900 m, approximately 550 m below the surface. The ore body is centered on melanocratic quartz diorite porphyry dikes and irregularly shaped intrusions that intruded into the Balili volcaniclastic rocks to about 300 m elevation (Fig. 2-1). These 50 to 150 m wide intrusive bodies contain >30% phenocrysts of plagioclase, quartz, hornblende, and biotite. A series of leucocratic quartz diorite dikes that are typically 20 to 40 m wide extends up to 500-700 m elevation and cuts the earlier melanocratic quartz diorite intrusions. In contrast to the earlier dikes, the leucocratic quartz diorite is only weakly mineralized. Both sets of dikes are intersected by a hydrothermal breccia pipe that is steeply dipping and up to 400 m wide (Concepcíon and Cinco, 1989; Hedenquist et al., 1998; Imai, 2000).

The primary ore minerals at Far Southeast are bornite and chalcopyrite. The sulfide minerals typically occur in veins containing euhedral quartz in addition to anhydrite, sericite, pyrite, or hematite. In many cases, the quartz veins are enveloped by centimeter- to meter-wide bleached halos of chlorite-sericite alteration (Hedenquist et al., 1998). Gold occurs as electrum in textural association with the bornite and chalcopyrite, as well as with locally occurring Bi-Te-rich tennantite (Concepcíon and Cinco, 1989; Garcia, 1991; Imai et al., 1994). The Far Southeast porphyry deposit contains a total of 356 Mt of ore grading 0.73% Cu and 1.24 g/t Au (Chang et al., 2011).

The alteration halo associated with the Far Southeast porphyry deposit exhibits a cupola-shaped configuration of alteration zones around the melanocratic quartz diorite intrusions (Fig. 2-1). Potassic alteration is most pervasive in the deep centre of the alteration halo (Concepcíon and Cinco, 1989; Garcia, 1991; Imai, 2000). It is comprised of biotite-magnetite ± K feldspar and associated with veins of vitreous, anhedral quartz (Hedenquist et al., 1998). Potassic alteration is partially to pervasively overprinted by chlorite-sericite alteration consisting of chlorite, hematite, and/or sericite (sericite is a

field term for fine-grained muscovite and/or illite). The zone of chlorite-sericite alteration grades outward into a distal zone of propylitic alteration characterized by the presence of epidote, calcite, and chlorite (Concepcíon and Cinco, 1989; Garcia, 1991; Imai, 2000).

To the northwest, the Far Southeast porphyry deposit is overlain by the ore body of the Lepanto epithermal deposit. The ore zone of this deposit is approximately 3 km long and consists of breccia and replacement ores stretching along the Lepanto fault, one of several northwest-trending splays off the northwest-trending Abra River fault, which forms part of the Philippine fault system. The enargite-luzonite ores of the Lepanto deposit are located at an elevation of 700 to 1200 m at the intersection of the steeply dipping Lepanto fault with the unconformity between the basement rocks and the Imbanguila hornblende-bearing dacite. The Lepanto deposit was mined out in 1996 with a total of 36.3 Mt of ore grading 2.9 % Cu, 3.4 g/t Au, and 14 g/t Ag (Chang et al., 2011).

Arribas et al. (1995) and Hedenquist et al. (1998) showed that the mineralization at Far Southeast and Lepanto formed contemporaneously during the Early Pleistocene. Hornblende from least-altered Imbanguila dacite that predates mineralization yielded K/Ar ages of 2.19 ± 0.62 to 1.82 ± 0.36 Ma. Ages for hydrothermal minerals from the Far Southeast deposit include 1.45 ± 0.04 to 1.34 ± 0.05 Ma for biotite from the potassic alteration halo and 1.37 ± 0.05 to 1.22 ± 0.06 Ma for illite from the chlorite-sericite alteration zone. Ore-stage alunite from the Lepanto deposit dated at 1.56 ± 0.29 to 1.17 ± 0.16 Ma. Hornblende and biotite from the post-mineralization Bato dacite are significantly younger, with K/Ar ages ranging from 1.18 ± 0.08 to 0.96 ± 0.29 Ma.

2.3 Materials and Methods

The detailed investigations of the present study focus on a porphyry vein collected from Far Southeast drill hole E-10 at an elevation of 80 m (Fig. 2-1). Preliminary fluid inclusion petrography and microthermometric investigations on this vein (sample U86-6-2045) have been reported previously by Hedenquist et al. (1998).

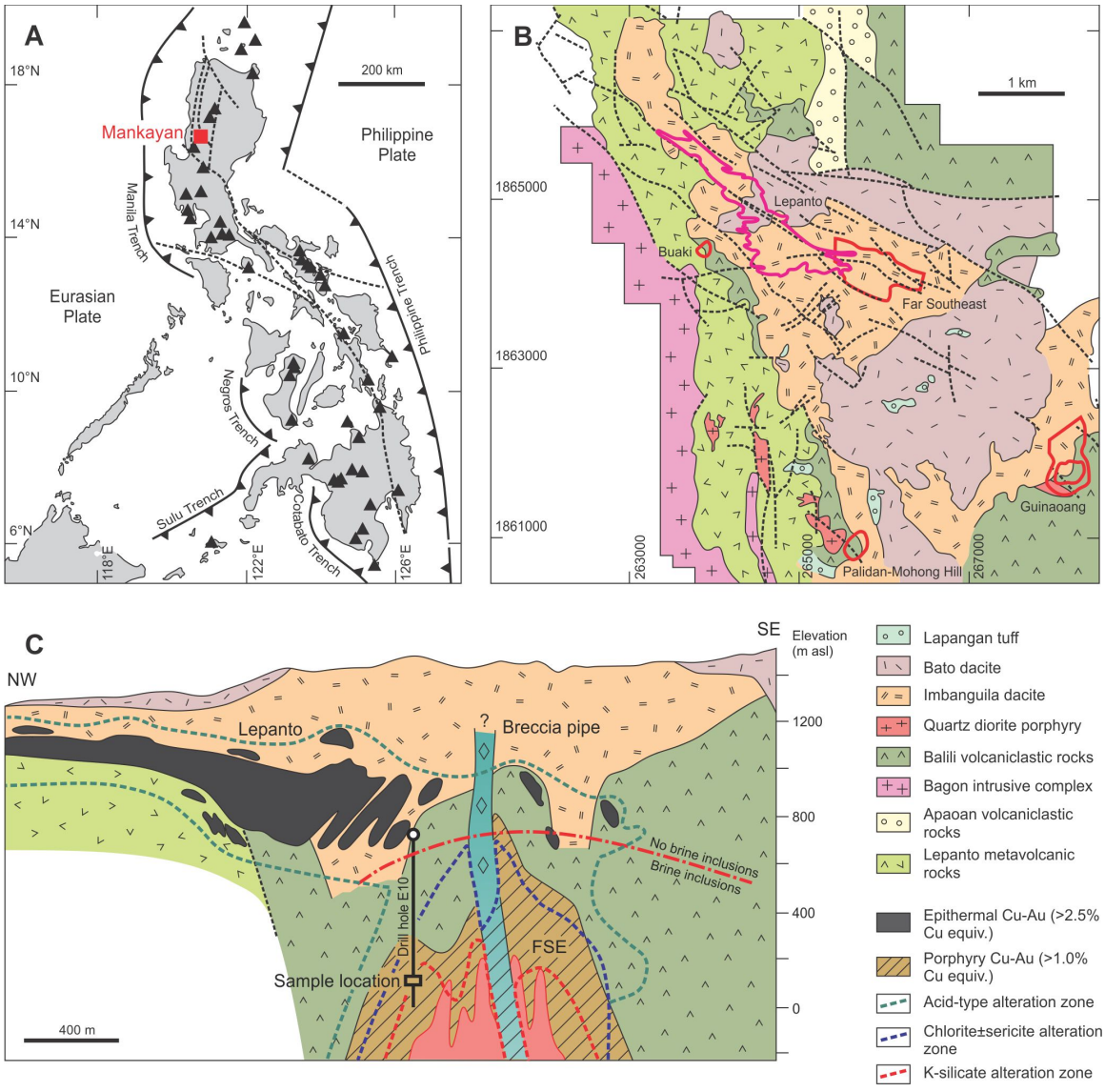

FIG. 2-1: Geology of the Far Southeast porphyry Cu-Au deposit. (A) Location of the Mankayan district in northern Luzon, Philippines. The triangles represent active arc volcanoes. (B) Geological map of the Mankayan mining district. The economically most important deposits in the district are highlighted. (C) Schematic northwest-southeast longitudinal section through the Far Southeast porphyry Cu-Au deposit and the associated Lepanto epithermal deposit. The section shows the distribution of lithological units, alteration styles, and ore zones. Note the sampling location of sample U86-6-2045 (drill hole E-10) that is described in detail in the present study. The figures are modified from Hedenquist et al. (1998) and Chang et al. (2011).

Initially, optical microscopy and fluid inclusion petrography were performed on the quartz vein sample with an Olympus BX51 microscope using a series of doubly polished, 60 μm-thick sections. Microthermometric data on selected fluid inclusions were collected using a Fluid Inc.-adapted U.S. Geological Survey gas-flow heating and freezing stage that was calibrated using synthetic fluid inclusions. Freezing temperatures were accurate to ±0.1°C. The accuracy of heating measurements ranged from approximately ±2°C at 200°C to approximately ±10°C at temperatures above 600°C. Imaging of representative fluid inclusions was conducted using an Optronics Microfire A/R camera.

Subsequent to the fluid inclusion petrography, the thick sections were carbon coated for the CL investigations. A HC5-LM hot cathode CL microscope by Lumic Special Microscopes, Germany, was used, allowing inspection of the thick sections under electron bombardment in a modified Olympus BXFM-S optical microscope. The microscope was operated at 14 kV and with a current density of ca. 10 μA mm^{-2} (Neuser, 1995). CL images were captured using a high sensitivity, double-stage Peltier cooled Kappa DX40C CCD camera, with acquisition times ranging from 8 to 10 seconds. CL spectra were collected on selected spots (ca. 30 μm spot diameter) located as far away from anhydrite inclusions as possible. The spectral data were acquired over a wavelength range of 380 to 1000 nm using an Acton Research SP-2356 digital triple-grating spectrograph equipped with a Princeton Spec-10 CCD detector attached to the CL microscope by a silica-glass fiber cable. Wavelength calibration of the spectrograph was performed with a Hg-halogen lamp.

Trace element (Al, K, and Ti) mapping in selected areas of the thick sections was performed by wave-length dispersive spectrometry using a JEOL JXA 8900 electron microprobe operated at 20 kV accelerating voltage, 100 nA current (measured on Faraday cup), and a focused beam with dwell times of one second per pixel. The trace element maps for the four elements were collected simultaneously, during which Al was collected on one spectrometer using a TAP analyzing crystal, K was collected on one spectrometer using PET analyzing crystal, and Ti was collected on three spectrometers using LiF analyzing crystals. In addition to the qualitative trace element maps, quantitative trace ele-

ment analyses were conducted along traverses across the quartz. Traverses were analyzed using 10 µm distances between spots. The operating conditions for spot analyses were 20 kV, 50 nA (measured on Faraday cup), and a beam defocused to 5 µm to minimize specimen damage. The Al Kα X-ray line was analyzed with a TAP crystal and the K Kα X-ray line with a PET crystal. The Ti Kα X-ray line was measured simultaneously with LiF crystals on the three other spectrometers. Count times of 10 minutes on the peak and 5 minutes on each the high and low backgrounds were applied. Alternating on and off peak acquisition was used to account for carbon contamination build up during the long analysis times. Aggregate intensities of the on- and off-peak positions of the duplicate elements and a blank correction were used to improve the counting statistics (Donovan et al., 2011). Calculated detection limits on spot analyses are 8 ppm for Al, 16 ppm for K, and 16 ppm for Ti.

2.4 Results

2.4.1 Optical Microscopy

The sample investigated represents an approximately 10 mm-wide vitreous quartz vein hosted by altered andesitic tuff of the Late Oligocene to Middle Miocene Balili volcaniclastic rocks. The quartz vein is surrounded by a distinct 4 mm-wide, grayish-yellow halo in which the wall rock has been pervasively replaced by sericite (fine-grained muscovite or illite) and fine-grained quartz. Disseminated chalcopyrite, bornite, and anhydrite are present within the alteration halo. Rutile represents a minor phase occurring in the alteration halo and probably formed as a result of hydrothermal alteration of Ti-bearing primary phases. Another accessory phase recognized is apatite, which likely represents a primary magmatic phase. The sericite alteration appears to overprint earlier potassic alteration. Kaolinite occurs locally.

The vitreous quartz vein is largely composed of large (ca. 250 to 1000 µm), sub- to anhedral quartz grains, referred to as Q1 in the present contribution. The Q1 grains can be easily identified based on the high abundance of fluid inclusions (Fig. 2-2A). The sub- to anhedral Q1 grains are blocky to slightly elongate. Under crossed-polarized light, Q1

grains extinct homogeneously (Fig. 2-2B), although the extinction angle may vary between adjacent grains. The sub- to anhedral Q1 grains are typically separated by irregular grain boundaries. In many cases, narrow (≤ 125 µm) zones of equant subgrains having different extinction angles are developed along grain boundaries.

Under crossed-polarized light, a progression of recrystallization of Q1 grains can be identified. In many cases, the large Q1 grains consist of domains of slightly different orientation (Fig. 2-2B). Narrow zones containing subgrains with undulose extinction can be observed along fractures transecting individual Q1 grains (Fig. 2-2C). In several locations within the vein, the large Q1 grains are transected by an up to 500 µm wide fracture-controlled zone of finely recrystallized Q1 grains (30 to 50 µm) that are equant in shape and have undulose extinction. Within these zones, sulfide minerals and anhydrite occur (Fig. 2-2D, E).

Some Q1 grains have distinct inclusion-poor rims that are occasionally separated from the inclusion-rich crystal cores by narrow zones of quartz with inclusion characteristics that differ from Q1. These narrow (≤ 70 µm) zones represent a quartz type not recognized by Hedenquist et al. (1998), referred to as Q2 in this contribution (Fig. 2-2F). The inclusion-poor rims represent the youngest quartz type, referred to as Q3. In most cases, no distinct grain boundaries can be observed between Q1 and the younger quartz generations forming the rims. In addition to inclusion-poor rims, Q3 quartz also forms distinct euhedral crystals that have grown into open space (Fig. 2-2F). These euhedral Q3 grains range from 50 to 250 µm in size and abundantly occur along the fractures that contain sulfide minerals and anhydrite (Fig. 2-2E, F). The same relationships can be observed within vugs in the wall-rock. Euhedral Q3 crystals commonly show homogeneous extinction, but undulose extinction also occurs.

Sulfide minerals and anhydrite commonly infill the space between euhedral Q3 crystals (Fig. 2-2F). Anhydrite and sulfide grains typically range in size from 40 to 600 µm and 40 to 350 µm, respectively. Distinctly small anhydrite and sulfide grains (<30 µm) and rare sericite flakes can be entirely encapsulated by euhedral Q3 quartz. These

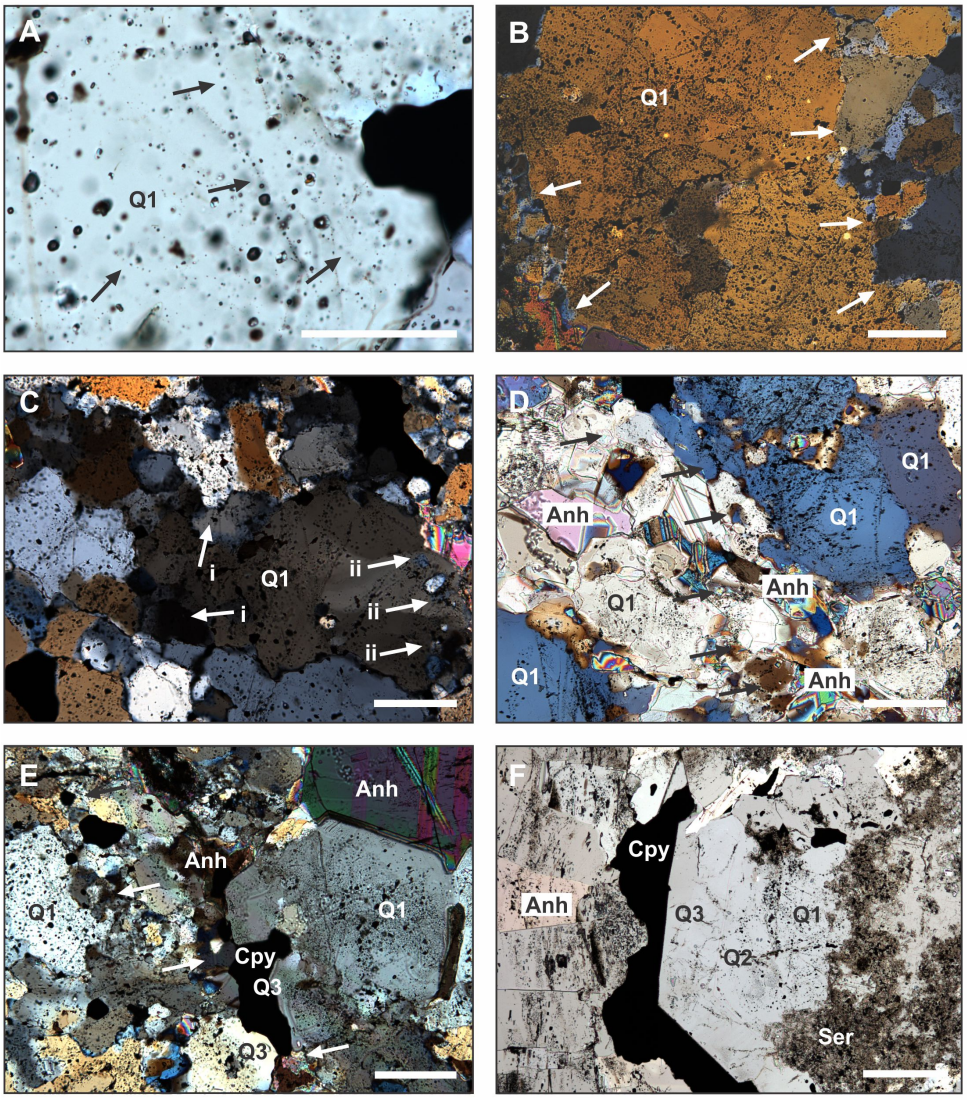

FIG. 2-2: Transmitted light photomicrographs of vein quartz from Far Southeast. (A) Plane polarized light image of a large, anhedral Q1 crystal that contains abundant fluid inclusions. The inclusions occur randomly throughout the quartz or along defined secondary inclusion trails (arrows). Scale bar is 100 µm. (B) Crossed-polarized light image of a large Q1 grain that shows homogeneous extinction. The grain boundary of the large quartz grain is irregular in shape and marked by the occurrence of equant-shaped subgrains (arrows). Scale bar is 200 µm. (C) Crossed-polarized light image of a large Q1 grain showing domains of slightly different orientation (i, arrows). The Q1 grain is crosscut by a narrow zone of equant-shaped subgrains (ii, arrows). Scale bar is 200 µm. (D) Crossed-polarized light image of the vein centre that is typified by the occurrence of numerous small, equant-shaped recrystallized Q1 grains (arrows) that are intergrown with anhydrite and sulfide minerals. Scale bar is 200 µm. (E) Crossed-polarized light image of the vein centre. Abundant anhydrite and sulfide minerals are intergrown with equant-shaped recrystallized Q1 grains (arrows). Chalcopyrite is intergrown with small euhedral Q3 grains that are largely devoid of fluid inclusions. Scale bar is 200 µm. (F) Plane polarized light image of inclusion-poor euhedral Q3 quartz crystals that are intergrown with chalcopyrite. The euhedral Q3 grains represent an overgrowth on an inclusion-rich core consisting of Q1 and Q2. The wall-rock contains abundant sericite. Scale bar is 400 µm. Note that all images were collected on thick sections. Anh = anhydrite, Cpy = chalcopyrite, Ser = sericite.

textural relationships imply that the sulfide formation occurred during, or shortly after, the formation of Q3.

2.4.2 Fluid Inclusion Petrography

The early anhedral Q1 quartz is characterized by the abundant presence of fluid inclusion assemblages comprising 5-10 μm brine inclusions (B_{Q1}) with medium to large vapor bubbles and coexisting 1-10 μm vapor rich inclusions, referred to as V_{Q1} in the present contribution (Fig. 2-3A-B). The inclusions are equant to negative-crystal shaped, indicating a relatively high entrapment temperature (cf. Bodnar et al., 1985). The B_{Q1} and V_{Q1} inclusions form clusters or distinct inclusion trails within Q1. Alignment of these inclusions along growth zones of Q1 quartz occurs, but is exceedingly rare. Based on the petrographic evidence, the majority of B_{Q1} and V_{Q1} inclusions are interpreted to be secondary in nature. However, as these inclusions have not been observed in the younger quartz generations, their entrapment is interpreted to have occurred in close association with the formation of Q1 quartz. Microthermometry of B_{Q1} inclusions coexisting with V_{Q1} inclusions yielded maximum homogenization by disappearance of the vapor bubble at 450°C to 550°C, with the dissolution of halite taking place between 425°C and 475°C. Lower homogenization temperatures also occur commonly. The B_{Q1} inclusions have a salinity of 50-55 wt % NaCl equiv. (cf. Hedenquist et al., 1998). Some B_{Q1} inclusions contain hematite accidentals in addition to halite. Anhydrite was identified as an additional daughter mineral in some of these inclusions.

As noted above, the anhedral zones of Q2 quartz occupying the space between Q1 quartz and the distinct late euhedral Q3 quartz can only be petrographically identified based on their distinct fluid inclusion assemblages. Inclusions within Q2 quartz consist of 2-10 μm brine inclusions (B_{Q2}) with a small vapor bubble. The B_{Q2} inclusions are distinctly irregular in shape (Fig. 2-3C), suggesting entrapment of these secondary inclusions at lower temperatures (cf. Bodnar et al., 1985). The equant to negative-crystal shaped B_{Q1} and V_{Q1} inclusions were never observed in Q2 quartz. The results of microthermometric investigations of two B_{Q2} inclusion assemblages were inconclusive, due

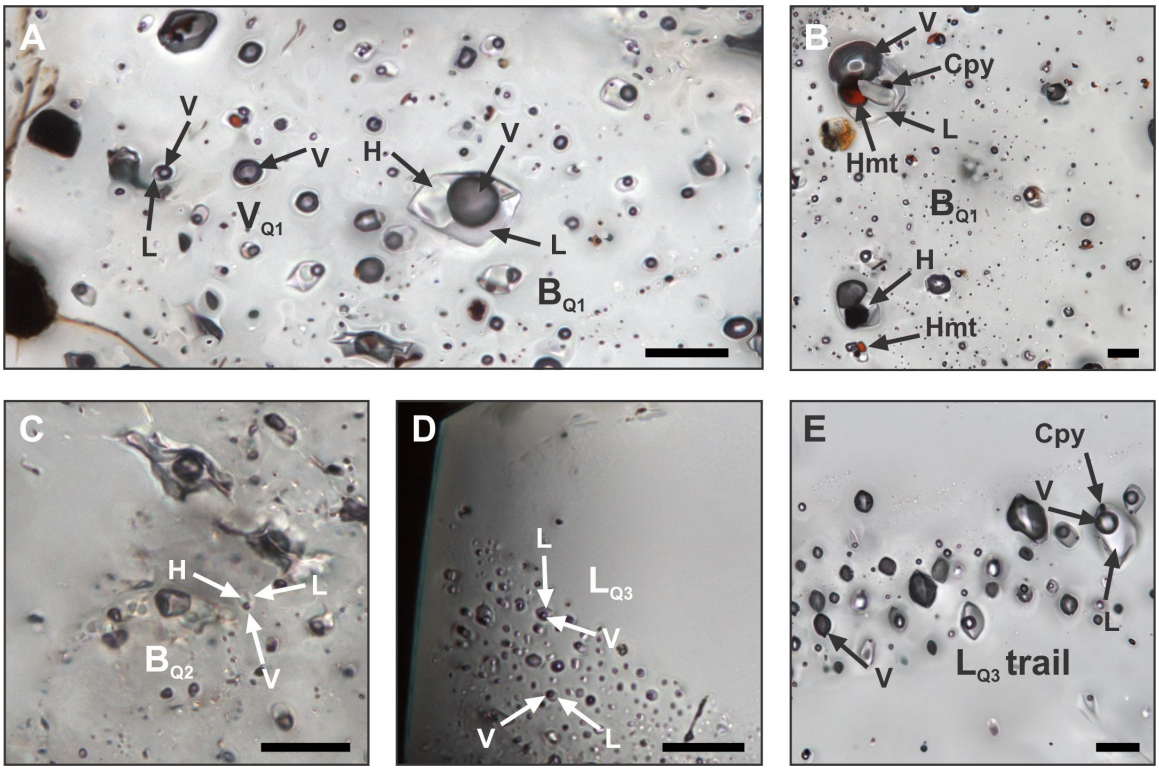

FIG. 2-3: Photomicrographs showing the different fluid inclusion assemblages encountered in the quartz from Far Southeast. (A) Brine B_{Q1} inclusions containing a halite daughter mineral and large vapor bubble. (B) Brine B_{Q1} inclusions containing (accidental ?) hematite and chalcopyrite daughter crystals in addition to halite. (C) Vapor V_{Q1} inclusions containing >80 vol. % vapor. The brine B_{Q1} inclusions and the vapor V_{Q1} inclusions are hosted by the early anhedral Q1 quartz. (D) Irregular-shaped brine B_{Q2} inclusions containing a small halite and anhydrite daughter crystals and a small vapor bubble. The inclusions are hosted by Q2 quartz. (E) Liquid L_{Q3} inclusions containing small vapor bubbles. The inclusions are hosted by altered Q1. (F) Secondary trail of low-salinity liquid L_{Q3} inclusions hosted by altered Q1. Formation of these secondary trails is associated with the formation of euhedral Q3 quartz. See text for detailed description of the fluid inclusion assemblages and their textural settings. L = liquid, V= vapor, Cpy = chalcopyrite, H = halite, Hmt = hematite. All scale bars are 10 μm.

to necking or leaking of the inclusions or the small size of the inclusions, which prohibited reliable observation of halite dissolution. A single pristine B_{Q2} inclusion homogenized by dissolution of halite at 295°C, and may be representative of an intermediate formation temperature between B_{Q1} and lower-temperature fluid inclusion assemblages described below. B_{Q2} inclusions have a salinity of >26 wt % NaCl equiv. based on the presence of halite at room temperature.

The late euhedral Q3 quartz is largely devoid of fluid inclusions. Only in a few locations, NaCl-undersaturated liquid inclusions (L_{Q3}) containing small vapor bubbles have been recognized in Q3 quartz (Fig. 2-3D,E). The inclusions range from <1 to 5 µm in size and are equant to irregular-shaped, generally suggesting entrapment at relatively low temperatures. It is difficult to discern whether L_{Q3} inclusions found in the euhedral Q3 quartz are truly primary, as there are too few inclusions to confidently correlate inclusion assemblages with growth zoning. Rarely, L_{Q3} inclusions are also observed along subgrain boundaries in Q2 quartz and as secondary fluid inclusion trails in Q1 and Q2 quartz. The L_{Q3} inclusions sometimes contain chalcopyrite daughter crystals (Fig. 2-3E). In the sample investigated, L_{Q3} inclusions have homogenization temperatures of ca. 280°C and salinities of 3 wt % NaCl equiv. Only in one secondary fluid inclusion trail, coexistence of L_{Q3} inclusions with vapor inclusions, referred to as V_{Q3}, was observed (Fig. 2-3E).

2.4.3 Cathodoluminescence Microscopy

CL microscopy showed that the vein quartz is characterized by a short-lived light blue CL color that fades away during continued electron bombardments (Fig. 2-4). Following approximately 100 seconds of exposure by the electron beam, two different types of hydrothermal quartz showing stable CL colors can be observed. Most of the quartz contained in the vein is characterized by a stable, bright blue luminescence. The quartz grains showing a bright blue CL are crosscut and surrounded by zones of quartz that shows a long-lived, red-brown luminescence (Fig. 2-5).

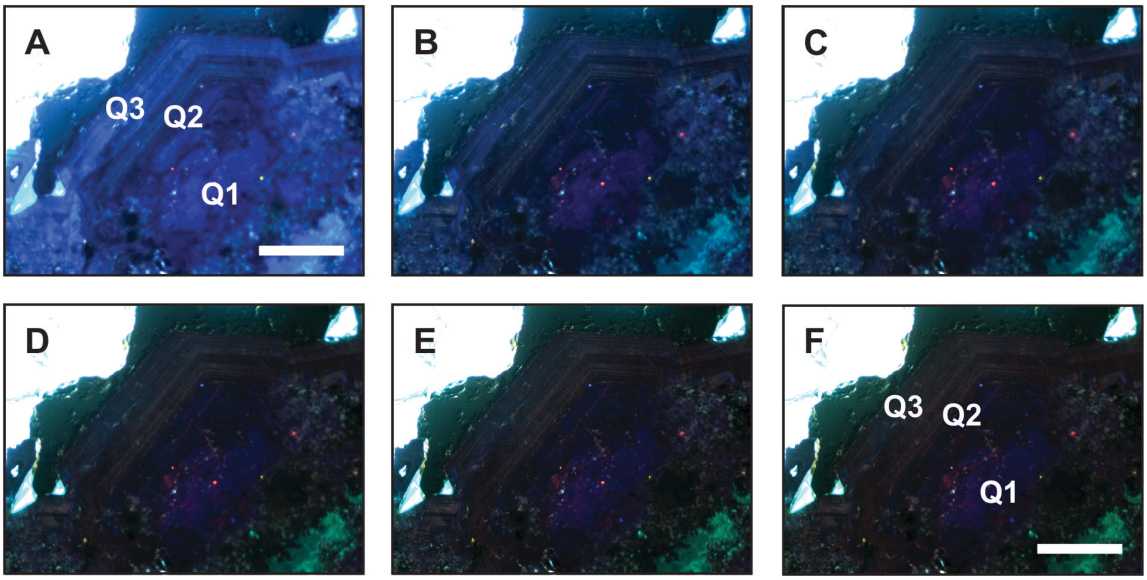

FIG. 2-4: Series of CL photomicrographs of a large euhedral quartz grain collected during continued electron bombardment. The core of the euhedral grain is rich in fluid inclusions and interpreted to represent Q1.This core is surrounded by a narrow zone of Q2 typified by irregularly shaped B_{Q2} inclusions. The outermost portion of the grain consists of Q3 that is largely devoid of fluid inclusions. The grain is the same shown in plane polarized light in Fig. 2-2F. (A) After 10 seconds of exposure to the electron beam, the quartz grain shows a short-lived, blue CL emission. (B-E) With continued exposure, the short-lived, blue luminescence gradually fades away (B after 20 seconds; C after 40 seconds; D after 80 seconds; E after 100 seconds). (F) After 120 seconds of continuous exposure to the electron beam, the short-lived CL of the hydrothermal quartz has been completely replaced by a stable CL signal. Q1 quartz in the core of the grain shows a stable blue luminescence while the remainder of the grain is typified by a long-lived red-brown CL emission. Note that the very bright luminescent mineral is anhydrite. It shows an intense greenish CL that is overexposed in the images because quartz is typified by a much less intense CL signal. Scale bar is 400 μm.

The frequently occurring bright blue quartz grains show well-defined oscillatory growth zoning (Fig. 2-5A), revealing that the quartz must have grown from the vein walls inwards towards the vein center. Careful correlation shows that quartz showing a bright blue CL color universally contains abundant B_{Q1} and V_{Q1} inclusions, implying that the quartz having a bright blue CL can be classified as Q1 (Fig. 2-5A,B).

The large blue luminescent Q1 grains showing oscillatory growth zoning are frequently crosscut by a network of quartz that shows a stable red-brown CL (Fig. 2-5A,C). The zones of red-brown CL occur along grain boundaries between adjacent Q1 grains having different extinction angles in crossed-polarized light or along fractures transecting multiple Q1 grains. The red-brown zones crosscutting the blue Q1 quartz have variable widths, ranging from <10 to ~300 μm. In cases where the grain boundaries and fractures are marked by the occurrence of narrow zones of subgrains, the band of red-brown CL encompasses almost all of the subgrains (Fig. 2-5A,C). Only some of the largest subgrains retain a tint of the blue CL, giving them a purplish appearance.

Locally, the red-brown CL zones developed along grain boundaries between Q1 crystals and fractures crosscutting Q1 grains form networks, resulting in the development of a breccia-like texture containing pseudoclasts of blue quartz in the red-brown pseudomatrix (Fig. 2-5A, 6). The blue pseudoclasts have variable sizes and CL intensities. In general, the intensity of the blue CL color corresponds to the size of the pseudoclasts. Bright blue CL is only observed in the largest pseudoclasts whereas many of the smaller pseudoclasts exhibit a purplish CL (Fig. 2-6).

The finely recrystallized Q1 grains occurring along the fracture-controlled zones that contain sulfide minerals and anhydrite also show a homogeneous red-brown CL (Fig. 2-5C,D). The contact between these zones of recrystallized Q1 quartz and adjacent bright blue luminescent Q1 grains are typically sharp. However, gradational contacts exist between these fracture-controlled zones and the pseudobreccias described above, which are best developed on either side of the fracture-controlled zones containing sulfide minerals and anhydrite (Fig. 2-6).

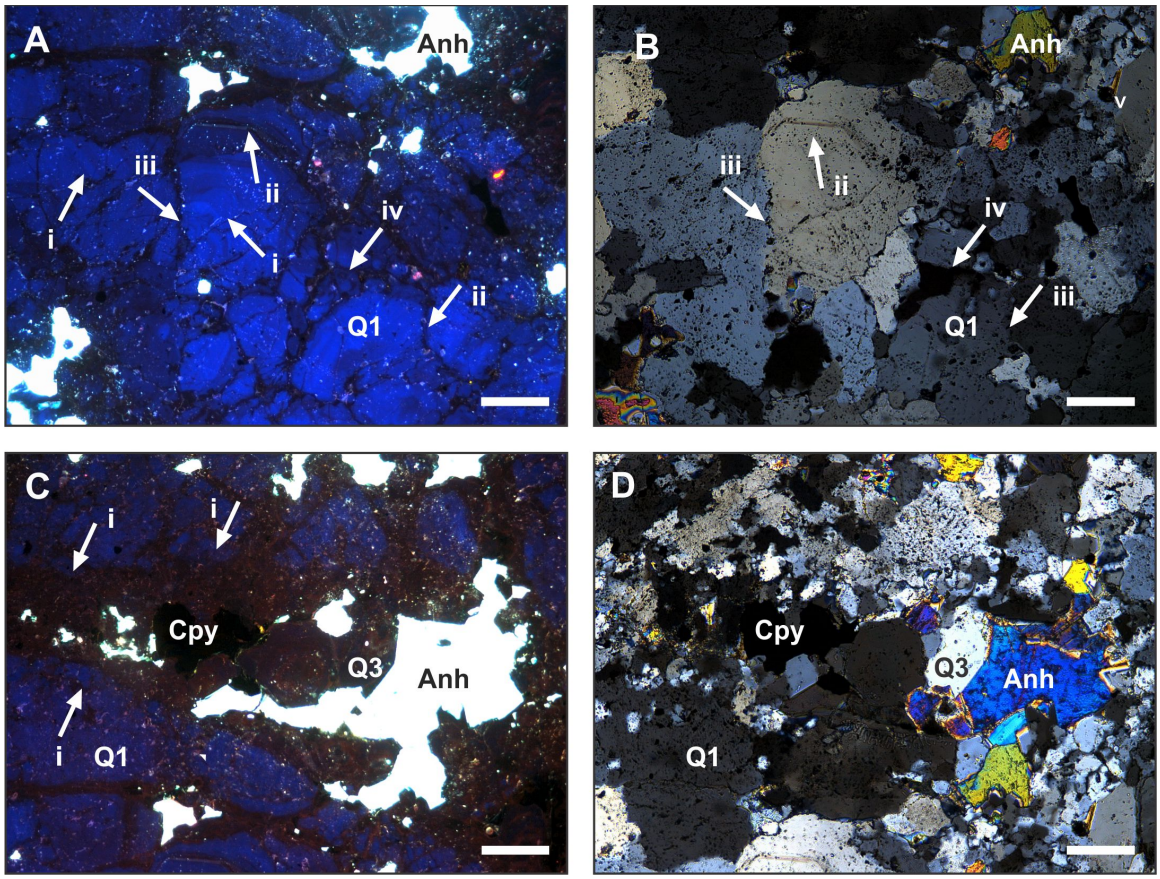

FIG. 2-5: CL photomicrographs and corresponding crossed-polarized light images of vein quartz from Far Southeast. (A+B) Thin section area dominated by blue luminescent Q1 quartz. Some of the large blue quartz grains exhibit oscillatory growth zoning (i, arrows). The quartz showing blue luminescence is rich in B_{Q1} and V_{Q1} inclusions. A 10-20 µm wide band of sub-micrometer anhydrite inclusions parallels growth zoning in Q1 near the crystal margin. The band of anhydrite inclusions can also be seen in transmitted light (ii, arrow). Red-brown luminescent quartz occurs primarily along grain boundaries marked by the occurrence of subgrains (iii, arrows). Locally, a breccia-like texture containing pseudoclasts of blue quartz in a red-brown pseudomatrix is developed. In transmitted light, this breccia-like texture coincides with the occurrence of finely recrystallized Q1 quartz (iv, arrows). (C+D) Fracture-controlled zone of red-brown quartz that crosscuts the blue Q1 quartz. Breccia-like textures of pseudoclasts of blue quartz in a red-brown pseudomatrix primarily occur along the margins of the fracture-controlled zone of red-brown quartz (i, arrows). Euhedral Q3 occurs in close association with the sulfide minerals and the anhydrite. Anh = anhydrite, Cpy = chalcopyrite. All scale bars are 200 µm.

Careful correlation between the occurrence of fluid inclusions and the distribution of CL colors further substantiates that the red-brown quartz commonly represents altered Q1 quartz. In many locations, abundant B_{Q1} and V_{Q1} inclusions can be found in the red-brown zones crosscutting Q1 grains and within the pseudomatrix of the breccia-like quartz (Fig. 2-7). The presence of these inclusions demonstrates that the CL signature of Q1 quartz changed during alteration, but that the fluid inclusion inventory has been preserved. The fluid inclusions in these zones of altered Q1 quartz are petrographically unmodified.

Although much of the red-brown quartz in the vein may represent altered Q1 quartz, the distribution of fluid inclusion types in the red-brown quartz can be complex. In some of the red-brown zones, the fluid inclusion inventory grades from B_{Q1} to B_{Q2} inclusions in quartz adjacent to the bright blue Q1 grains to inclusion-poor quartz with rare low salinity liquid inclusions at the fracture center. This suggests that the red-brown quartz notable under CL represents a composite of altered Q1, pristine or altered Q2 and newly formed Q3.

Further evidence for the fact that the different quartz types cannot be distinguished based on their CL color without the aid of optical microscopy and fluid inclusion petrography is provided by the fact that grains confidently identified as Q2 and Q3 also show stable red-brown luminescence. The euhedral quartz adjacent to sulfide minerals and anhydrite that is largely devoid of fluid inclusions universally shows a red-brown CL color (Fig. 2-4 to 2-6). Some of the euhedral Q3 grains show well-developed fine-scale oscillatory zoning, which becomes less apparent as the luminescence changes from short-lived blue to red-brown (Fig. 2-4). Locally, Q3 grains can have rare zones that are non-luminescent after the short-lived CL has faded away.

Anhydrite present in the vein samples is characterized by a bright green-white to greenish-rose CL. Most anhydrite grains show pronounced oscillatory growth zoning although more irregular, wavy zoning has also been recognized. The CL of the anhydrite is much more intense than the emission of the vein quartz (Fig. 2-4 to 2-6).

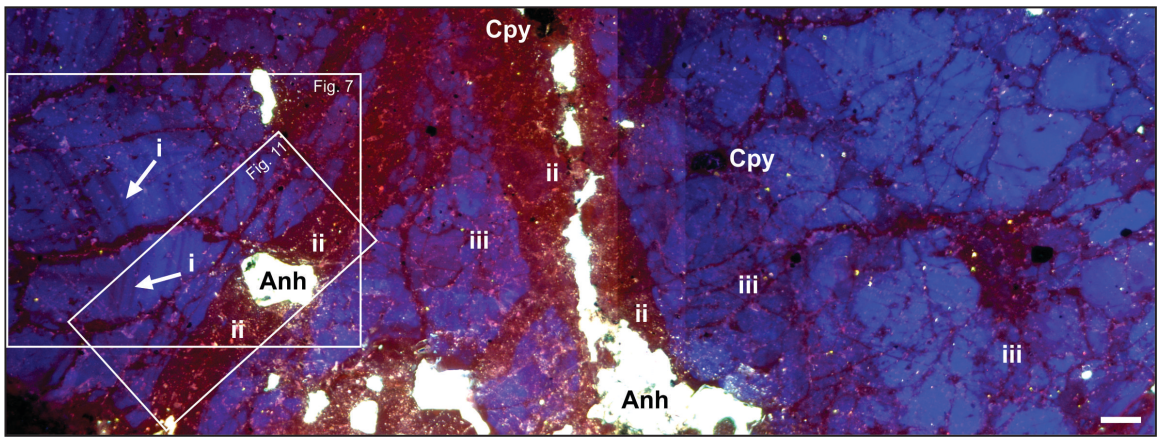

FIG. 2-6: CL photomosaic across the central portion of the porphyry vein. The large blue luminescent Q1 grains exhibit oscillatory growth zoning (i, arrows), suggesting that they have grown towards the vein centre. The quartz showing blue luminescence contains abundant B_{Q1} and V_{Q1} inclusions. Zones of red-brown luminescent quartz occur crosscut the blue quartz. Anhydrite and sulfide minerals occur in close spatial association with the red-brown quartz (ii). Breccia-like textures containing pseudoclasts of blue quartz in the red-brown pseudomatrix are well developed (iii). The color of the pseudoclasts depends on the clast sizes. Bright blue CL is only observed in the largest pseudoclasts whereas many of the smaller pseudoclasts exhibit a purplish CL. Anh = anhydrite, Cpy = chalcopyrite. Scale bar is 100 µm.

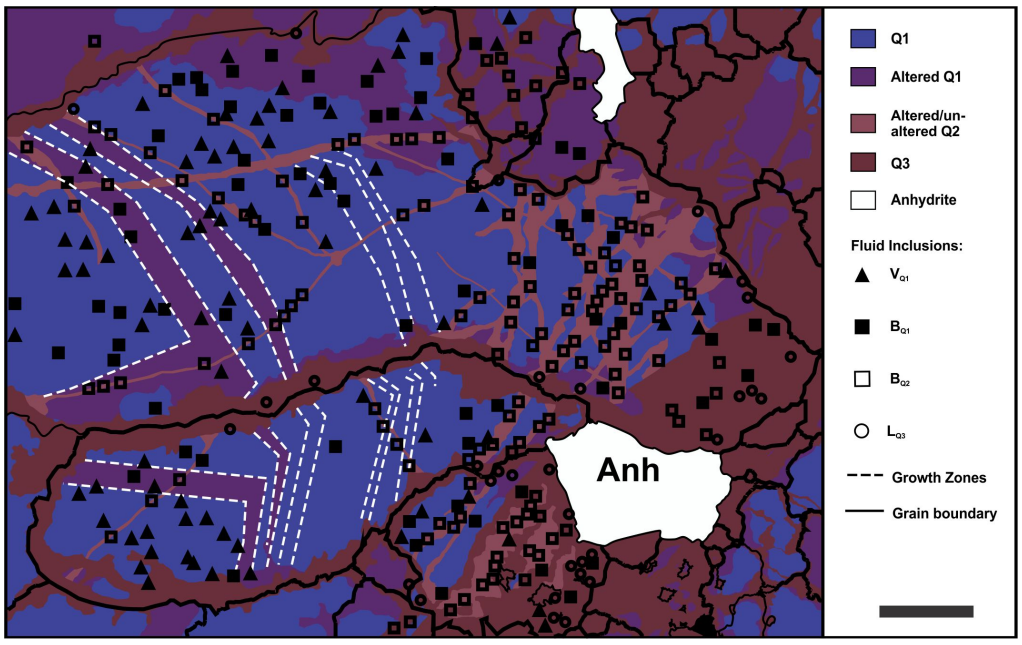

FIG. 2-7: Sketch showing fluid inclusion distribution relative to CL textures in an area that has a breccia-like texture. B_{Q1} and V_{Q1} inclusions are dispersed throughout Q1 quartz, but are also present within the zone of red-brown quartz that crosscuts the Q1 grains. This suggests that red-brown quartz, at least in part, represents altered Q1. Narrow zones of red-brown quartz contain abundant B_{Q2} inclusion and may represent altered Q1 quartz or newly formed Q2. Rare L_{Q3} inclusion trails occur locally within the red-brown quartz. Anh = anhydrite, Cpy = chalcopyrite. Scale bar is 100 µm.

2.4.4 Cathodoluminescence Spectroscopy

The spectral properties of the long-lived CL color were measured in four representative locations. Two spectral measurements were conducted within the bright blue and dark blue zones of the oscillatory growth zones of Q1 quartz. The other two measurements were performed on a red-brown Q2 grain and a euhedral Q3 crystal (Fig. 2-8). All CL spectra were gathered at sufficient distance from the intensely luminescent anhydrite grains to avoid spectral overlap.

All four spectra are characterized by two broad CL bands in the blue and red regions (Fig. 2-8). The blue emissions for all quartz types fall within a narrow range of intensity values while more significant differences can be observed for the red CL emission band. The spectra collected on the light and dark blue luminescent Q1 quartz have the lowest intensities of the red emission band. The difference between the light and dark blue emission of the Q1 quartz is thereby caused by relative variations in the intensities of the blue and red bands. The red-brown Q2 and Q3 grains have the most intense red emissions. Q2 has a slightly more intense red emission than the Q3 grain (Fig. 2-8).

The spectral measurements indicate that the CL emission of all quartz types encountered at Far Southeast result from similar defects. The intrinsic blue emission (peak maximum at 470 nm) is probably associated with the recombination self-trapped excitons (Stevens-Kalceff, 2009) that are formed by electron-phonon interactions (Fisher et al. 1990). Spectral analysis showed that the broad red emission band is composed of at least two, possibly three, overlapping peaks. The most intense peak in the red region matches the intrinsic 650 nm emission band described by Götze et al. (2001), and can likely be attributed to non-bridging oxygen hole centers (Siegel and Marrone, 1981; Stevens-Kalceff, 2009).

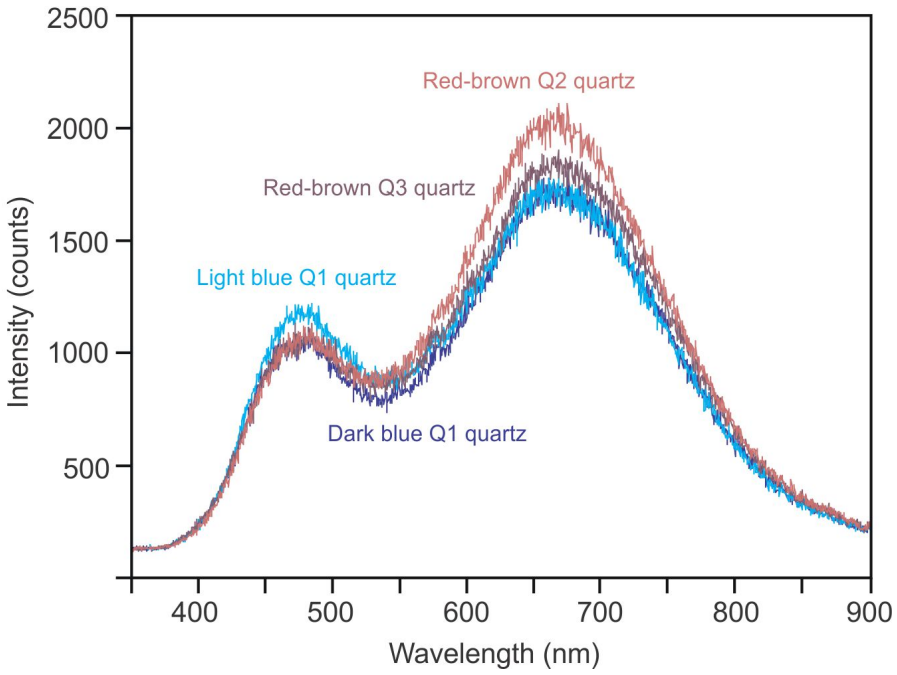

FIG. 2-8: Emission spectra of the long-lived CL of porphyry quartz from Far Southeast. Two spectra were collected on the growth zones of a blue luminescent Q1 grain. In addition, the red-brown emissions of a Q2 quartz and a euhedral Q3 grain were analyzed. All four emission spectra show pronounced emission bands in the blue and red regions.

2.4.5 Electron Microprobe Analyses

The distribution of Al, K, and Ti was mapped in three selected, petrographically well-characterized, areas of the quartz vein using wavelength dispersive X-ray spectroscopy (Fig. 2-9 to 2-11). The trace element maps were calibrated using electron microprobe analyses conducted along nine traverses (Table 2-1).

Trace element mapping and spot analyses along several traverses were conducted in one area of the porphyry quartz vein that is characterized by the occurrence of a large blue luminescent Q1 grain that is transected by smaller zones of red-brown quartz. Based on fluid inclusion petrography, the Q1 grain containing abundant B_{Q1} and V_{Q1} inclusions is partially surrounded by a rim of Q2 quartz containing abundant B_{Q2} inclusions. The area also covered several euhedral Q3 grains that occur in close spatial association with anhydrite and sulfide minerals (Fig. 2-9; 2-12).

Trace element mapping showed that there is, in general, a strong correlation between the trace element abundances within the quartz and the different quartz types identified by CL imaging and fluid inclusion petrography. The blue luminescent Q1 quartz characterized by abundant negative-crystal shaped B_{Q1} and V_{Q1} inclusions has the highest Ti concentrations (up to 262 ppm; *n = 37*). Oscillatory growth zones within Q1 grains are typified by slightly variable Ti concentrations, with the dark blue zones typically having lower Ti contents (up to 86 ppm; *n = 10*). Measurable concentrations of Al and K in the blue Q1 quartz are low and variable, ranging from below detection limit to 973 ppm and 360 ppm, respectively (*n = 37*). The brighter growth zones having elevated Ti concentrations typically also show higher Al contents.

Quartz that shows a red-brown CL emission or is non-luminescent is characterized by distinctly low Ti contents (<98 ppm; *n = 63*). This includes the red-brown quartz zones occurring along fractures crosscutting Q1 that contain trails of B_{Q2} and L_{Q3} inclusions, the red-brown Q2 or Q3 overgrowth on the larger Q1 grains, and the euhedral Q3 quartz crystals that are intergrown with anhydrite and sulfide minerals. However, the different types of red-brown quartz show distinct variations in their Al and K concentrations.

The bright red-brow Q2 quartz identified by its irregularly-shaped brine B_{Q2} inclusions exhibits low Ti concentrations, but anomalously high Al (481 to 5179 ppm; *n = 13*) and K (113 to 1497 ppm; *n = 13*) values (Fig. 2-9; 2-12; Table 2-1). In several locations where the blue Q1 is crosscut by red-brown quartz, trace element mapping shows that only the outer portions of the zones is enriched in Al and K, suggesting that Q2 quartz forms the rim of these zones.

The red-brown euhedral Q3 quartz is characterized by generally low trace element abundances (Fig. 2-9; 2-12). The Ti and K contents of the Q3 quartz are typically below the detection limit, but can reach up to 28 ppm Ti and 308 ppm K (*n = 18*). The Q3 quartz contains Al concentrations that are significantly lower than the concentrations of this element measured in the bright red-brown Q2 quartz (Table 2-1). The Al content in red-brown Q3 quartz range from the detection limit up to 994 ppm (*n = 18*).

A second area selected for trace element mapping and spot analysis covers the red-brown zone of quartz transecting blue luminescent Q1 quartz (Fig. 2-10). Trace element mapping showed that light blue luminescent Q1 quartz has comparably high Ti (45 to 203 ppm; *n = 21*) concentrations. The Al content varies from 50 to 683 ppm (*n = 21*), while the concentrations of K are typically below detection. The quartz in the red-brown zones transecting the blue quartz shows low Ti contents (<16 to 141 ppm; *n = 17*) despite the fact that it hosts B_{Q1} and V_{Q1} inclusions (Fig. 2-7). This suggests that alteration of Q1 has resulted in a chemical modification of the quartz, but that preexisting fluid inclusions were preserved, at least locally. The alteration of Q1 must have been associated with the formation of Q2 or Q3, which is consistent with the occurrence of B_{Q2} and L_{Q3} inclusions in this zone of red-brown quartz. Quartz interpreted to be Q2 has Al concentrations ranging from 486 to 2417 ppm and K concentrations of <16 ppm to 865 ppm (*n = 8*). Quartz identified as Q3 contains 54 to 362 ppm Al and K contents <16 ppm (*n = 9*).

Trace element mapping and spot analyses were also performed across the outermost growth zones of a Q1 quartz crystal that is in immediate contact with anhydrite. The crystal is unusual in comparison to other Q1 grains as it contains a band of anhydrite inclusions that parallels the oscillatory growth zoning visible in CL (Fig. 2-11). The growth zone immediately adjacent to this band of anhydrite inclusions shows a dark red CL. Trace element mapping shows that the oscillatory growth zoning of the quartz visible under CL correlates with small variations in the abundances of Ti and Al. The light blue CL growth bands have slightly higher Ti (151 and 160 ppm; *n = 2*) and Al (166 and 173 ppm; *n = 2*) concentrations when compared to the dark blue CL growth bands (Ti of 60 to 118 ppm and Al of 47 to 138 ppm; *n = 10*). The K concentrations in the blue Q1 quartz were below detection limit. The zone of anhydrite inclusions is distinctly enriched in Al and K (2921 ppm Al and 498 ppm K; *n = 1*) while the red growth zone immediately adjacent to this zone has only slightly elevated Al concentrations (335 ppm; *n = 1*). The Ti content of this growth zone is below the detection limit. The outermost portion of the grain is characterized by narrow zones of Al and K enrichment that are wavy in character and not parallel to the crystal face (Fig. 2-11, 2-13; Table 2-1).

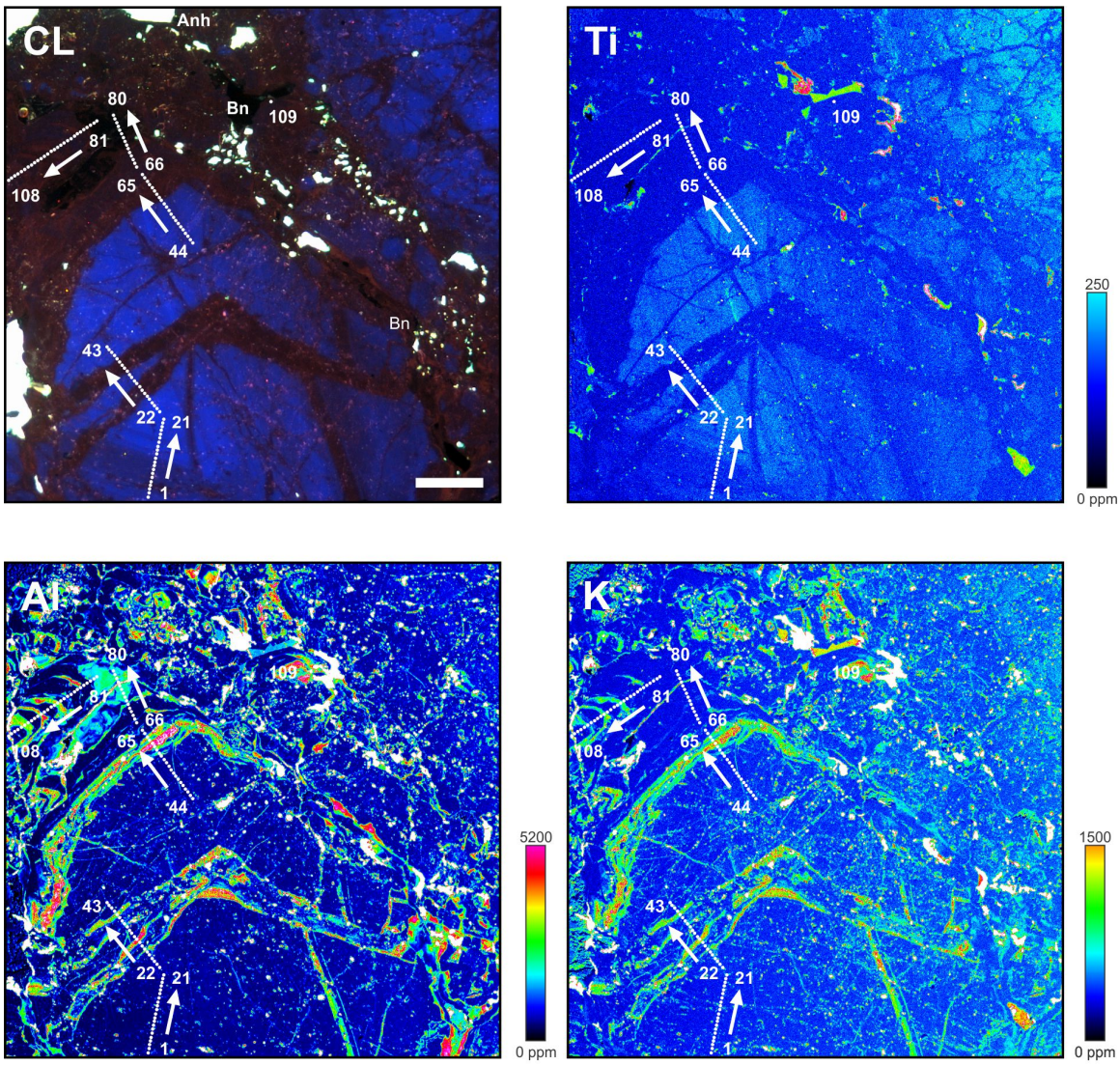

FIG. 2-9: Cathodoluminescence image and corresponding trace element maps of the central portion of the quartz vein. (A) CL image showing a large Q1 grain that exhibits oscillatory zones that are dark blue and light blue in color. The quartz grain is crosscut by a zone of quartz that shows a red-brown CL. The quartz is surrounded by red-brown quartz that is intergrown with anhydrite and sulfide minerals. (B) Electron microprobe map of Ti concentrations. The bright growth zones visible in CL correspond to zones of elevated Ti concentrations. (C) Electron microprobe map of Al concentrations. The map shows that the zone of red-brown quartz crosscutting the Q1 crystal is composed of two different types of quartz, one having low and one having high Al abundances. (D) Electron microprobe map of K concentrations. The distribution of K is generally similar to that of Al. Anh = anhydrite. Bn = bornite. Locations of microprobe spot analyses are given and keyed to Table 2-1. Scale bar is 100 μm.

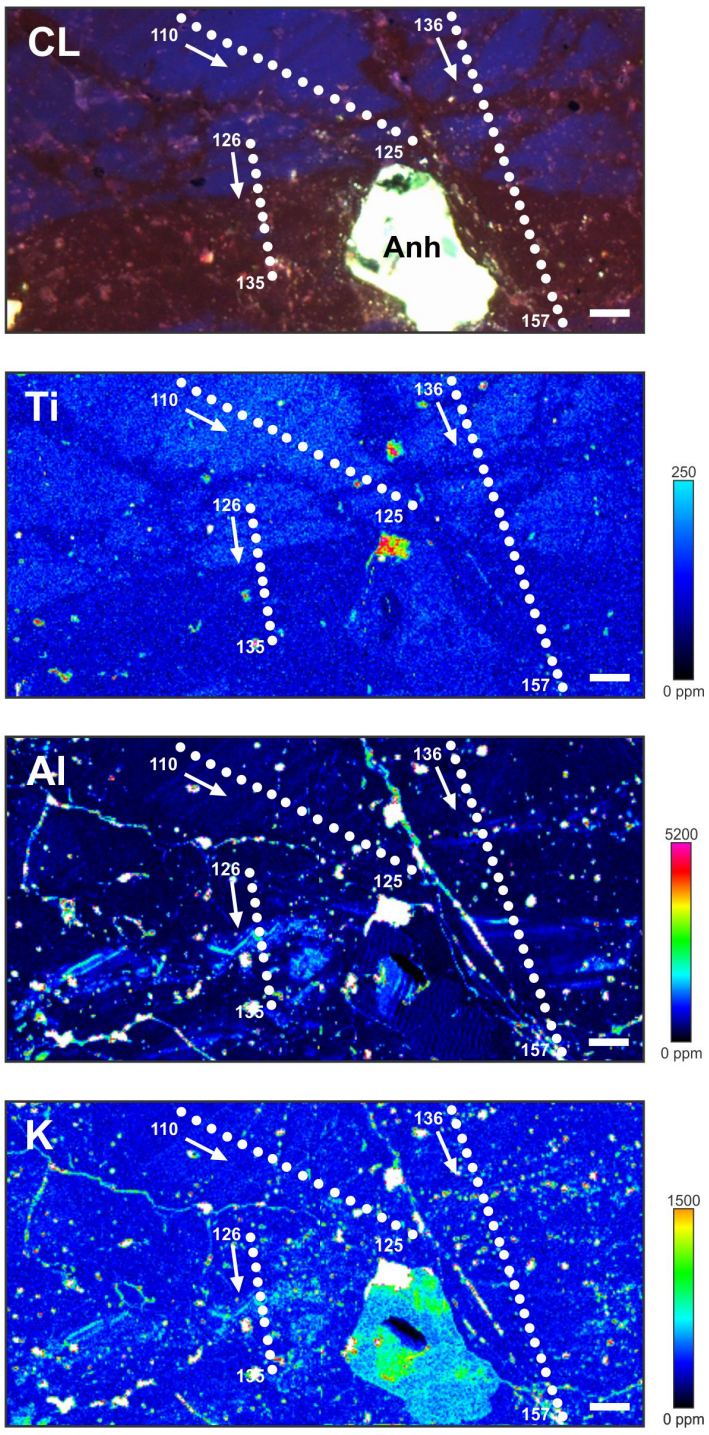

FIG. 2-10: Cathodoluminescence image and corresponding trace element maps of Q1 quartz that is crosscut by a zone of red-brown quartz. (A) CL image of Q1 quartz that is dark blue to light blue in color. The quartz is crosscut by a zone of red-brown quartz that hosts a large anhydrite crystal. (B) Electron microprobe map of Ti concentrations. The differences in composition between the blue quartz and the red-brown quartz are subtle. (C) Electron microprobe map of Al concentrations. The red-brown quartz shows a slightly elevated Al content. (D) Electron microprobe map of K concentrations. Compositional differences between the different quartz types visible in CL are insignificant. Anh = anhydrite. Locations of microprobe spot analyses are given and keyed to Table 2-1. Scale bar is 50 µm.

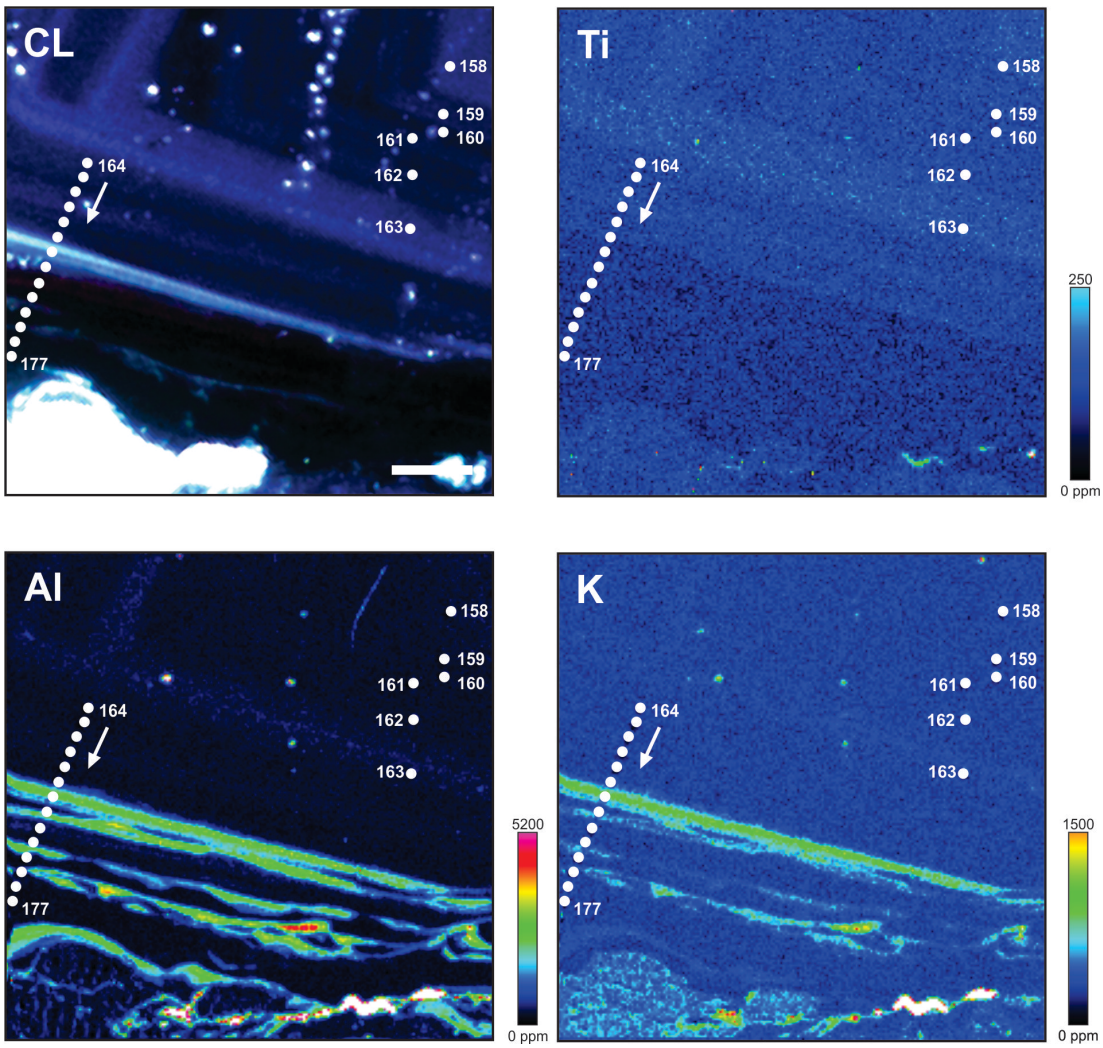

FIG. 2-11: Cathodoluminescence image and corresponding trace element maps of a Q1 grain. (A) CL image showing that the Q1 quartz exhibits well-developed oscillatory growth zones that are dark blue and light blue in color. One of the outermost growth zones contains abundant anhydrite inclusions. The growth band immediately adjacent to the zone of anhydrite inclusions shows a red-brown CL. The outermost growth bands are unusually wavy. (B) Electron microprobe map of Ti concentrations. The bright growth zones visible in CL correspond to zones of elevated Ti concentrations. (C) Electron microprobe map of Al concentrations. The central portion of the Q1 grain generally shows low abundances of Al although the Al content of the bright blue oscillatory growth zone is slightly elevated in comparison to the dark blue growth zones. The outer growth zones of the Q1 crystal show distinct enrichment in Al, especially the zone hosting the anhydrite inclusions. (D) Electron microprobe map of K concentrations. The concentrations of this element mimic the distribution of Al. Note the wavy nature of the outermost growth zones. Locations of microprobe spot analyses are given and keyed to Table 2-1. Scale bar is 50 µm.

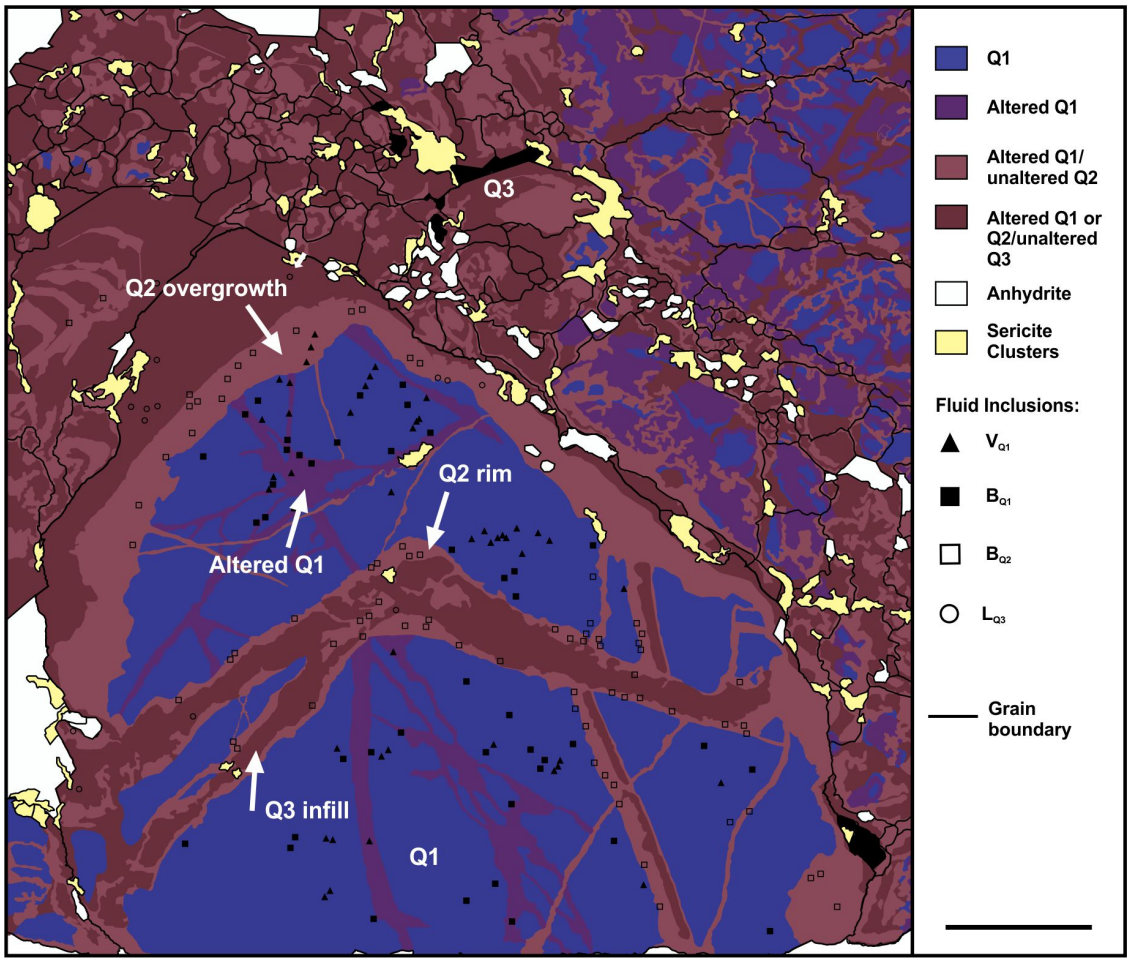

FIG. 2-12: Interpretation of textural relationship between different quartz types in a porphyry vein from Far Southeast. The area shown corresponds to Fig. 2-9. The map shows the distribution of fluid inclusions in unaltered Q1, altered Q1, unaltered/altered Q2, and Q3 quartz. The different types of quartz were identified through a combination of fluid inclusion petrography, CL microscopy, and electron microprobe mapping. Brine B_{Q1} inclusions are observed within unaltered blue Q1 and within crosscutting red-brown zones of altered Q1 quartz. Large through going red-brown fractures consist of an outer filling of Q2 quartz that contains rare B_{Q2} inclusions and an inner filling of Q3 quartz. Isolated clasts of Q2 quartz exist within the Q3 fracture filling, and are only observable using trace element mapping. Rare L_{Q3} inclusions can be found within the inner fracture filling and in the latest overgrowth of Q3 on the margins of the crystal. Scale bar is 200 μm.

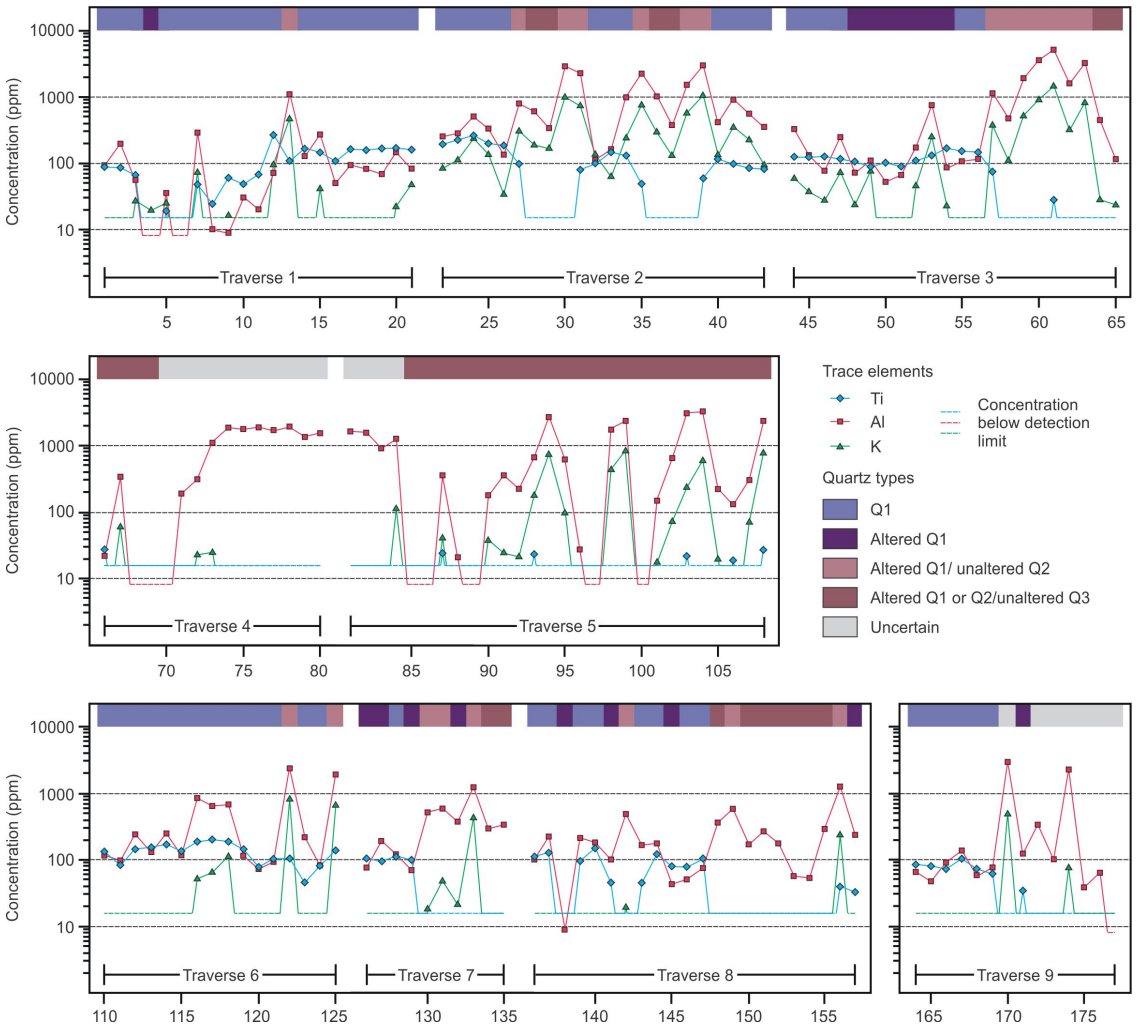

FIG. 2-13: Trace element profiles across different quartz types. The CL color of the quartz is shown. Positions of the profiles are given in Fig. 2-9, 2-10, 2-11. Spot numbers are keyed to Table 2-1.

Table 2-1: Electron microprobe spot analyses of quartz from Far Southeast. - = below detection limit. All data in ppm.

Spot	CL property	Interpretation	Ti	Al	K
Traverse 1 (Fig. 2-9)					
1	Dark blue	Q1	86	91	-
2	Dark blue	Q1	85	194	-
3	Dark blue	Q1	66	56	28
4	Dark blue-purple	Altered Q1	-	-	20
5	Dark blue	Q1	19	35	26
6	Dark blue	Q1	-	-	-
7	Dark blue	Q1	48	283	75
8	Dark blue	Q1	24	10	-
9	Dark blue	Q1	60	9	17
10	Dark blue	Q1	48	31	-
11	Dark blue	Q1	67	20	-
12	Light blue	Q1	262	73	96
13	Light blue-purple	Altered Q1 or Q2	109	1082	475
14	Light blue	Q1	163	129	-
15	Light blue	Q1	145	269	43
16	Light blue	Q1	106	50	-
17	Light blue	Q1	164	92	-
18	Light blue	Q1	158	82	-
19	Light blue	Q1	165	67	-
20	Light blue	Q1	167	140	23
21	Light blue	Q1	160	82	49
Traverse 2 (Fig. 2-9)					
22	Light blue	Q1	192	257	87
23	Light blue	Q1	225	274	116
24	Light blue	Q1	257	503	245
25	Light blue	Q1	194	328	140
26	Light blue	Q1	184	136	35
27	Red-brown	Q2	98	798	313
28	Red-brown	Q3	-	600	193
29	Red-brown	Q3	-	337	171
30	Red-brown	Q2	-	2816	1010
31	Red-brown	Q2	79	2267	757
32	Light blue	Q1	101	111	140
33	Light blue	Q1	149	161	64
34	Light blue	Q1	130	973	248
35	Red-brown	Q2	49	2191	762
36	Red-brown	Q3	-	994	308
37	Red-brown	Q3	-	370	134
38	Red-brown	Q2	-	1478	578
39	Red-brown	Q2	59	2896	1072
40	Light blue	Q1	113	410	137
41	Light blue	Q1	96	892	360
42	Light blue	Q1	83	553	233
43	Light blue	Q1	84	354	95

Table 2-1 (continued).

Spot	CL property	Interpretation	Ti	Al	K
Traverse 3 (Fig. 2-9)					
44	Light blue	Q1	124	332	61
45	Light blue	Q1	126	130	39
46	Light blue	Q1	129	78	29
47	Light blue	Q1	117	244	75
48	Light blue-purple	Altered Q1	107	73	25
49	Light blue-purple	Altered Q1	90	110	80
50	Light blue-purple	Altered Q1	102	52	-
51	Light blue-purple	Altered Q1	90	66	-
52	Light blue-purple	Altered Q1	109	174	48
53	Light blue-purple	Altered Q1	133	740	265
54	Light blue-purple	Altered Q1	170	87	24
55	Light blue	Q1	153	106	-
56	Light blue	Q1	144	118	-
57	Red-brown	Q2	75	1133	392
58	Red-brown	Q2	-	481	113
59	Red-brown	Q2	-	1917	543
60	Red-brown	Q2	-	3570	936
61	Red-brown	Q2	28	5179	1497
62	Red-brown	Q2	-	1630	336
63	Red-brown	Q2	-	3272	842
64	Red-brown	Q3	-	453	30
65	Red-brown	Q3	-	117	25
Traverse 4 (Fig. 2-9)					
66	Red-brown	Q3	28	22	-
67	Red-brown	Q3	-	342	63
68	Red-brown	Q3	-	-	-
69	Red-brown	Q3	-	-	-
70	Non-luminescent	Uncertain	-	-	-
71	Non-luminescent	Uncertain	-	191	-
72	Non-luminescent	Uncertain	-	312	24
73	Non-luminescent	Uncertain	-	1111	26
74	Non-luminescent	Uncertain	-	1876	-
75	Non-luminescent	Uncertain	-	1773	-
76	Non-luminescent	Uncertain	-	1911	-
77	Non-luminescent	Uncertain	-	1712	-
78	Non-luminescent	Uncertain	-	1932	-
79	Non-luminescent	Uncertain	-	1384	-
80	Non-luminescent	Uncertain	-	1543	-
Traverse 5 (Fig. 2-9)					
81	Non-luminescent	Uncertain	-	1652	-
82	Non-luminescent	Uncertain	-	1584	-
83	Non-luminescent	Uncertain	-	933	-
84	Red-brown	Uncertain	-	1264	118
85	Red-brown	Q3	-	-	-
86	Red-brown	Q3	-	-	-
87	Red-brown	Altered Q2	24	356	42
88	Red-brown	Q3	-	21	-

Table 2-1 (continued).

Spot	CL property	Interpretation	Ti	Al	K
89	Red-brown	Q3	-	-	-
90	Red-brown	Altered Q2	-	180	39
91	Red-brown	Altered Q2	-	355	25
92	Red-brown	Altered Q2	-	229	22
93	Red-brown	Altered Q2	23	662	185
94	Red-brown	Altered Q2	-	2723	776
95	Red-brown	Altered Q2	-	629	101
96	Red-brown	Q3	-	27	-
97	Red-brown	Q3	-	-	-
98	Red-brown	Altered Q2	-	1779	460
99	Red-brown	Altered Q2	-	2356	873
100	Red-brown	Q3	-	-	-
101	Red-brown	Altered Q2	-	153	18
102	Red-brown	Altered Q2	-	638	75
103	Red-brown	Altered Q2	22	3057	239
104	Red-brown	Altered Q2	-	3242	623
105	Red-brown	Altered Q2	-	223	20
106	Red-brown	Altered Q2	19	129	-
107	Red-brown	Altered Q2	-	305	71
108	Red-brown	Altered Q2	27	2407	808
Spot analyses (Fig. 2-9)					
109	Red-brown	Q3	21	243	-
Traverse 6 (Fig. 2-10)					
110	Dark blue	Q1	130	116	-
111	Light blue	Q1	82	97	-
112	Light blue	Q1	145	241	-
113	Light blue	Q1	154	131	-
114	Light blue	Q1	171	249	-
115	Light blue	Q1	134	118	-
116	Light/dark blue	Q1	190	843	53
117	Light blue	Q1	203	643	68
118	Light blue	Q1	188	683	121
119	Light blue	Q1	144	117	-
120	Light blue	Q1	79	74	-
121	Light blue	Q1	103	94	-
122	Red-brown	Q2	105	2417	865
123	Light blue	Q1	46	221	-
124	Light blue	Q1	82	84	-
125	Red-brown	Q2	141	1925	687
Traverse 7 (Fig. 2-10)					
126	Purple to red-brown	Altered Q1	105	77	-
127	Purple to red-brown	Altered Q1	95	191	-
128	Light blue	Q1	116	121	-
129	Purple to red-brown	Altered Q1	99	70	-
130	Red-brown	Q2	-	520	19
131	Red-brown	Q2	-	597	50
132	Light blue-purple	Altered Q1	-	378	22
133	Red-brown	Q2	-	1241	457
134	Red-brown	Q3	-	299	-
135	Red-brown	Q3	-	336	-

Table 2-1 (continued).

Spot	CL property	Interpretation	Ti	Al	K
Traverse 8 (Fig. 2-10)					
136	Light blue	Q1	112	100	-
137	Light blue	Q1	125	222	-
138	Purple to red-brown	Altered Q1	-	9	-
139	Light blue	Q1	94	210	-
140	Light blue	Q1	149	181	-
141	Purple to red-brown	Altered Q1	45	100	-
142	Red-brown	Q2	-	486	20
143	Light blue	Q1	45	165	-
144	Light blue	Q1	122	176	-
145	Light blue-purple	Altered Q1	78	42	-
146	Light blue	Q1	80	50	-
147	Light blue	Q1	104	74	-
148	Red-brown	Q3	-	362	-
149	Red-brown	Q2	-	577	-
150	Red-brown	Q3	-	169	-
151	Red-brown	Q3	-	264	-
152	Red-brown	Q3	-	174	-
153	Red-brown	Q3	-	57	-
154	Red-brown	Q3	-	54	-
155	Red-brown	Q3	-	287	-
156	Red-brown	Q2	39	1238	246
157	Light blue-purple	Altered Q1	32	236	-
Spot analyses (Fig. 2-11)					
158	Light blue	Q1	151	166	-
159	Dark blue	Q1	118	121	-
160	Dark blue	Q1	60	117	-
161	Dark blue	Q1	105	93	-
162	Dark blue	Q1	84	103	-
163	Light blue	Q1	160	173	-
Traverse 9 (Fig. 2-11)					
164	Dark blue	Q1	83	65	-
165	Dark blue	Q1	79	47	-
166	Dark blue	Q1	73	91	-
167	Dark blue	Q1	103	138	-
168	Dark blue	Q1	70	57	-
169	Dark blue	Q1	62	77	-
170	Zone with Anh	Uncertain	-	2921	498
171	Purple to red-brown	Altered Q1	34	121	-
172	Red-brown	Uncertain	-	335	-
173	Non luminescent	Uncertain	-	103	-
174	Wavy light blue	Uncertain	-	2235	79
175	Wavy light blue	Uncertain	-	39	-
176	Non luminescent	Uncertain	-	63	-
177	Non luminescent	Uncertain	-	-	-

The deviating CL characteristics, the elevated Al and K contents of the outer growth zones, and the unusual wavy nature of the zones of Al and K enrichment suggests that the outer portion of the Q1 grain has been affected by secondary processes. It is possible that the anhydrite inclusions in the Q1 are not primary and have formed through fluid infiltration and diffusion along an oscillatory growth zone of Q1.

2.5 Discussion

2.5.1 Identification of Quartz Generations

The investigated sample of a vitreous quartz vein from the Far Southeast porphyry consists of at least three generations of quartz, defined on the basis of optical microscopy, fluid inclusion petrography, CL microscopy, and electron microprobe analysis (Fig. 2-14). Confident identification of the characteristics of the three quartz generations was only possible after careful study of the thin sections and selection of areas where textural relationships are simple and easy to interpret.

The earliest generation Q1 encompasses the large anhedral quartz crystals containing equant-shaped B_{Q1} inclusions and coexisting vapor inclusions, referred to as V_{Q1}. The quartz is typified by a long-lived bright blue CL emission and commonly exhibits well-defined oscillatory growth zoning under electron bombardment. The Q1 quartz is generally typified by high Ti concentrations (>50 ppm) and low Al (<500 ppm) and K (<200 ppm) contents. The Ti and Al concentrations can vary between adjacent oscillatory growth zones defined by CL microscopy.

The second quartz generation Q2 forms quartz overgrowth on preexisting Q1 quartz or infills fractures transecting the anhedral Q1 grains. Q2 is less abundant in thin section than the earlier Q1. The Q2 quartz is characterized by irregular-shaped brine B_{Q2} fluid inclusions. Under electron bombardment, the quartz shows a red-brown CL. Q2 grains contain high concentrations of Al (>500 ppm). The quartz is also typified by high concentrations of K (typically >200 ppm). Although the quartz structure can accommodate elevated Al and K concentrations (cf. Götze et al., 2004), it is likely that the high

concentrations of these elements in Q2 quartz are related to the abundant occurrence of submicroscopic inclusions in the quartz. This highlights that Q2 quartz formed under physicochemical conditions that differed from those during Q1 and Q3 formation.

The third quartz generation Q3 comprises small euhedral quartz crystals that have grown into open space. These crystals are fairly rare in thin section. In addition to these easily identifiable quartz crystals, Q3 quartz may also occur throughout the vein along fractures transecting earlier formed quartz. However, confident distinction between altered preexisting quartz and newly formed Q3 is not always possible. The euhedral Q3 quartz contains liquid L_{Q3} inclusions previously measured by Hedenquist et al. (1998), yielding salinities of ≤3 wt.% NaCl equiv. The euhedral quartz crystals are characterized by a long-lived red-brown CL. In some locations, the quartz is non-luminescent. Q3 quartz contains low concentrations of all elements measured, except for Al (up to 1000 ppm).

2.5.2 Hydrothermal Alteration of Quartz

Inspection of the quartz vein shows that the textural relationships between the three different quartz generations are often complex. Due to overprinting and alteration of preexisting quartz during the formation of each new quartz generation, a considerable proportion of the quartz vein is composed of altered quartz that has characteristics transitional between those described above.

The most obvious result of quartz alteration is the widespread modification and quenching of the bright blue CL of the early Q1 quartz. Modification and quenching of the original CL color occurs, for instance, along grain boundaries between adjacent Q1 grains. Similar changes can be observed along narrow bands that cross-cut Q1 grains. An entire progression of changes in CL intensity and color is observed in detail, ranging from the occurrence of dark purple luminescence along growth zones and within small Q1 fragments to the development of distinctly red-brown emission in crystals cut by abundant microfractures or subgrain boundaries. Areas of Q1 quartz showing modifica-

tion of the original CL emission typically contain small islands of blue CL that decrease in abundance and size with increasing alteration intensity.

Trace element analysis and mapping shows that these areas of modified CL appearance in Q1 grains are commonly depleted in Ti when compared to the neighboring least-altered blue luminescent Q1 quartz. The observed compositional changes suggest that changes of the CL signal are accompanied by structural rearrangement of the quartz. A reduction in the Ti content in the altered quartz requires changes in the tetrahedral sites of the quartz structure as Ti is incorporated into the crystal structure of quartz through substitution for Si (cf. Götze et al., 2001, 2004).

Evidence that the areas of red-brown CL within the blue luminescent Q1 grains indeed represent altered Q1 and not simply newly precipitated Q2 or Q3 is provided by the highly irregular contacts between the blue luminescent Q1 quartz and altered Q1 quartz showing a red-brown CL. Moreover, quartz showing a red-brown CL commonly contains clearly identifiable equant-shaped B_{Q1} and V_{Q1} inclusions, implying that fluid inclusions originally present in the Q1 quartz are inherited to its altered equivalent. Thus, alteration of the Q1 quartz during the hydrothermal event forming Q2 or Q3 resulted in changes in the CL properties and trace element abundances of the Q1 quartz, but did not necessarily modify the petrographic appearance of fluid inclusions.

Comparison between images taken in crossed-polarized light and under electron bombardment suggests that the degree of structural rearrangement can vary substantially. In some cases, areas of altered Q1 show the same extinction behavior as the adjacent apparently least-altered quartz that shows a blue luminescence. However, closer to the vein centre and in areas of increased abundance of anhydrite and sulfide minerals, the early Q1 quartz must have been affected by an increasing amount of structural rearrangement as evidenced by the formation of subgrains. Wholesale recrystallization appears to have occurred were the vein consists only of 30 to 50 µm large Q1 grains that are equant in shape and have undulose extinction.

The case study at Far Southeast illustrates that quartz does not represent a stable phase resistant to processes of secondary alteration and that the assumption that the CL properties and trace element content of quartz are related to the primary growth of quartz is not necessarily correct in environments of high fluid flux such at the porphyry veins. This finding is in agreement with a number of recent studies summarized by Kempe et al. (2012), documenting that similar processes of quartz alteration occur in other hydrothermal deposit types. As pointed out by Kempe et al. (2012), the susceptibility of quartz to undergo significant structural changes in response to secondary hydrothermal alteration may be related to the fact that water molecules are able to hydrolyze Si-O bonds in quartz at elevated temperatures and pressures. This can enhance diffusion of chemical compounds through the quartz structure and cause hydrolytic weakening of the quartz (Griggs and Blacic, 1965). It appears possible that the progression of alteration effects from incipient alteration causing changes of the CL behavior and trace element content through the development of subgrains to the formation of mosaic quartz consisting of small recrystallized grains with equant shapes is an indirect reflection of the degree of fluid-mineral interaction.

2.5.3 Use of CL Microscopy in Fluid Inclusion Studies

The observations of the present study have significant implications for the use of CL microscopy in fluid inclusion studies. The widely held assumption that quartz generations can be distinguished based solely on their CL emission is not always valid. In the case of the quartz vein from Far Southeast, CL microscopy allowed rapid identification of unaltered Q1 quartz that shows a long-lived blue CL. However, all other types of quartz were found to have a similar CL response. The hydrothermal alteration of Q1 quartz resulted in a quenching of the blue CL color of this quartz. Intensely altered Q1 quartz shows a red-brown CL color that is indistinguishable from the CL responses of pristine or altered Q2, and newly formed Q3.

Due to the occurrence of CL quenching of quartz within reopened porphyry veins, CL microscopy alone cannot be used to map out the distribution of the different types of

quartz on the thin section scale. As demonstrated in the present study, CL quenching can be recognized by combining CL microscopy with other techniques such as careful petrography, fluid inclusion microscopy, and electron microprobe mapping. The study at Far Southeast demonstrates that quartz affected by CL quenching can still contain its original fluid inclusion inventory. Petrographically unmodified fluid inclusions can even be hosted in quartz that has been affected by changes in its composition as constrained by electron microprobe analysis. The inheritance of fluid inclusions could not be recognized without careful fluid inclusion petrography.

In the light of these results, it is also important to note that paragenetic relationships in which fluid inclusion data are interpreted require careful scrutiny. In the case of Far Southeast, the intermediate Q2 quartz generation was not recognized by Hedenquist et al. (1998) despite careful thin section and fluid inclusion petrography. Only the combination of CL microscopy and trace element mapping carried out as part of the present study led to recognition that the brine B_{Q2} inclusions occur in texturally distinct zones that are interpreted to be altered Q1 or newly formed Q2. Without application of these advanced analytical techniques, it would not have been apparent that the difference in shape between the brine B_{Q1} and B_{Q2} inclusions records a change in the physicochemical environment of quartz formation, which is related to the progressive evolution of the hydrothermal system.

At the same time, CL microscopy showed that the ore minerals in the porphyry veins are texturally closely associated with quartz showing a red-brown CL signal. The results of the present study reveal that this quartz represents altered Q1 or pristine or altered Q2, or newly formed Q3. Euhedral grains of Q3 quartz, which show a clear textural relationship to the ore minerals, are generally rare and mostly devoid of fluid inclusions. As a consequence, incorrect interpretation of the CL observations coupled with the above described occurrence of inherited fluid inclusions could have easily lead to the incorrect conclusion that the B_{Q1} and B_{Q2} inclusions abundantly present in the red-brown quartz represent the ore-forming hydrothermal fluids.

2.5.4 Reconstruction of the Fluid Evolution

The fluid inclusion inventory, CL characteristics, and trace element signatures of the three quartz types recognized in the vein quartz from Far Southeast can be used to reconstruct the progressive evolution of the hydrothermal system at the sampling location through different stages of deposit genesis (Fig. 2-14). The model proposed here represents a refinement of that of Hedenquist et al. (1998).

The textural evidence demonstrates that Q1 quartz crystallized early in the paragenesis and records the first stage of vein mineral precipitation. Fluid inclusions entrapped in Q1 quartz are dominantly brine B_{Q1} liquid inclusions. Although these inclusions are not strictly primary as alignment of these inclusions along growth zones in Q1 is rare, formation of the B_{Q1} inclusions is closely related to Q1 formation. Microthermometric data obtained on B_{Q1} coexisting with V_{Q1} inclusion indicates that the inclusions were entrapped from a high-temperature hypersaline liquid at maximum temperatures of 450 to 550°C. As the microthermometric data were obtained on fluid inclusion assemblages entrapped during phase separation, the inclusion data provides the most reliable constraint on the temperature of quartz formation.

Formation of Q1 quartz at high temperatures is consistent with the distinct enrichment of Ti in the Q1 quartz. Unfortunately, Ti geothermometry using the calibration of Wark and Watson (2006) cannot be applied in the present case as the vein quartz formed under open system conditions. Although the Q1 quartz formed under lithostatic conditions, the well-developed oscillatory growth zoning within the Q1 grains possibly suggests that the quartz precipitated rapidly into open-space. This open-space may have been produced by hydrofracturing and was probably transient in nature (cf. Weis et al., 2012). The hypersaline liquid forming Q1 quartz was K-feldspar and biotite stable as evidenced by the potassic alteration surrounding the quartz vein.

The hypersaline liquid entrapped as B_{Q1} inclusions could have formed as a product of phase separation of from a magmatic fluid exsolved from a parent magma at depth at

near-magmatic conditions (Hedenquist et al., 1998). The coexistence of B_{Q1} and V_{Q1} inclusions in the sample provides unequivocal evidence for phase separation. Assuming that the exsolved magmatic fluid had a salinity of 5 to 7 wt.% NaCl, as observed in other porphyry deposits (Redmond et al., 2004; Landtwing et al., 2005, 2010; Klemm et al., 2008; Rusk et al., 2008a; Pudack et al., 2009), formation of the hypersaline liquid having a salinity of 50-55 wt % NaCl must have occurred through condensation. At a temperature of 550°C, condensation of a hypersaline liquid with such a salinity occurs at a pressure of about 490 to 540 bars in the H_2O-NaCl system. The corresponding vapor produced would have a salinity of 0.3 to 0.5 wt% NaCl (Driesner and Heinrich, 2007). Mass balance constraints imply that a small amount of hypersaline liquid and a large volume of co-existing low-salinity vapor were generated (9 to 13% hypersaline liquid and 87 to 91% low-salinity vapor). As the pressure regime was presumably lithostatic, phase separation of the magmatic fluid would have occurred under an overburden of about 1850 to 2040 m. These estimated conditions appear to be realistic as the quartz sample investigated was collected at a depth of 1370 m below present surface.

Condensation of a hypersaline liquid would have produced a large amount of low-salinity vapor. The vapor produced would have been highly buoyant, whereas the hypersaline liquid would have stayed at depth (Hedenquist et al., 1998). As a consequence, the vapor would have ascended rapidly into the near-surface environment. Condensation of the vapor into ambient groundwater would have produced a highly acidic liquid, causing advanced argillic alteration and the formation of an extensive zone of vuggy quartz (Fig. 2-14, 2-15). The results of K/Ar dating confirm that the acid-type alteration at shallow depth, produced by the vapor, overlaps in age with the potassic alteration at depth, which is caused by the corresponding hypersaline liquid (Arribas et al., 1995; Hedenquist et al., 1998).

The second quartz generation recognized in the vein sample from Far Southeast also formed from a hypersaline liquid. Although microthermometric data could not be obtained on entire fluid inclusion assemblages, the shape of the inclusions confirms that Q2 formed at lower temperatures than Q1. The B_{Q2} inclusions were not observed to be

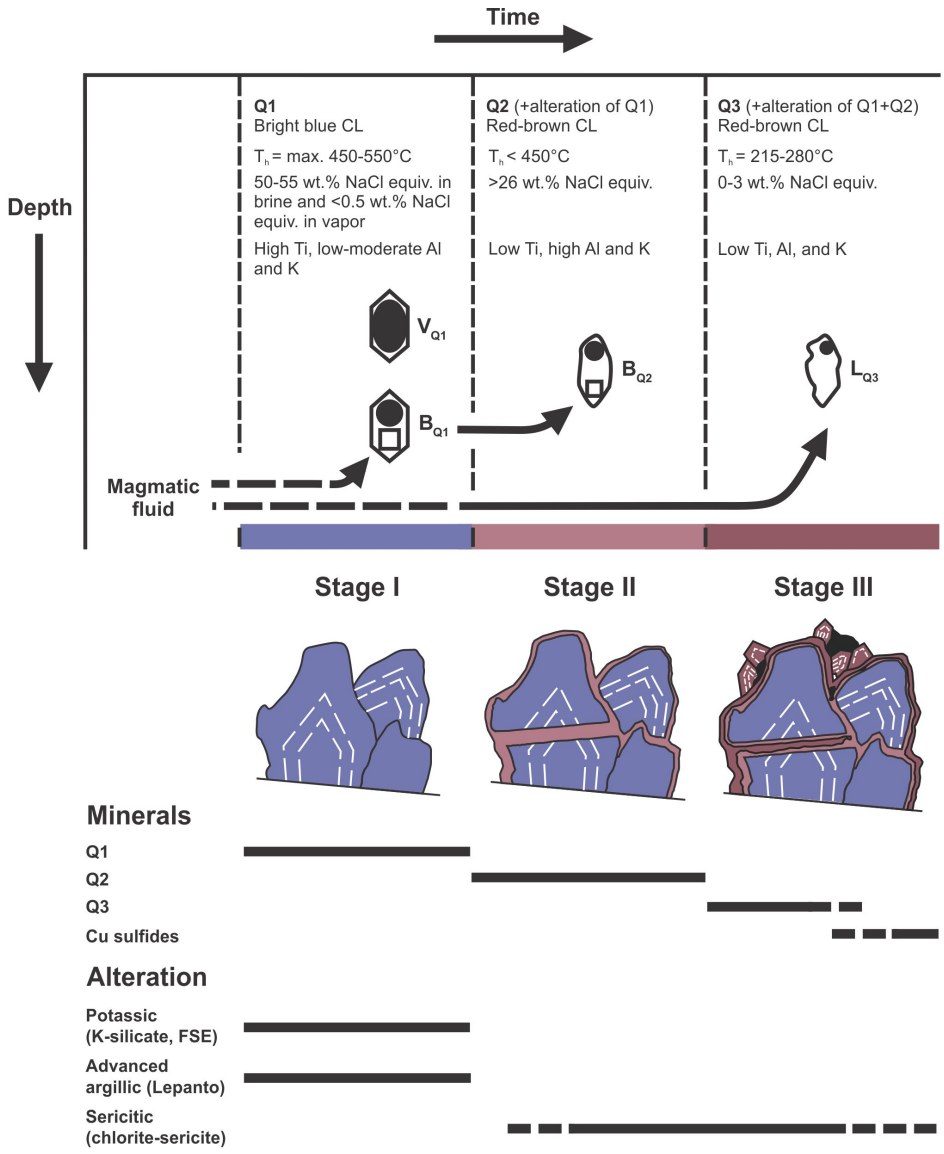

FIG. 2-14: Relationships between the formation of different quartz generations in the porphyry environment and inferred fluid evolution at Far Southeast. Stage I: Precipitation of Q1 quartz from a hypersaline liquid (50-55wt% NaCl equiv.) and a coexisting low-salinity vapor. Quartz precipitation took place at lithostatic pressure conditions and maximum temperatures of 450 to 550°C. The hypersaline liquid and the vapor are responsible for potassic alteration in the deep porphyry system and advanced argillic alteration in the associated epithermal environment, respectively. Stage II: Precipitation of Q2 was associated with the dilution and cooling of the hypersaline liquid. The formation of Q2 quartz possibly overlapped with the initiation of chlorite-sericite alteration, as suggested by the high Al and K contents of Q2 quartz. Stage III: Precipitation of Q3 occurs late in the paragenesis from a low-salinity liquid (0-3 wt.% NaCl). Formation of this quartz took place at temperatures <350°C. The low-temperature liquid forming Q3 quartz resulted in the pervasive sericitic alteration at Far Southeast. The precipitation of sulfide minerals such as chalcopyrite and bornite likely occurred from this hydrothermal liquid upon further cooling. The same liquid is interpreted to have formed the ores of the Lepanto epithermal deposit. The liquid is interpreted to have originated from isochemical contraction of a deep single-phase fluid of magmatic origin.

associated with vapor inclusions, implying that the measured homogenization temperature of 295°C represents a minimum temperature. Q2 formed largely through fracturing and reopening of the preexisting Q1 quartz veins. Despite this overprinting relationship, the formation of Q2 is envisaged here to have occurred essentially from the same fluid that precipitated Q1, following its evolution towards lower temperatures (Fig. 2-15).

Although the existence of Q2 as a discrete quartz generation has not been previously documented at Far Southeast (cf. Hedenquist et al., 1998), inclusions with similar petrographic and homogenization behavior have been previously reported to occur at the Santa Rita porphyry in New Mexico. At this location, brine inclusions which homogenize to the liquid by halite dissolution have homogenization temperatures ranging from 260° to 520°C with salinities between 35 and 55 wt.% NaCl equiv. (Reynolds and Beane, 1985). The findings at Far Southeast suggest that these inclusions may be the hallmark of a separate period of quartz precipitation and alteration not recognized as such in other deposits. The evidence suggests that formation of these inclusions may have occurred during or immediately after the transition from lithostatic to hydrostatic conditions, allowing a hypersaline liquid to cool without a coexisting vapor phase being present (this is implied by homogenization of the fluid inclusions through halite dissolution).

The hydrothermal system underwent significant changes following the formation of the Q2 quartz. The third quartz generation Q3 recognized formed from a lower temperature hydrothermal liquid that also had a distinctly lower salinity (Fig. 2-14, 2-15). Rare primary L_{Q3} inclusions in the quartz sample investigated here and by Hedenquist et al. (1998) homogenize at less than 280°C and have salinities of ≤3 wt % NaCl equiv. Evidence for phase separation is restricted to one secondary trail of L_{Q3} inclusions in the sample investigated. However, Q3 quartz in samples collected from the center of the deposit contain L_{Q3} inclusions that occasionally coexist with V_{Q3} inclusions (Hedenquist et al., 1998), indicating that the hydrothermal liquid was boiling in the central upflow zone of the system at the time of precipitation of Q3. This would only be possible if hydrostatic conditions prevailed during the formation of the third quartz generation. The estab-

lishment of open fluid pathways is consistent with the observation that Q3 commonly forms euhedral quartz crystals infilling open space in the veins and wall rocks.

Based on the observed homogenization temperatures, the Q3 quartz formed under chlorite-sericite stable conditions during development of the chlorite-sericite alteration halo. In fact, Q3 grains sometimes enclose sericite inclusions. In addition, the veins containing Q3 quartz are surrounded by a chlorite-sericite alteration halo, with the chlorite-sericite alteration overprinting the earlier potassic alteration of the wall rocks. K/Ar dating of hydrothermal biotite and illite suggests that the shift from K-feldspar and biotite-stable alteration associated with the formation of Q1 and possibly Q2 to chlorite-sericite-stable conditions associated with the precipitation of Q3 took place in a very short time interval, probably ≤100 ka (Arribas et al., 1995; Shinohara and Hedenquist, 1997; Hedenquist et al., 1998).

The Q3 quartz formed by reopening of the previously existing quartz vein consisting of Q1 and Q2. In contrast to the earlier period of fracturing associated with the deposition of Q2, the formation of euhedral Q3 grains immediately followed, or was accompanied by, extensive alteration of the preexisting quartz. This is presumably related to the fact that the fluid flux associated with Q3 formation was more substantial and sustained than during Q2 quartz deposition.

Textural relationships between the sulfide minerals and euhedral Q3 grains demonstrate beyond any doubt that sulfide precipitation at Far Southeast occurred during, or more likely, after the growth of this third and last quartz generation. Although sulfide mineral precipitation was not accompanied by the formation of secondary fluid inclusions in the euhedral Q3 grains that could be investigated, sulfide deposition must have occurred from a fluid that was akin to that precipitating Q3 quartz. The Cu sulfide minerals at Far Southeast, therefore, precipitated under chlorite-sericite stable conditions.

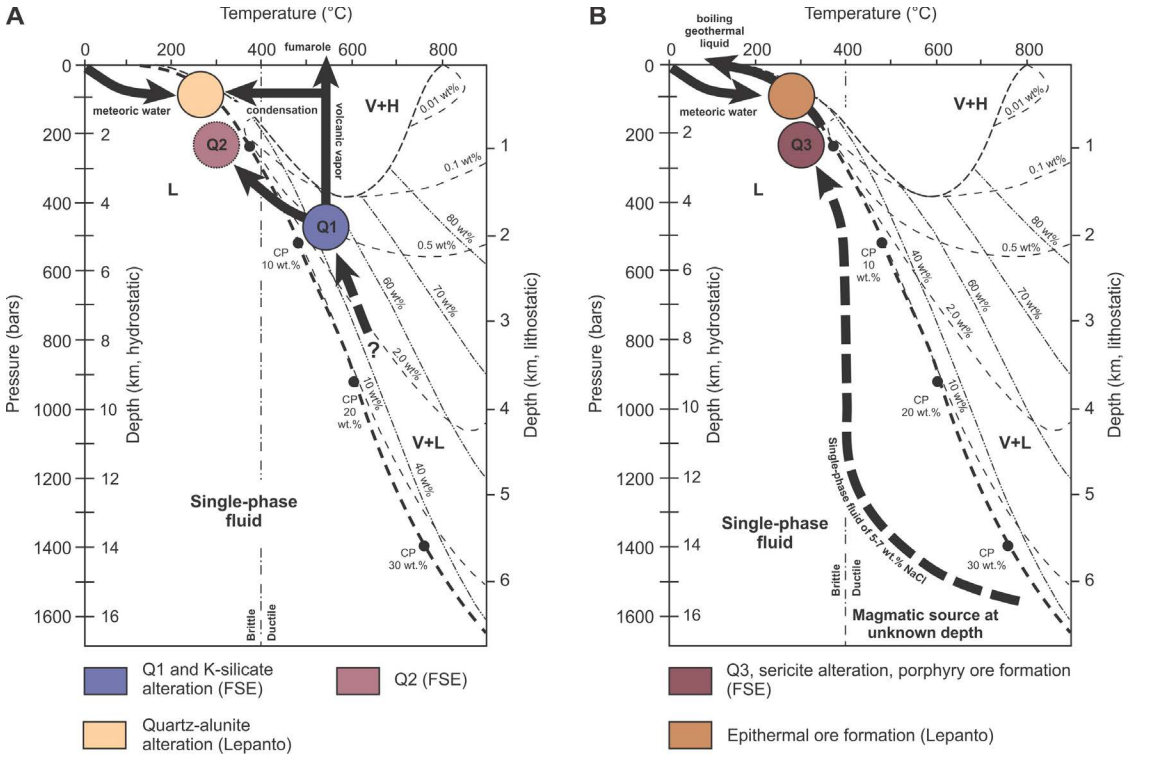

FIG. 2-15: P-T diagrams showing phase relations for the system H_2O-NaCl and the inferred evolution of the hydrothermal fluids. (A) Formation of Q1 quartz occurred in the two-phase field of the H2O-NaCl system where a hypersaline liquid coexisted with a low-salinity vapor phase. Quartz formation was accompanied by potassic alteration in Far Southeast. The later Q2 quartz formed during cooling of the hypersaline liquid in the single-phase field. The vapor produced was buoyant and ascended into the epithermal environment. Condensation of the vapor into groundwater resulted in the acidic alteration at Lepanto. (B) The hydrothermal fluids during the mineralization stage were presumably derived from a magmatic source at greater depth and evolved within the single-phase field. During cooling, the fluid contracts and becomes a liquid. This liquid forms the Q3 quartz and the associated chlorite-sericite alteration at Far Southeast. In the epithermal environment, the liquid deposited the enargite of the Lepanto deposit. Evolution from the porphyry to the epithermal environment involved cooling and dilution by groundwater. Inferred fluid evolution is based on p-T-X_{NaCl} data from fluid inclusion microthermometry from Hedenquist et al. (1998) and this study. Arrows represent the interpreted migration of fluids through space and time required to produce the observed fluid inclusion properties. Depths are based on a 1 g/cm^3 hydrostatic load and a 2.5 g/cm^3 lithostatic load. Isopleths of NaCl in the liquid and in the vapor are shown in the liquid plus vapor field by the dashed-double-dot lines and the dashed lines, respectively. The vertical dot-dash line shows the approximate location of the brittle-ductile boundary at a strain rate of 10^{-14} s^{-1}. CP = critical point, H = halite, L = liquid, and V= vapor. Diagram adapted from Muntean and Einaudi (2001).

Measurement of L_{Q3} inclusions in euhedral Q3 grains showed that the salinity of these inclusions varies from about 1 to 7 wt.% NaCl equiv. (Hedenquist et al. (1998). Based on isotopic investigations, Hedenquist et al. (1998) showed that this liquid is also of magmatic origin. In fact, such a liquid could have originated from a magmatic fluid if this fluid would ascend through the porphyritic stock without intersecting its solvus. If the fluid evolution would take place entirely within the single-phase field of the H_2O-NaCl system, the a single-phase magmatic fluid could isochemically contract into a liquid during cooling to temperatures below the critical temperature of pure water (see Heinrich, 2007, for discussion on this process).

According to Hedenquist et al. (1998), the hydrothermal liquid produced this way deposited the ore minerals within the porphyry environment due to the temperature-dependent solubility of sulfide minerals. During further ascent in the epithermal environment, this liquid cooled and started to mix with ambient meteoric water, causing a decrease in temperature and salinity with increased transport distance (Mancano and Campbell, 1995). Sulfide precipitation from this hydrothermal liquid ascending into the epithermal environment is interpreted to have resulted in the formation of the Lepanto ore body that was emplaced into volcanic rocks that underwent previous acid-type alteration.

2.5.5 Comparison to other Porphyry Deposits

Recent studies on Grasberg, Indonesia (Penniston-Dorland, 2001; Rusk et al., 2008b); Butte, Montana (Rusk and Reed, 2002; Rusk et al., 2006); Bingham Canyon, Utah (Redmond et al., 2004; Landtwing et al., 2005, 2010; Redmond and Einaudi, 2010); El Teniente, Chile (Klemm et al., 2007); Questa, New Mexico (Klemm et al., 2008); Nevados de Famatina, Argentina (Pudack et al., 2009); Oyu Tolgoi and Zesen Uul, southern Mongolia (Müller et al., 2010); and the Pebble deposit, Alaska (Marsh, 2012) have shown that the textural relationships observed in quartz veins at Far Southeast may be an ubiquitous feature of this deposit type. In all of these cases, porphyry veins were interpreted to consist of two or more quartz generations that formed at distinctly different times during the evolution of the magmatic-hydrothermal system.

Early quartz associated with the formation of potassic alteration in these deposits has been reported to have characteristics that are generally comparable to those of Q1 quartz at Far Southeast. For instance, at Grasberg, Indonesia, quartz veins contain a significant proportion of early quartz grains that show distinct oscillatory growth zoning and appear to have grown inwards towards the vein center (Penniston-Dorland (2001). Rusk and Reed (2002) as well as Rusk et al. (2006) reported the occurrence of similar bright luminescent quartz in stockwork veins from Butte, Montana using the CL signal of a scanning electron microscope. This quartz formed at temperatures of approximately 550°C (Rusk and Reed, 2002) and was found to be enriched in Ti, with variation in CL intensity between oscillatory growth zones correlating with variations in the Ti content (Rusk et al., 2006). At Bingham Canyon, Utah, early anhedral and moderate- to bright luminescent quartz has homogenization temperatures ranging up to 560°C and salinities between 38 and 50 wt. % NaCl equiv. (Redmond et al., 2004). The quartz has oscillatory growth zoning and Ti contents ranging from 65 to 240 ppm (Landtwing and Pettke, 2005; Landtwing et al., 2005). Similarly high Ti contents also occur in early oscillatory zoned quartz from Oyu Tolgoi and Zesen Uul, southern Mongolia (Müller et al., 2010).

In analogy to Far Southeast, dull luminescent quartz is also intergrown with hypogene sulfide minerals at the other well-studied porphyry deposits mentioned above (Penniston-Dorland, 2001; Rusk and Reed, 2002; Redmond et al., 2004; Landtwing et al., 2005, 2010; Rusk et al., 2006; Pudack et al., 2009; Müller et al., 2010; Redmond and Einaudi, 2010; Marsh, 2012). Particularly notable is the study by Penniston-Dorland (2001) that described the occurrence of quartz with dark CL in contact with sulfide grains from the Grasberg porphyry Cu-Au deposit, Indonesia. This quartz was found to contain anomalous Fe contents (up to 4900 ppm) that were interpreted to be the result of the diffusion of Fe into the quartz after precipitation of the quartz. At Bingham Canyon, quartz intergrown with sulfide minerals contains brine inclusions (38 - 45 wt% NaCl equiv.) that homogenize at temperatures between 330 and 380°C (Redmond et al., 2004). This quartz is typified by low Ti concentrations and generally low Al and K contents (Landtwing et al., 2005), resembling those of Q3 of the present study.

Previous authors have highlighted the importance of dissolution processes occurring after the deposition of the early quartz associated with potassic alteration and prior to the formation of the late quartz that is intergrown with sulfide minerals (Rusk and Reed, 2002; Landtwing et al., 2010). In the case of Bingham Canyon, it has been proposed that these dissolution processes were important in providing secondary pore space that could subsequently be infilled by the ore minerals (Landtwing et al., 2010). The results of the present study show that hydrothermal alteration and structural rearrangement of quartz is a much more important process associated with the reopening and dilation of the veins at Far Southeast. In contrast to Bingham Canyon, there is no clear textural evidence for the dissolution of earlier vein quartz and subsequent quartz precipitation from the same fluid during continued cooling (Fig. 2-5).

2.6 Conclusions

The present study on the Far Southeast deposit provides critical new constraints on the processes of quartz vein formation and the relative timing of ore deposition in the porphyry environment. It is demonstrated that porphyry veins are composite structures that formed during multiple discrete stages of quartz precipitation and alteration over the lifetime of the evolving magmatic-hydrothermal system. Early quartz was found to be linked to the development of potassic alteration of the porphyry whereas texturally late quartz is associated with chlorite-sericite alteration around the veins. The textural relationships suggest that hypogene sulfide mineralization occurred in close association with the formation of this late quartz generation, implying that sulfide deposition at Far Southeast took place under chlorite-sericite stable conditions.

The detailed investigations at Far Southeast suggest that hydrothermal alteration of quartz may be a phenomenon that is more important than previously recognized. Repeated reopening of the veins during the evolution of the hydrothermal system has resulted in complex overprinting relationships. Hydrothermal alteration of quartz can involve various changes, ranging from the modification and quenching of the CL to changes in its trace element abundances. In areas that have not undergone wholesale recrystallization

during alteration, the fluid inclusion inventory of the original quartz may be preserved. The complex alteration patterns observed in the present study are not apparent on the hand specimen scale and even difficult to identify in thin section without the use of complementary analytical techniques. In the light of these findings, it cannot be expected that correct interpretation of paragenetic relationships in porphyry deposits is possible using macroscopic observations only.

CHAPTER 3

CATHODOLUMINESCENCE AND FLUID INCLUSION CHARACTERISTICS OF PORPHYRY VEIN QUARTZ: A COMPARISON OF WORLD-CLASS DEPOSITS

3.1 Introduction

Porphyry deposits represent one of the world's premier metal resources, providing most of the copper and molybdenum, as well as s substantial part of the global gold and silver production (Seedorff et al., 2005). The deposits form from hydrothermal fluids of magmatic origin that precipitate metals within well-defined ore zones characterized by a dense stockwork of quartz veins (Lowell and Guilbert, 1970; Gustafson and Hunt, 1975; Titley and Beane, 1981; Seedorff et al., 2005).

Over the past decades, a large number of fluid inclusion studies have been conducted on quartz veins from porphyry deposits. These studies showed that the magmatic-hydrothermal fluids in the porphyry environment evolve through time and space due to progressive changes in the pressure and temperature conditions during deposit formation. As the phase behavior of hydrothermal fluids is pressure and temperature dependent (Driesner and Heinrich, 2007), significant variations in the character of the hydrothermal fluids can be observed. The fluid salinity in porphyry deposits generally varies from <1 to 70 wt.% NaCl equiv., with fluid densities ranging from <0.1 to >1.3 g/cm^3. Quartz vein formation occurs at temperatures between 200 and 800°C and pressure conditions that vary from lithostatic to vaporstatic at depths between <1 and 10 km from surface (Reynolds and Beane, 1985; Bodnar, 1995; Redmond et al., 2004; Landtwing et al., 2010; Rusk et al., 2008a; Klemm et al., 2007, 2008; Pudack et al., 2009).

Significant advances in the understanding of the evolution of the magmatic-hydrothermal fluids in the porphyry environment have been made recently through the integration of fluid inclusion petrography and microthermometry with CL microscopy

(Rusk and Reed, 2002; Redmond et al., 2004; Landtwing and Pettke, 2005; Landtwing et al., 2005, 2010; Rusk et al., 2006, 2008a; Klemm et al., 2007, 2008; Pudack et al., 2009; Müller et al., 2010; Redmond and Einaudi, 2010; Marsh, 2012). The use of CL microscopy allows the identification of complex textural relationships in porphyry veins that cannot be visualized by any other technique and enables a more rigorous interpretation of the textural setting of fluid inclusions.

The present chapter reports on the findings of CL investigations conducted on porphyry vein quartz from several porphyry deposits that have been the focus of previous fluid inclusion studies. Particular emphasis is placed on the examination of the CL characteristics of the vein quartz to test whether similar CL patterns can be observed in the different deposits and to what extent CL and fluid inclusion characteristics can be correlated. Based on the findings at Butte in Montana (Rusk, 2003; Rusk et al., 2004, 2008a; Reed et al., 2013); Bingham Canyon in Utah (Redmond, 2002; Redmond et al., 2004; Landtwing et al., 2005, 2010; Redmond and Einaudi, 2010); and deposits in the Maricunga belt of Chile (Muntean and Einaudi, 2000, 2001), a refined model of porphyry deposit formation is proposed that links the formation of distinctly different generations of quartz to the temperature and pressure evolution of the magmatic-hydrothermal systems through time. The study highlights the role of the depth of the host intrusion.

3.2 Materials and Methods

The present study is based on selected archival samples that have been previously studied for their fluid inclusion inventories. Quartz vein samples from Butte in Montana were obtained from B. Rusk; P. Redmond contributed samples from Bingham Canyon in Utah; and J. Muntean provided vein samples from the Maricunga belt in Chile (Table 3-1).

Initially, optical microscopy and fluid inclusion petrography were performed on the quartz vein sample using an Olympus BX51 microscope. Images were collected with an attached Optronics Microfire A/R camera. Subsequent to the fluid inclusion

Table 3-1: Porphyry quartz vein samples investigated in the present study.

Sample	Description
Butte, Montana	
11135-3872	Quartz-molybdenite vein
11052-6383	Gray sericite vein
Bingham Canyon, Utah	
5090-1700B	Sheeted A2 vein
5090-1510	A3-A4 vein with an overprint of A5 quartz
5090-1528	A3-A4 vein with an overprint of A5 quartz
211-211.5	A3 vein with a crosscutting A4 vein
Maricunga belt, Chile	
ALC-1 292.8 m	A veins from Cerro Casale
RP054	Banded vein from Pancho
DD26 36-38 m	Banded vein from Verde
RV027	Banded vein from Verde
CAV-1 110.1 m	Hybrid A-banded veins with crosscutting D veins from Cavancha
CAV-2 203 m	Hybrid A-banded veins with crosscutting D veins from Cavancha

petrography, the sections were carbon coated for the CL investigations. CL microscopy was performed with a HC5-LM hot cathode microscope by Lumic Special Microscopes, Germany. The microscope was operated at 14 kV and with a current density of ca. 10 μA mm^{-2} (Neuser, 1995). CL images were captured using a high sensitivity, double-stage Peltier cooled Kappa DX40C CCD camera, with acquisition times ranging from 5 to 10 seconds.

3.3 Butte, Montana

The Butte Cu-Mo deposit in Montana represents one of the largest porphyry deposits in the world. A total of ~9.8 Mt Cu, 90,000 t Mo, 20,300 tons Ag, and 82.8 tons Au have been mined at Butte between 1880 and 2005 (Czehura, 2006), with approximately 10% of the Cu production derived from the porphyry ore body and 90% from late Cordilleran-style lode veins (Houston and Dilles, 2013). A resource of 4.9 Gt of ore with an average grade of 0.49% Cu and 0.033% Mo is estimated to remain at Butte (Czehura,

2006). The deposit is thought to have formed at an unusually great depth of ~5 to 9 km below surface (Seedorff et al., 2005; Rusk et al., 2008a). As samples are available from deep drilling, the Butte deposit offers exceptional insights into the formation of porphyry deposits emplaced at the deeper end of the spectrum (Rusk et al., 2008a).

3.3.1 Deposit Geology and Vein Types

The Butte porphyry deposit is hosted by the Butte granite at the southern end of the Boulder batholith (Lund et al., 2002; Butte Quartz Monzonite of Tilling et al., 1968; Brimhall, 1977). The Butte granite, which has a U-Pb age of 74.5 ± 0.9 Ma (Lund et al., 2002), is largely hosted by Middle Proterozoic to Mesozoic sedimentary rocks. Along its southern margin, the granite intruded into Archean crystalline basement (Meyer et al., 1968; Tilling, 1973). The medium to coarse-grained equigranular granite consists of approximately equal proportions of quartz and K feldspar, which together constitute approximately 40 to 45 modal% of the rock. Plagioclase ranges in abundance from 36 to 42 modal%. Biotite and hornblende together form 15 to 20 modal% of the granite (Meyer et al., 1968; Brimhall, 1977). Magnetite, titanite, ilmenite, apatite, tourmaline, and zircon are present as accessory phases (Roberts, 1975; Brimhall, 1977).

The Butte granite is cut by a swarm of steeply dipping, east-west-trending quartz porphyry dikes (Meyer et al., 1968; Brimhall, 1977). The dikes are tan in color with an aphantic to fine-grained groundmass (Lund et al., 2002). They contain phenocrysts of K feldspar and partially resorbed bipyramidal quartz. Smaller, typically altered, plagioclase and biotite phenocrysts are present (Meyer et al., 1968; Lund et al., 2002; Rusk et al., 2008a). Zircon U/Pb ages of 66.5 ± 1.0 Ma and 65.7 ± 0.9 Ma place the intrusion of the quartz porphyry dikes about 10 million years after the emplacement of the Butte granite (Lund et al., 2002).

Mineralized breccias and stockwork veins of the so-called pre-Main Stage are centered on the late quartz porphyry dikes (Rusk et al., 2008a). The pre-Main Stage ores resemble those of typical hypogene porphyry Cu-Mo deposits. The pre-Main Stage ores

occupy two dome-shaped orebodies termed the Anaconda dome in the west and the Pittsmont dome in the east. Both are separated by an up to 1.2 km-wide zone of intensely quartz-sericite-pyrite-altered Butte granite (Rusk et al., 2004, 2008a).

Based on variations in the alteration mineral associations, several different pre-Main Stage vein types can be distinguished. The earliest pre-Main Stage veins at Butte are the early dark micaceous veins that contain quartz, pyrite, chalcopyrite, and magnetite (Meyer, 1965; Roberts, 1975; Brimhall, 1977; Rusk et al., 2008a). In general, quartz is the dominant mineral in the early dark micaceous veins, constituting more than 90% of the vein material, whereas sulfide minerals are much less abundant and collectively make up <5% of the veins. The early dark micaceous veins are complex both in their mineral composition and the composition of the surrounding alteration halos. Significant variations occur with depth (Rusk et al., 2008a; Reed et al., 2013). In the deep parts of the deposit, the veins are chalcopyrite-poor and quartz dominated. They are surrounded by alteration halos that contain biotite, K feldspar, quartz, and sericite (Meyer, 1965). In addition, anhydrite, andalusite, corundum, and secondary plagioclase occur (Rusk et al., 2008a). Shallow early dark micaceous veins contain more pyrite, chalcopyrite, and magnetite. The alteration halos have a higher proportion of sericite. Anhydrite, corundum, and secondary plagioclase are missing (Rusk et al., 2008a). Muscovite and biotite from early dark micaceous veins yielded $^{40}Ar/^{39}Ar$ ages of 63.6 ± 0.2 Ma, confirming a genetic relationship between the east-west-trending quartz porphyry dikes and the porphyry mineralization at Butte (Lund et al., 2002).

Green sericite veins occur upward and outward from the early dark micaceous veins. These veins are interpreted to be the upward continuation of the early dark micaceous veins and transitions between both vein types have been observed (Rusk et al., 2008a; Reed et al., 2013). The pale-green sericite veins consist of quartz, magnetite, chalcopyrite, and pyrite. They contain in excess of 50% opaque phases. The alteration selvages of the veins are typified by K feldspar, quartz, green sericite, chlorite, and minor calcite (Roberts, 1975; Brimhall, 1977; Rusk et al., 2008a; Reed et al., 2013). Most of the

Cu in pre-Main Stage veins at Butte is contained in the early dark micaceous veins and the pale-green sericite veins (Meyer et al., 1968; Rusk et al., 2004, 2008a).

The early dark micaceous and pale-green sericite veins are both crosscut by barren quartz and quartz-molybdenite veins (Brimhall, 1977), which occur dominantly in the deeper parts of the deposit. Except for the presence of molybdenite, the barren quartz and quartz-molybdenite veins are identical in appearance and transitions between both vein types have been observed. In addition to quartz and molybdenite, the veins contain purple anhydrite, rutile hairs, K feldspar, and calcite. Veins from moderate depths lack most of these minerals and only contain rutile hairs (Rusk et al., 2008a). Barren quartz and quartz-molybdenite veins in the deep part of the deposit are bordered by potassic alteration halos composed of K feldspar, whereas more shallow veins lack visible alteration halos (Rusk et al., 2008a; Reed et al., 2013).

All earlier vein types are cut by gray sericite veins consisting of abundant pyrite (commonly >80%) in addition to euhedral quartz. The alteration selvages are composed of muscovite, quartz, pyrite, and minor magnesian chlorite (Rusk et al., 2008a; Reed et al., 2013). The gray sericite veins and associated sericitic alteration halos closely resemble quartz-sericite-pyrite veins described in other porphyry deposits (Seedorff et al., 2005; Sillitoe, 2010).

All of the pre-Main Stage vein types at Butte are cut by large, through-going polymetallic base metal Cordilleran-style Main Stage veins consisting of quartz and Cu-, Zn-, Pb-, and Ag-sulfide minerals (Meyer et al., 1968). Main Stage veins are zoned from a Cu-rich core in the centre of the deposit, outward through an intermediate Cu-Zn zone, to a more peripheral Ag, Pb, Zn, and Mn zone. The veins are associated with sericitic and intermediate to advanced argillic alteration halos (Meyer et al., 1968). Although the terminology used at Butte suggests a relationship between the veins formed during the pre-Main Stage and the rich ores of the Main Stage, a number of studies have demonstrated that both types of mineralization are not necessarily directly related (Lang and Cheney,

1971; Brimhall, 1979; Lund et al., 2002; Rusk et al., 2008c). For this reason, the characteristics of the Cordilleran-style Main Stage veins are not further discussed here.

3.3.2 Fluid Inclusion Characteristics Identified in Previous Studies

Previous studies have shown that quartz in the early dark micaceous veins as well as in the barren quartz and quartz-molybdenite veins sampled from the deep part of the deposit (>1,400 m below present surface) contain abundant rectangular to negative-crystal shaped intermediate density fluid inclusions (0.63 to 0.73 g/cm^3) that consist of 30 to 50 vol.% vapor (referred to as B35 inclusions by Rusk, 2003; Rusk et al., 2004, 2008a). Approximately 20% of the inclusions contain an opaque or transparent daughter mineral, with chalcopyrite being the most common opaque phase (Rusk et al., 2004, 2008a). The inclusions are variably scattered across multiple quartz crystals and appear as clusters within grains. Assemblages occurring along growth zones in the quartz that are clearly primary are very rare (Rusk et al., 2004, 2008a). The intermediate density inclusions homogenize to the liquid in the range of 300 to 400^{o}C. They contain 1 to 8 wt.% NaCl equivalent and 3 to 7 mol % CO_2 (Rusk et al., 2008a).

In contrast to the deep portion of the deposit, quartz in the early micaceous veins as well as in the barren quartz and quartz-molybdenite veins from shallow depth (<1,400 m below present surface) contains abundant scattered or clustered equant to negative-crystal shaped intermediate density inclusions that consist of 50 to 75 vol.% vapor at room temperature (B60 inclusions of Rusk, 2003; Rusk et al., 2004, 2008a). The same type of inclusions with large vapor bubbles also occurs in the pale-green sericite at shallow depth (<900 m below present surface). It is the dominant inclusion type in the late gray sericite veins, irrespective of the depth within the deposit (Rusk et al., 2004, 2008a). The inclusions have generally similar characteristics to those described above, except that their density is lower, ranging from 0.4 to 0.55 g/cm^3. Only approximately 15% of the inclusions contain daughter minerals, with chalcopyrite being the dominant opaque phase (Rusk et al., 2004, 2008a). The inclusions have salinities ranging from 1 to 8 wt.% NaCl

equiv., CO_2 contents ranging from 4 to 9 mol %, and homogenize to the liquid, vapor, or by critical behavior between 356 and 452°C (Rusk et al., 2008a).

At shallow depth in the deposit (<1,400 m), brine and vapor inclusions occur in quartz of all vein types (B15H and B85 inclusions of Rusk, 2003; Rusk et al., 2004, 2008a). Brine inclusions are particularly common at those depths in the early dark micaceous veins and the pale-green sericite veins. Vapor inclusions are most common in the pale-green sericite and gray sericite veins. Both types of inclusions typically occur in the same veins and assemblages containing both brine and vapor inclusions are common. The brine inclusions contain 10 to 20 vol.% vapor in addition to the halite crystal. Approximately 5% of the brine inclusions contain hematite daughter crystals. Over 70% of the brine inclusions homogenize by halite dissolution above the temperature of liquid-vapor homogenization, whereas the remaining 30% of the inclusions homogenize by liquid-vapor homogenization after halite dissolution. Halite dissolution occurs at temperatures between 175 and 412^{o}C (Rusk et al., 2008a). The inclusions have salinities ranging from 30 to 48 wt.% NaCl equivalent (Rusk et al., 2004, 2008a). The vapor inclusions consist of more than 75 vol.% vapor and contain up to 18 mol% CO_2 (Rusk et al., 2008a). The presence of fluid inclusion assemblages containing coexisting brine and abundant vapor inclusions at shallow levels suggests that the pressure conditions in this part of the deposit dropped to levels low enough to promote fluid unmixing of the homogeneous intermediate density single-phase fluid described above (Rusk et al., 2008a).

Veins from all depths at Butte contain equant low-salinity liquid inclusions (B20 inclusions described by of Rusk, 2003, and Rusk et al., 2008a). These liquid inclusions are most abundant in the gray sericite veins, but have also been noted in all other vein types. CL investigations indicate that most of the liquid inclusions form secondary trails developed in late crosscutting quartz, although rare scattered clusters of the liquid inclusions also occur (cf. Rusk et al., 2006). The liquid inclusions contain 10 to 30 vol.% vapor. Opaque daughter minerals are not common and only occur in 10% of the inclusions. Scattered liquid inclusions show a wide range of salinities (6 to 28 wt.% NaCl equivalent) and homogenization temperatures. Homogenization occurs to the liquid between

195 and 420°C (Rusk et al., 2008a). Liquid inclusions in the gray sericite veins show less variability in salinity and homogenization temperature. They reportedly contain >10 wt.% NaCl equivalent and homogenize at 200 to 330°C (Rusk et al., 2008a).

3.3.3 Correlation between Fluid Inclusion Types and the Cathodoluminescence of the Vein Quartz

Two samples from the original study by Rusk (2003) and Rusk et al. (2008a) were investigated as part of the present study. These originated from the quartz-molybdenite and gray sericite vein types at Butte, respectively.

The investigated quartz-molybdenite vein (sample 11135-3872) from 1191 m depth within the Pittsmont dome is composed of over 95% quartz and less than 3% molybdenite. The vein is surrounded by a selvage of potassic alteration. The bulk of the quartz within the vein displays a homogeneous bright blue CL (Fig. 3-1A). Where examined, oscillatory growth zoning is missing. The quartz showing the blue CL is dominated by intermediate density fluid inclusions with large bubbles, although variations in bubble size were observed (B60 and some B35 inclusions of Rusk, 2003; Rusk et al., 2004, 2008a). Rare brine and vapor inclusions occur, which are mostly aligned along secondary trails. The quartz showing a blue CL is weakly overprinted by later quartz that displays a stable red-brown CL (Fig. 3-1A).

The gray sericite vein examined in the present study (sample 11052-6383) originated from within the bulb-shaped, central zone of pervasive sericitic alteration spatially above and between the Anaconda and Pittsmont domes. This sample is composed of early bright blue luminescent quartz (Fig. 3-1B). The early quartz contains abundant intermediate density fluid inclusions with large bubble sizes (B60 inclusions of Rusk, 2003; Rusk et al., 2004, 2008a) and few intermediate density fluid inclusions with distinctly smaller bubble sizes (B35 inclusions of Rusk, 2003; Rusk et al., 2004, 2008a). Brine and vapor inclusions are comparably rare (Fig. 3-1C).

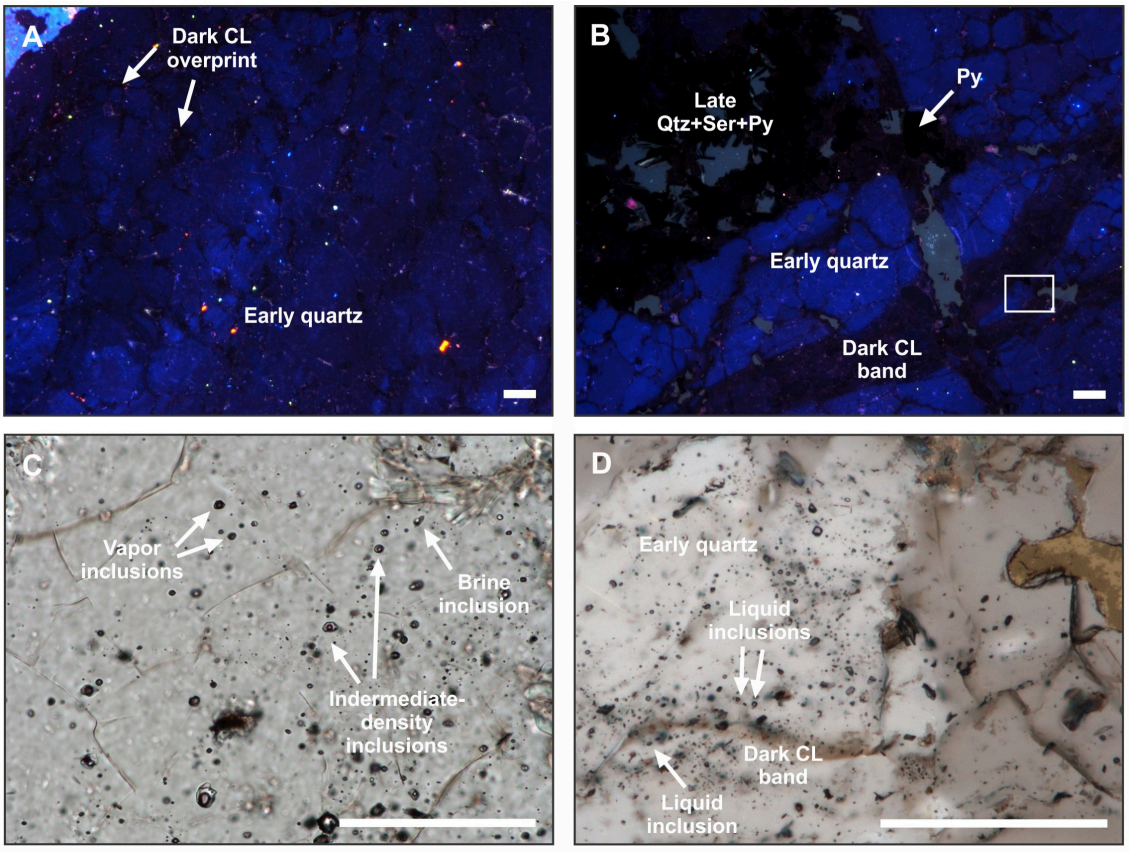

FIG. 3-1: Plane polarized light and cathodoluminescence photomicrographs of porphyry quartz veins from Butte, Montana. (A) CL image of early quartz in a quartz-molybdenite vein showing a mottled blue CL with a partial red-CL quartz overprint. Sample 11135-3872. (B) CL image of a gray sericite vein. The vein consists of early blue quartz that is pervasively overprinted by later red CL quartz. The late quartz forms dark bands that crosscut the early quartz veins. Sample 11052-6383. (C) Intermediate density inclusions and fewer brine and vapor inclusions contained in early quartz in a gray sericite vein. Sample 11052-6383. (D) Plane polarized light image showing the fluid inclusion distribution in a gray sericite vein. The dark CL bands contain low salinity liquid inclusions. The location of the photomicrograph is indicated in image (B). Sample 11052-6383. Py = pyrite, Qtz = quartz, Ser = sericite (illite/muscovite). All scale bars are 100 μm.

The blue luminescent quartz in the gray sericite vein is pervasively overprinted by quartz that has a red-brown CL and cannot be readily identified in transmitted light (Fig. 3-1B). The red-brown quartz is best developed along grain boundaries of the blue quartz and along wider fracture-controlled zones that typically contain low-salinity liquid inclusions (Fig. 3-1D; B20 inclusions of Rusk, 2003; Rusk et al., 2004, 2008a). The contacts between the late quartz with the red-brown CL and the early blue quartz are irregular and lobate. Some of the wider fracture-controlled zones of red-brown quartz crosscutting the early quartz grains contain faintly visible blue to purple pseudoclasts. Intermediate density fluid inclusions (B60 inclusions of Rusk, 2003; Rusk et al., 2004, 2008a) occur within these pseudoclasts, implying that the faintly visible blue to purple quartz represents early quartz that has been altered during the fluid-flow event that formed the red-brown quartz. Pyrite is texturally closely associated with the late quartz that shows a red-brown CL.

3.4 Bingham Canyon, Utah

The Bingham Canyon Cu-Au(-Mo) deposit, located in the central Oquirrh Mountains 30 km southwest of Salt Lake City in Utah, contains 3.23 Gt of ore at grades of 0.88 wt.% Cu, 0.02 wt.% Mo, and 0.497 g/t Au (Cooke et al., 2005). The orebody at Bingham is thought to have formed within a depth window of approximately 1.8 to 3.3 km from paleosurface (Redmond and Einaudi, 2010). Deep drilling below the deposit has provided a unique opportunity to sample the deep and largely unmineralized part of the porphyry in addition to the ore zone itself, giving unique insights into the evolution of the hydrothermal fluids over a vertical distance of 2.3 km (Gruen et al., 2010; Redmond and Einaudi, 2010).

3.4.1 Deposit Geology

The Bingham Canyon porphyry deposit is hosted by the Bingham stock, a late Eocene subvolcanic, composite monzonitic pluton, emplaced into Late Pennsylvanian quartzite, calcareous quartzite, and limestone (James et al., 1961; Lanier et al., 1978;

Redmond and Einaudi, 2010). The Bingham stock consists of four main intrusions described in detail by Redmond and Einaudi (2010).

The oldest intrusive unit is an equigranular monzonite that was emplaced at 38.55 ± 0.19 Ma (zircon U-Pb age date from Parry et al., 2001). The equigranular monzonite has been intruded by three different types of porphyritic dikes (Lanier et al., 1978; Redmond et al., 2001; Redmond and Einaudi, 2010). The earliest intrusion is a quartz monzonite porphyry, which consist of 50 to 60 vol. % phenocrysts in a groundmass of subequal amounts of aplitic quartz and orthoclase. Phenocrysts include 25-30 vol.% plagioclase, 6-12 vol.% orthoclase, 12-15 vol.% hornblende, 2-3 vol.% biotite, and rare quartz (Redmond and Einaudi, 2010). The quartz monzonite porphyry represents the primary ore host at Bingham Canyon, and is the volumetrically largest porphyry intrusion associated with the deposit (Redmond et al., 2001; Redmond and Einaudi, 2010).

The quartz monzonite porphyry is crosscut by latite porphyry that forms a series of north-northeast striking dikes and sills, extending for more than 3 km to the northwest of the Bingham stock. The latite porphyry is texturally and compositionally similar to the quartz monzonite porphyry, but contains fewer plagioclase and hornblende phenocrysts and a slightly higher proportion of groundmass (Redmond and Einaudi, 2010).

Thee quartz monzonite porphyry and the latite porphyry are both cut by biotite porphyry that is significantly darker in color than the other intrusive phases at Bingham Canyon. The biotite porphyry contains 12-15 vol.% biotite phenocrysts in addition to groundmass biotite. K feldspar and plagioclase phenocrysts are locally rounded and embayed due to resorption in the magma. Xenoliths of the earlier quartz monzonite porphyry and the latite porphyry are common (Redmond and Einaudi, 2010).

Highly irregular bodies of quartz latite porphyry breccia cut all earlier intrusive units. The breccia contains abundant wall-rock xenoliths that make up 20 to 50 vol.% of the breccia (Redmond and Einaudi, 2010). The quartz latite porphyry breccia itself is cut by quartz latite porphyry dikes. The quartz latite porphyry contains 30 to 40 vol. % phe-

nocrysts, which includes 3 to 7 % quartz crystals. The quartz latite porphyry ranges in color from dark green to medium brown, depending on the intensity of the biotite alteration (Redmond and Einaudi, 2010).

The Cu orebody occupies a bell-shape region draped above the quartz monzonite porphyry, with grades increasing from 0.35% Cu in equigranular monzonite and quartzite to >1% Cu in the central quartz monzonite porphyry. A zone averaging 1 g/t Au is located at the base of the central Cu ore shell (Gruen et al., 2010).

The emplacement of each of the four dike intrusions was followed by the formation of a set of hydrothermal veins. Quantitatively, most of the veining and Cu mineralization occurred after the emplacement of the quartz monzonite porphyry and prior to the latite porphyry (Redmond et al., 2001; Redmond and Einaudi, 2010).

The earliest veins formed are volumetrically minor wispy biotite veinlets, which are barren. These veins are postdated by early dark micaceous veins (Redmond and Einaudi, 2010). Thin (<3 mm) quartz centerlines in the early dark micaceous veins were potentially deposited after reopening of the veins during formation of the overprinting quartz stockwork veins (Landtwing et al., 2010).

The two types of early veins are crosscut by stockwork quartz veins. These veins are typically 0.5 to 2 cm wide, although they can range in width up to about 15 cm. Within the ore body, the stockwork veins comprise 25 vol.% of the quartz monzonite porphyry. The veins contain digenite, bornite, and chalcopyrite (Redmond and Einaudi, 2010). Based on vein morphology and crosscutting relationships, different types of stockwork quartz veins have been distinguished at Bingham Canyon (Redmond, 2002; Redmond and Einaudi, 2010). Early irregular A1 veins hosted by quartz monzonite porphyry are discontinuous and are crosscut by sheeted sets of sinuous 0.3-2 mm-wide A2 veinlets. Irregular 5-20 mm-wide A3 quartz veins are crosscut and offset by more straight walled A4 veins. The A4 quartz veins lack an obvious centerline. The A1 to A4 veins are com-

posed of anhedral, vitreous quartz that forms grains that are 0.1 to 5 mm in size (Redmond and Einaudi, 2010).

CL imaging has shown that the anhedral quartz in the A1 to A4 vein types is overprinted by later quartz generation that forms irregular networks, 0.01-0.1 mm-wide veinlets, and fillings in vugs. This late quartz occurs in close textural association with bornite, digenite, and chalcopyrite, indicating that formation of the ore minerals was associated with the precipitation of this type of quartz (Redmond and Einaudi, 2010).

The stockworks of A-veins are surrounded by alteration halos in which >25% of porphyry groundmass adjacent to veins as well as plagioclase phenocrysts are replaced by K-feldspar and quartz (Redmond et al., 2001; Redmond, 2002). Biotite within the alteration halos is medium brown in color and slight smaller and less abundant when compared to weakly altered rock. Only the late quartz latite porphyry is characterized by weak potassic alteration, in which <10% of the porphyry groundmass adjacent to porphyry veins and plagioclase phenocrysts are replaced by K-feldspar and quartz. Biotite is dark brown in color without any notable change in size or abundance (Redmond, 2002). $^{40}Ar/^{39}Ar$ isotope data collected by Parry et al. (2001) from hydrothermal biotite yielded ages ranging from 37.57 ± 0.11 to 37.07 ± 0.21 Ma, suggesting that hydrothermal activity at Bingham Canyon occurred over a period of approximately 0.5 Ma.

At Bingham Canyon, all stockwork quartz vein types are cut by later stage quartz-molybdenite veins (Redmond et al., 2001; Redmond and Einaudi, 2010), suggesting that this vein type formed after the emplacement of the quartz latite porphyry (Redmond and Einaudi, 2010). The veins are associated with areas of pervasive biotite alteration (Seo et al., 2012). The abundance of quartz-molybdenite veins is generally low within the Cu-Au orebody, but generally increases in the deep peripheral parts of the Cu ore shell (Gruen et al., 2010; Seo et al., 2012). The quartz-molybdenite veins are in turn crosscut by quartz-pyrite veins that may contain chalcopyrite and are characterized by sericite alteration halos (Redmond et al., 2001; Redmond, 2002; Gruen et al., 2010; Redmond and Einaudi,

2010). This overprinting phyllic alteration is rare within the ore body, and does not appear to be associated with significant ore grades (Redmond, 2002).

3.4.2 Fluid Inclusion Characteristics Identified in Previous Studies

The fluid inclusion inventory of stockwork quartz veins at Bingham Canyon has been described in detail by Redmond (2002), Landtwing (2004), Landtwing et al. (2005), Furrer (2006), Landtwing et al. (2010), and Redmond and Einaudi (2010).

In the deep root of the deposit beneath the central Au-Cu orebody, barren stockwork quartz veins are characterized by ubiquitous intermediate density fluid inclusions. These inclusions homogenize by critical behavior (fading of the liquid-vapor meniscus) or by homogenization to the vapor phase at temperatures of 365-429 ± 14^{o}C (Redmond, 2002; Landtwing et al., 2010). The intermediate density inclusions were also identified in quartz-molybdenite veins from the deep center of the deposit, and homogenize by the same behavior at 390 ± 30^{o}C. Intermediate density fluid inclusions in quartz veins from the deep peripheral Cu-rich zone examined by Furrer (2006) homogenize to the liquid phase at temperatures between 361 ± 4^{o}C and 384 ± 11^{o}C. The salinity of the inclusions ranges from 5.8 ± 1.4 to 7.2 ± 1 wt.% NaCl equiv.

The fluid inclusion inventory in quartz contained in stockwork veins changes with decreasing depth. Immediately below the ore zone, intermediate density fluid inclusions are observed in addition to abundant brine and vapor inclusions. Within the ore zone, the anhedral quartz in the stockwork quartz veins contains only negative-crystal to equant-shaped brine inclusions that coexist with vapor inclusions (Landtwing et al., 2005, 2010). The brine and vapor inclusions define abundant secondary trails and rare primary assemblages aligned along oscillatory growth zones in the quartz. The brine inclusions measured by Redmond (2002) homogenized between 347 and 561^{o}C and have salinities of 38 to 50 wt.% NaCl equiv. In some cases, brine and vapor inclusions are clearly cogenetic, indicating that phase separation of the hydrothermal fluids accompanied the precipitation of the quartz (Redmond, 2002; Landtwing et al., 2010). Fluid inclusions contained in

stockwork quartz veins associated with the later intrusions contain petrographically similar inclusions, but show declining temperatures reflecting the progressive cooling of the hydrothermal system. Brine inclusions in quartz veins crosscutting quartz latite porphyry homogenize at temperatures between 313 and 476^{o}C. These brine inclusions have salinities ranging from 38 to 43 wt.% (Redmond, 2002).

Redmond (2002), Redmond et al. (2004), and Landtwing et al. (2005, 2010) showed that early quartz in the stockwork quartz veins from Bingham Canyon is overprinted by the later quartz generation A5. This distinctly late quartz contains brine inclusions that are petrographically similar to those in the earlier quartz, although the abundance of inclusions in the quartz is generally lower. The brine inclusions have homogenization temperatures of 308-390^{o}C and salinities that range from 38 to 45 wt.% NaCl (Redmond, 2002). Close association between these brine inclusions and vapor inclusions indicates that phase separation of the hydrothermal fluids occurred during formation of the late quartz.

The quartz in the late quartz-pyrite veins is reported to contain liquid inclusions with a moderate- to small-sized vapor bubble (type A inclusions of Landtwing et al., 2005, 2010). These inclusions have a low salinity and sometimes contain sericite flakes, interpreted to have been accidentally entrapped from the altered wall rock. Similar liquid inclusions occur as late secondary inclusion trails in A1 to A5 quartz in the stockwork quartz veins, where they crosscut all types of quartz (Landtwing et al., 2010).

3.4.3 Correlation between Fluid Inclusion Types and the Cathodoluminescence of the Vein Quartz

As part of the present study, several quartz vein samples representing a range of A-vein types from within the high-grade Cu-Au orebody of the Bingham Canyon deposit were investigated (Fig. 3-2). These samples include a sheeted A2 vein sample cutting quartz latite porphyry (sample 5090-1700B) and two samples hosted in quartz monzonite porphyry consisting of A3-A4 and A5 quartz (samples 5090-1528 and 5090-1510). All

three samples were taken from the 5090 feet bench in the open pit. An additional sample from drill hole D211 originates from shallower depth. This sample consists of A3 and crosscutting A4 veins in quartz monzonite porphyry (sample 211-211.5).

CL microscopy showed that the A1 to A4 quartz veins are mostly composed of anhedral quartz that shows a bright blue CL emission and well-developed oscillatory growth zoning (Fig. 3-2B,D-F). Abundant brine and vapor inclusions are contained in this type of quartz (Fig. 3-2C). The inclusions form trails and clusters within the quartz grains. Alignment of assemblages along growth zones visible under CL that would suggest a primary origin of the inclusions was only rarely observed.

Oscillatory growth zoning in anhedral quartz is best developed in the A3 and crosscutting A4 veins from the 5184 feet level (sample 211-211.5; Fig. 3-2D). Samples from A1 toA4 veins collected from the 5090 feet level exhibit more irregular zoning when viewed using CL (sample 5090-1700b; Fig. 3-2E). In some cases, the oscillatory growth zoning shows disruptions where growth zones in the early blue CL quartz are truncated by growth zones of petrographically later quartz (sample 5090-1510; Fig. 3-2F). Vein selvages of the A1 to A4 veins and the adjacent quartz monzonite porphyry contain abundant K feldspar and biotite (sample 5090-1528; Fig. 3-2B, D). The K feldspar in the wall-rock is characterized by a bright light-blue luminescence. In the studied A2 vein, K feldspar forms narrow rims along the vein walls that exhibit wavy zoning (sample 5090-1510; Fig. 3-2F) or, more rarely, occurs as inwardly-oriented euhedral crystals with margins that impinge on the anhedral bright blue luminescent quartz that shows well-developed oscillatory growth zoning (sample 5090-1528; Fig. 3-2B).

CL microscopy showed that early quartz in the stockwork quartz veins is overprinted by late A5 quartz that exhibits a dull red CL color. This type of quartz occurs as overgrowth rims on the early blue quartz or irregular veinlets along microfractures. The dull red A5 quartz was observed in all of the vein samples examined during this investigation, but is present in significantly lower abundance in granular A4 quartz veins from the 5184 feet elevation level than in the other veins from slightly deeper in the deposit

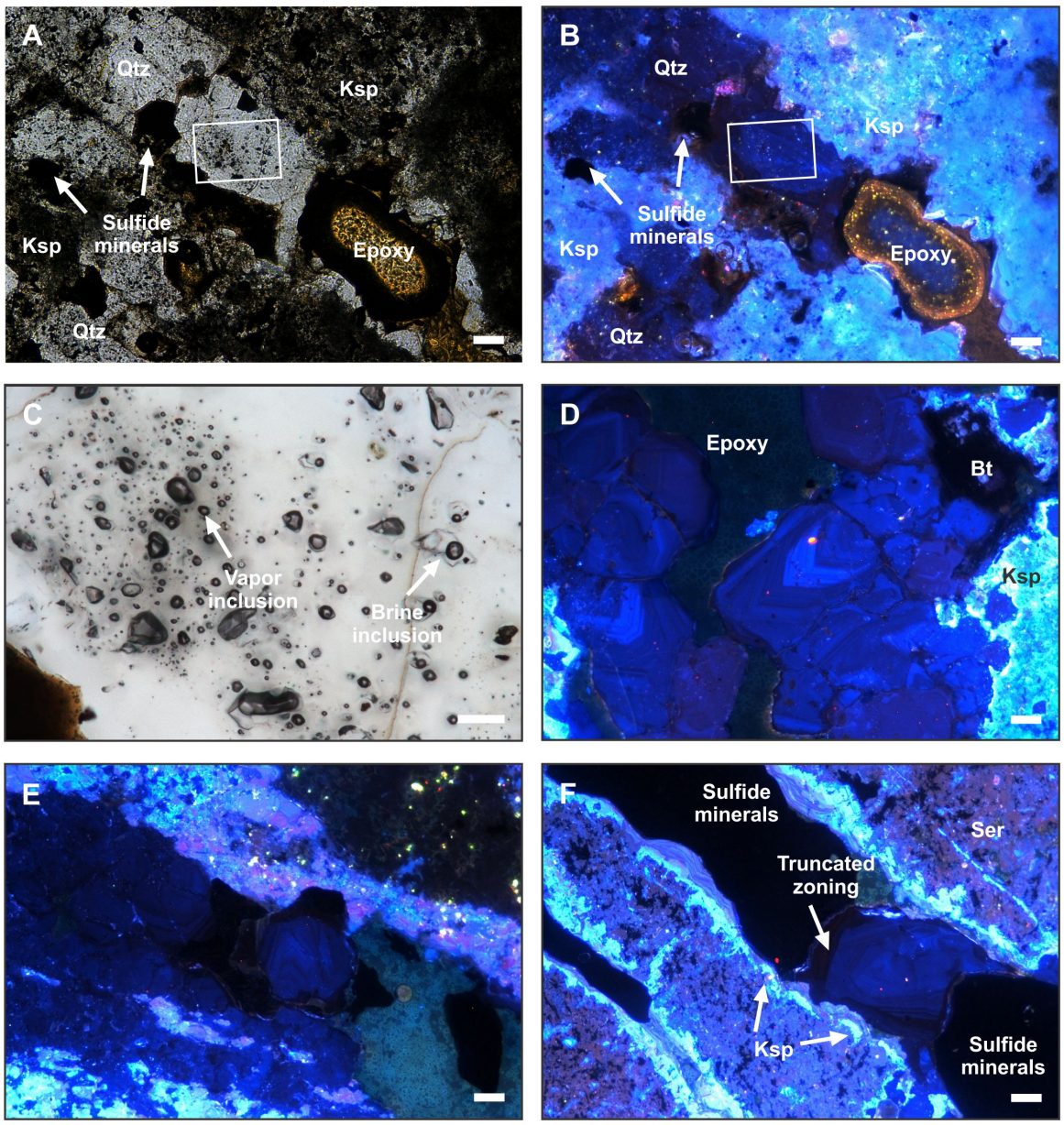

FIG. 3-2: Plane polarized light and cathodoluminescence photomicrographs of porphyry quartz veins from Bingham Canyon, Utah. (A) Plane polarized light image showing A2 vein textures. Multiple quartz types are not clearly apparent in the vein. Sample 5090-1528. (B) CL image showing luminescence textures within the same field of view as the previous image. A2 veins are composed of early blue-CL quartz with oscillatory growth zoning. A selvage of K feldspar showing light blue CL with turbulent growth zoning borders the quartz veins. Sample 5090-1528. (C) Brine inclusions containing a halite daughter mineral and a vapor bubble in the early blue quartz. The same vein contains abundant equant-shaped vapor inclusions. The image is taken in the area indicated in the two previous images. Sample 5090-1528. (D) Early blue-CL A vein quartz with strongly developed oscillatory growth zoning. Sample 211-211.5. (E) Early A vein quartz from deeper levels of the deposit showing blue CL with more irregular zoning. Sample 5090-1700b. (F) Early blue-CL quartz overprinted by late red-CL A5 quartz. Growth zones in early blue-CL quartz are truncated and crosscut by the late A5 quartz. Sample 5090-1510. Bt = biotite, Kspr = K feldspar, Qtz = quartz, Ser = sericite (illite/muscovite). Scale bars are 100 µm for images (A), (B), (D) and (F). Scale bar is 10 µm for image (C).

(Fig. 3-2D). Where observed, boundaries between the early blue quartz and the late dull red quartz are lobate and irregular (Fig. 3-2B,E,F). Oscillatory growth zones in A1 to A4 quartz are sometimes crosscut by the later dull red quartz (Fig. 3-2E,F). These CL textures were previously interpreted to represent dissolution textures formed through corrosion of the early quartz prior to precipitation of A5 quartz (Landtwing and Pettke, 2005; Landtwing et al., 2010). The dull red quartz is texturally associated with sulfide minerals and may have formed just before or during sulfide deposition.

The late dull-red quartz rarely contains small brine inclusions, which is consistent with the findings of Redmond (2002). However, no primary inclusions of this type were observed in the present study.

3.5 Maricunga Belt, Chile

The Maricunga belt, located about 700 km north of Santiago in northern Chile, is a metallogenic belt that includes several porphyry Au (±Cu) and associated high-sulfidation epithermal deposits that together contain a resource of ~40 million oz Au (Muntean and Einaudi, 2000). The porphyries are unique from other porphyry deposits as they were emplaced at depths of less than one kilometer (Muntean and Einaudi, 2000). As part of the present investigations, samples from the Cerro Casale in the Aldebarán district, the Pancho and Verde deposits in the Refugio district, and the Cavancha deposit in the La Pepa district were studied.

3.5.1 Deposit Geology

The porphyry deposits of the Maricunga belt are hosted by a thick succession of late Oligocene to late Miocene andesitic to dacitic volcanic rocks that are located within a north-northeast trending structural zone that is bordered by high-angle reverse faults. The late Oligocene to late Miocene volcanic rocks formed during four distinct episodes of volcanism (Muntean and Einaudi, 2000). Stratovolcanic complexes and dome fields were formed during the first and second episodes of volcanism, which occurred during the late

Oligocene to early Miocene (26-20 Ma) and middle Miocene (16-11 Ma), respectively. Extensive dacitic volcanism occurred during the third volcanic episode in the late Miocene (11-7 Ma) and the fourth period of volcanism in the late Miocene to early Pliocene (7-5 Ma). In the Maricunga belt, erosion of the late Oligocene to late Miocene volcanic rocks has exposed subvolcanic porphyry intrusions, many of which are hydrothermally altered and contain low-grade Au (±Cu) ore zones (Muntean and Einaudi, 2000). The basement to the late Oligocene to late Miocene andesitic to dacitic volcanic rocks of the Maricunga belt is comprised of Pennsylvanian to Triassic granitoids and intermediate to silicic volcanic rocks (Muntean and Einaudi, 2000, 2001).

The Aldebarán district is located at the southern end of the Maricunga belt. Hydrothermally altered rocks are exposed over a distance of approximately 5 km and a vertical range of about 1100 m (Muntean and Einaudi, 2001). Cerro Casale is the main deposit, located in eastern part of the district. The deposit coincides with an extensive zone of quartz veining hosted by a composite intrusion. The bulk of the intrusion is a medium-grained quartz diorite porphyry, which is cut by numerous irregular dikes of fine-grained feldspar porphyry, aplite, and intrusive breccia. Cerro Casale comprises a resource of 1114 Mt of ore grading 0.71 g/t Au and 0.26 % Cu (Muntean and Einaudi, 2001).

At Cerro Casale, A veins are associated with pervasive potassic alteration that consists of a peripheral zone of biotite and central alteration zone of quartz and K feldspar. Within the peripheral potassic zone, igneous biotite and hornblende phenocrysts in the groundmass are altered to shreddy-textured hydrothermal biotite. Rock textures are well preserved in this zone, and contain 1 to 5 vol.% magnetite. In the central and deep potassic zones, groundmass plagioclase is partially to pervasively altered to quartz and K feldspar, and brown biotite is replaced by green biotite, chlorite, and sericite. The original rock texture is largely destroyed and contains 4 to 10 vol.% magnetite that is partially altered to hematite. A veins in the deposit are characterized by anhedral granular quartz with sugary appearance and <1 vol.% chalcopyrite. Gypsum occurs in the oxidized zone close to surface. At Cerro Casale, banded quartz veins occur mostly in the periphery of

the ore body. They constitute <2 vol.% of the rock. The banded quartz veins crosscut and offset earlier A veinlets (Muntean and Einaudi, 2001).

At Cerro Casale, both the A veinlets and the banded quartz veins are crosscut by D veins that contain more than 50 vol.% pyrite with lesser amounts of quartz and up to 5 vol.% chalcopyrite. In many cases, the late D veins reopen earlier formed A veinlets. In addition, polymetallic veins occur on the northern and western side of the Cerro Casale deposit. These veins have centimeter-scale alteration halos composed of quartz, sericite, and pyrite. The polymetallic veins contain intergrown pyrite, chalcopyrite, sphalerite and tetrahedite/tennantite. They clearly cut A veinlets, but temporal relationships with the banded quartz veins and the D veins could not be established. Quartz-alunite replacement veins occur throughout the Aldebarán district and are particularly common to the west of Cerro Casale. At lower elevations, the quartz-alunite replacement veins are composed of quartz, alunite, pyrite, and rutile. At higher elevations, the veins are composed of a central core of vuggy residual quartz with pyrite, rutile, alunite, and diaspore. Locally, distinctly late enargite-quartz veins crosscut these veins. Due to their spatial separation from the deposit, crosscutting relationships with the A veinlets, the banded quartz veins, and the D veins could not be established (Muntean and Einaudi, 2001).

The Refugio district is located in the central portion of the Maricunga belt. The deposits of this district are hosted by an approximately 700 m-thick succession of late Oligocene to early Miocene (24-22 Ma) volcanic rocks, which include andesitic-dacitic flows and breccias as well as dacite domes. In the eastern portion of the district, this volcanic succession is covered by mid-Miocene volcanic rocks related to the La Laguna stratovolcano, which is located approximately 6 km to the east. Paleozoic to early Tertiary basement rocks are exposed in the western part of the district. This includes Late Pennsylvanian to Triassic rhyolitic pyroclastic deposits. Late Jurassic to early Tertiary red beds, andesite flows, and andesitic volcaniclastic rocks crop out to the south.

The main porphyry deposits in the district include the Verde and Pancho deposits. The Verde deposit, which had a pre-mining reserve of 101 Mt of 1.02 g/t Au at a cut-off

of 0.5 g/t and a Cu grade of 0.03 % (Brown and Rayment, 1991; Flores, 1993), comprises two separate coalescing annular-shaped zones of intense quartz veining, referred to as Verde West and Verde East. The orebodies have diameters of approximately 500 m, with an inner low-grade core that is about 100 to 150 m in thickness. The vertical extent of the ore zones is more than 500 m. The deposit is hosted by a dacite porphyry emplaced prior to mineralization and a large intrusive breccia body, 800 m in diameter, thought to have formed during the mineralizing event. Small stocks of a quartz diorite porphyry intrusion appear to have been emplaced immediately after the final stages of mineralization (Muntean and Einaudi, 2000). The mineralized zones at Verde spatially overlap with an alteration halo composed of chlorite, albite, and magnetite.

The earliest veins in the Verde deposit are narrow-discontinuous veinlets of andradite, chlorite, and magnetite. These veins do not show a spatial association with the gold zones, although they locally contain pyrite, chalcopyrite, and traces of galena. (Muntean and Einaudi, 2000). The andradite-chlorite-magnetite veins are overprinted and offset by banded quartz veins, which are the dominant vein type (>99 vol%) at Verde (Muntean and Einaudi, 2000, 2001). The banded quartz veins have slightly wavy, parallel walls and lack alteration halos. They are characterized by symmetric dark gray bands near vein margins. The dark bands show botryoidal textures and are typically continuous across quartz grains. Banded veins commonly contain granular quartz and have vuggy centers, although some inwardly-oriented crystals have been observed. The dark bands in the banded veins are related to the abundant presence of vapor inclusions and micrometer-sized magnetite grains. In addition to magnetite, the dark bands can contain micrometer-sized chalcopyrite, bornite, and sphalerite encapsulated in the quartz. Pyrite with minor magnetite, K feldspar, titanite, magnetite, and chlorite commonly occur in the vuggy vein centers, constituting less than 5 vol.% of the veins. The banded veins are host to the bulk of the gold at Verde. Based on crosscutting relationships, the majority of banded quartz veins must have formed after the emplacement of the intrusive breccia, but prior to the quartz diorite porphyry stock (Muntean and Einaudi, 2000). Steeply dipping quartz-alunite replacement veins are present at shallow levels in the Verde deposits. These replacement veins consist of quartz, alunite, and pyrite with smaller amounts of rutile,

dickite, and diaspore. The replacement veins can be up to 150 m long and 40 m wide. They are typically surrounded by sericitic alteration halos (Muntean and Einaudi, 2000, 2001). The quartz-alunite replacement veins clearly crosscut and postdate the banded quartz veins at Verde (Muntean and Einaudi, 2000, 2001).

The Pancho deposit, which has a resource of 68 Mt of 0.96 g/t Au (Brown and Rayment, 1991), is located in the northwest of the Refugio district. The deposit is centered on a quartz diorite porphyry stock that has a diameter of over 900 m. The quartz porphyry is cut by steeply dipping dikes of intrusive breccia. The ore zones of the deposit comprise an east-trending zone of abundant quartz veinlets that is 1.1 km long and 0.7 km wide (Muntean and Einaudi, 2000). The dominant alteration style at the Pancho deposit is a central potassic zone consisting of magnetite, K feldspar, and oligoclase. This zone grades outwards into a zone of secondary biotite that only contains traces of secondary K feldspar.

At Pancho, an extensive stockwork of quartz veinlets is associated with the potassic alteration zone. The veinlets are composed of quartz, magnetite, and sulfide minerals and can be classified as A veinlets according to the nomenclature of Gustafson and Hunt (1975). These A veinlets range from discontinuous and irregular veinlets containing magnetite, biotite, quartz, and minor chalcopyrite to continuous veins having a higher proportion of quartz and chalcopyrite. The quartz is pale gray and has a distinctive sugary texture in hand specimen. Fairly continuous zones of 0.5 to 1 g/t Au coincide with intense potassic alteration and the occurrence of A veinlets (Muntean and Einaudi, 2000). Similar to Verde, the Pancho deposit also contains abundant banded quartz veins. They are most abundant in the upper levels of the quartz diorite porphyry stock and in the overlying volcanic rocks (Muntean and Einaudi, 2000, 2001). Gold grades in whole rock samples commonly exceed 1 g/t in zones of abundant banded quartz veins. The banded quartz veins clearly crosscut and offset the earlier A veinlets. The banded quartz veins themselves are cut and offset by pyrite-quartz-sericite veins that resemble D veins of Gustafson and Hunt (1975). These veins are up to several centimeters in width and commonly occur as anastomosing networks. The pyrite-quartz-sericite veins consist of 10 to 60

vol.% pyrite with local chalcopyrite and molybdenite. The veins are enveloped by up to several centimeters wide alteration halos of quartz, pyrite, and sericite. Similar to the Verde deposit, quartz-alunite replacement veins have been recognized at Pancho. Their occurrence is restricted to the volcanic rocks at high elevation and crosscutting relationships with the other vein types could not be established. These replacement veins are anomalous in gold content, but do not form ore (Muntean and Einaudi, 2000).

The La Pepa district is located at the northern end of the Maricunga belt. In the district, an erosional window through late Miocene ignimbrites exposes late Oligocene to early Miocene volcaniclastic rocks in addition to porphyry dikes and stocks. The Cavancha deposit in the central part of the district is hosted by multiple intrusions of quartz diorite porphyry and intrusive breccia. The area of quartz veining is approximately 400 m in diameter. The ore zone is characterized by intense biotite alteration that is partially replaced by chlorite and hematite. Both A veinlets and banded quartz veins occur at the Cavancha deposit. However, the banded quartz veins appear to predate the A veinlets and many hybrid A-banded quartz veinlets occur that share characteristics of both vein types. D veins at Cavancha clearly postdate the banded quartz veins and A veinlets. They commonly contain >50 vol.% pyrite with quartz and minor sericite. The D veins contain early chalcopyrite, followed by bornite and enargite as well as late chalcopyrite and tennantite. Native gold commonly occurs in association with the bornite. In contrast to the other deposits of the Maricunga belt, high precious metal grades at Cavancha are related to quartz-alunite replacement veins, which average 20 g/t Au, but can contain up to 1000 g/t Au (Muntean and Einaudi, 2001).

$^{40}Ar/^{39}Ar$ dating by Muntean and Einaudi (2001) established the absolute timing of igneous and hydrothermal activity in the Maricunga belt. Cerro Casale hydrothermal biotite yielded a $^{40}Ar/^{39}Ar$ age of 13.89 ± 0.04 Ma while alunite from a quartz-alunite replacement vein gave an age of 13.91 ± 0.04 Ma. Hydrothermal biotite from the Pancho deposit yielded an age of 23.22 ± 0.06 Ma, which broadly overlaps with an igneous biotite age for the late quartz diorite porphyry stock at Verde West of 23.37 ± 0.06 Ma and Verde East of 23.28 ± 0.06 Ma. At the Cavancha deposit, $^{40}Ar/^{39}Ar$ dating of hydrother-

mal biotite gave an age of 23.81 ± 0.08 Ma while alunite from the replacement veins yielded age of 23.50 ± 0.06 Ma and 23.25 ± 0.08 Ma.

3.5.2 Fluid Inclusion Characteristics Identified in Previous Studies

The fluid inclusion characteristics of quartz from the A veinlets occurring in the various porphyry deposits of the Maricunga belt have been summarized by Muntean and Einaudi (2001). The vitreous quartz in these veins contains abundant equant to negative crystal shaped brine inclusions. These inclusions may contain sylvite and hematite daughter crystals in addition to halite. The brine inclusions coexist with less abundant vapor inclusions that contain <10% visible liquid (Fig. 3-3A). Microthermometry performed by Muntean and Einaudi (2001) indicates trapping temperatures between 315^{o} and 675^{o}C and salinities between 35 and 84 wt % NaCl.

The fluid inclusion inventory of banded veins has been studied in detail at Refugio by Muntean and Einaudi (2000). These authors demonstrated that the banded appearance of these quartz veins is caused by dark bands composed of abundant (>99%) vapor inclusions that can range up to 50 μm in size. The dark bands are botryoidal (Fig. 3-3B-D) and continuous across quartz grain boundaries, suggesting that they crystallized from a vapor-charged silica gel (Muntean and Einaudi, 2000). Besides vapor inclusions, rare brine and liquid inclusions (<1%) are present in the bands that can be up to 25 μm in size. In addition to halite, up to three unidentified opaque and non-opaque daughter minerals may be present in the brine inclusions. The light and dark bands in the banded quartz veins contain similar relative proportions of vapor and brine or liquid inclusions, but the dark bands are characterized by a larger number of fluid inclusions. Trapping temperatures of brine or liquid inclusions coexisting with vapor inclusions in banded quartz veins from the Verde deposit range from 220 to 350^{o}C. The salinity vary from 3.4 to 34 wt.% NaCl equiv. (Muntean and Einaudi, 2000) The banded quartz veins contain mineral inclusions of magnetite and rare native gold, bornite, and chalcopyrite.

Quartz in D veins from the porphyry deposits of the Maricunga belt is clear and forms small euhedral crystals that show oscillatory growth zoning (Muntean and Einaudi,

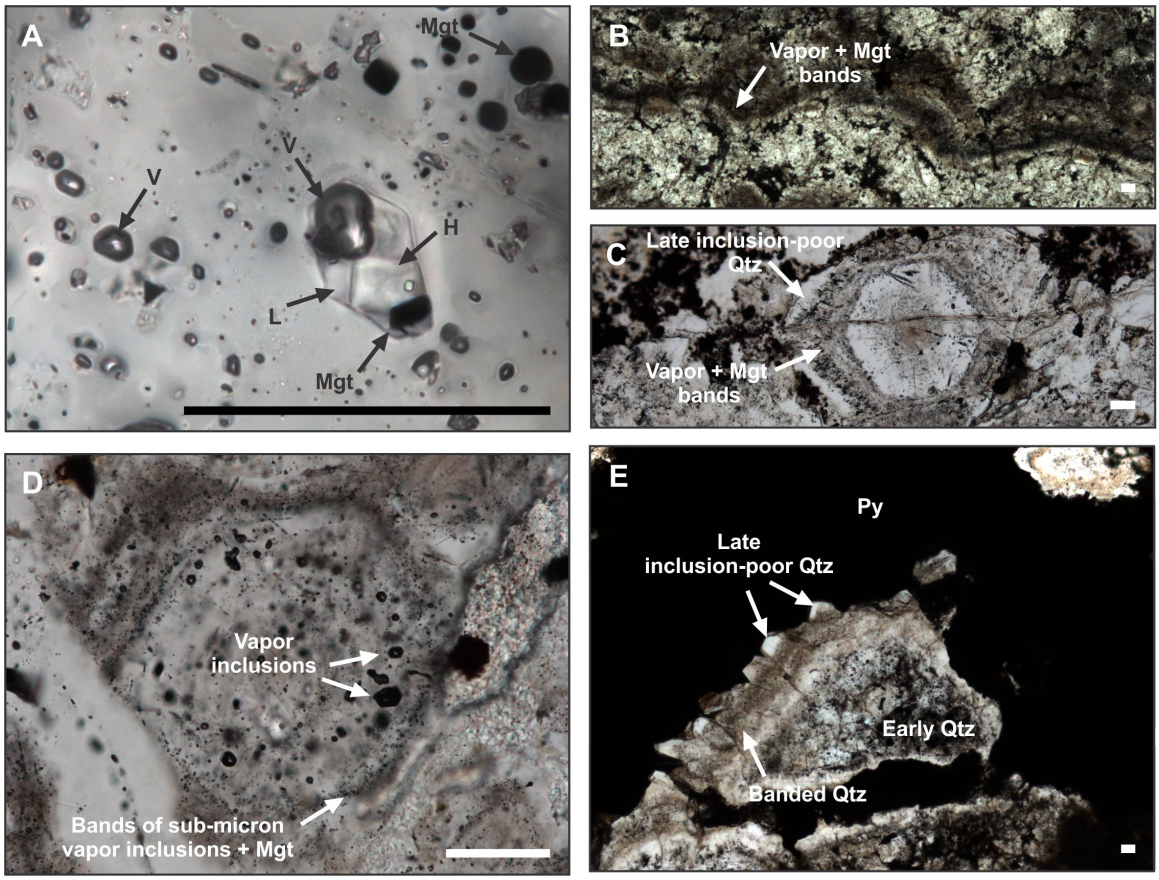

FIG. 3-3: Plane polarized light photomicrographs depicting the fluid inclusion inventory of quartz veins from porphyry deposits of the Maricunga belt, Chile. (A) Equant-shaped brine inclusions within A-vein quartz from the Cavancha deposit at La Pepa. These inclusions contain a large halite crystal and multiple additional daughter minerals. Sample CAV-2 203 m. (B) Plane polarized light image of veins containing botryoidal vapor-rich bands from the Verde deposit at Refugio. Sample DD26 36-38 m. (C) Plane polarized light image of similarly banded quartz from the Pancho deposit viewed down the c-axis of a large quartz grain. Sample RP054. (D) Abundant vapor inclusions located along botryoidal bands in quartz from the Pancho deposit. Sample RP054. (E) Hybrid A-banded vein and D-vein intersection from the Cavancha deposit. Sample CAV-2203 m. Mgt = magnetite, Qtz = quartz. All scale bars are 50 μm.

2001). Figure 3-3E shows an example of a hybrid A-banded-vein from the Cavancha deposit that is intersected by a D vein. The quartz in the A veinlet hosts brine and vapor inclusions, and is overgrown by quartz with a banded appearance that contains abundant vapor and rare liquid inclusions. The banded quartz is overgrown by a late generation of small euhedral inclusion-poor quartz typical of D veins that share grain boundaries with pyrite, which forms a volumetrically large portion of the D vein. Muntean and Einaudi (2001) reported that the clear quartz in D veins contains sub-micrometer irregular shaped liquid inclusions with or without halite. These inclusions occur in association with vapor inclusions. Limited microthermometric data suggest that the quartz formed at temperatures of less than 400^{o}C (Muntean and Einaudi, 2001).

3.5.3 Correlation between Fluid Inclusion Types and the Cathodoluminescence of the Vein Quartz

A spectrum of quartz veins was re-examined for their fluid inclusion contents and CL characteristics during this study. These included A veins from the Cerro Casale porphyry deposit in the Aldebarán district (sample ALC-1 292.8 m), banded veins from the Pancho (sample RP054) and Verde (samples DD26 36-38 m and RV027) deposits in the Refugio district, and hybrid A-banded veins with crosscutting D veins from the Cavancha porphyry deposit at La Pepa (samples CAV-1 110.1 m and CAV-2 203 m).

The investigated A veinlets from the Cerro Casale porphyry deposit at Aldebaran, Chile are composed of early blue to purplish quartz that shows weakly developed oscillatory growth zoning and contains abundant brine inclusions (Fig. 3-4A). The early blue quartz is crosscut by quartz that shows a red luminescence. The red quartz occurs along fractures and as an infill within vug space. There is a clear textural relationship between the red quartz and sulfide minerals. In the investigated sample, the relative proportion of red quartz is small, suggesting that the overprint of the earlier quartz was only weak.

Banded quartz exhibits bright blue luminescence. The luminescence is continuous across the light and dark bands visible in plane polarized light. At Pancho, the blue quartz

is overprinted by a later quartz type that is red under the CL microscope. This red quartz occurs as an overgrowth on the blue quartz, as a fracture fill, or as distinct euhedral crystals (Fig. 3-4B). Dark vapor-rich bands in the banded quartz veins are disrupted by zones of inclusion-poor quartz where they are crosscut by the red quartz. Banded quartz from Verde shows similar overprinting textures, but the quartz showing the botryoidal bands of vapor inclusions is slightly purplish in CL (Fig. 3-4C). Pervasive overprinting sometimes gives grains the appearance of blue islands encapsulated in red quartz. Quartz showing a red CL is generally inclusion-poor, but rarely contains low salinity liquid inclusions. The irregular, rounded overgrowth boundary between these two quartz types is optically continuous in plane light, and is only observable using CL.

Blue-banded quartz contains some irregular patches that exhibit bright pink CL. These areas correlate with zones of abundant subparallel subgrains and undulatory extinction when viewed under crossed polarized light, and appear to relate to partial recrystallization of the early bright blue-CL quartz. The most complex textures are encountered at Pancho within a vein consisting of large blue, banded quartz crystals and fragments cut by a trail of smaller bright pink quartz crystals (Fig. 3-4D). Pink quartz contains fewer large vapor inclusions and rare small brine inclusions that may be relics of inclusions contained in earlier quartz. Both the blue and pink quartz are cemented by a later generation of red quartz, resulting in a quartz microbreccia texture.

Several hybrid A-banded veins with crosscutting D-veins were examined from the Cavancha deposit. Figure 3-4E shows the intersection of an early A-banded quartz vein and a later D vein. Quartz of the early A veinlet exhibits a bright blue to purplish luminescence and contains brine and vapor inclusions. The early quartz of the A veinlet is overgrown by blue-CL banded quartz that contains abundant vapor and rare liquid inclusions, similar to equivalent banded quartz from Refugio and Pancho. Banded quartz is overgrown by a thin margin of euhedral, inclusion-poor quartz that shares grain boundaries with the pyrite of the D vein. The euhedral quartz is characterized by a short-lived blue CL that fades to a stable dull red to grey-black color during continuous electron bombardment. Figure 3-4F shows A-vein quartz from the same sample. Quartz in this

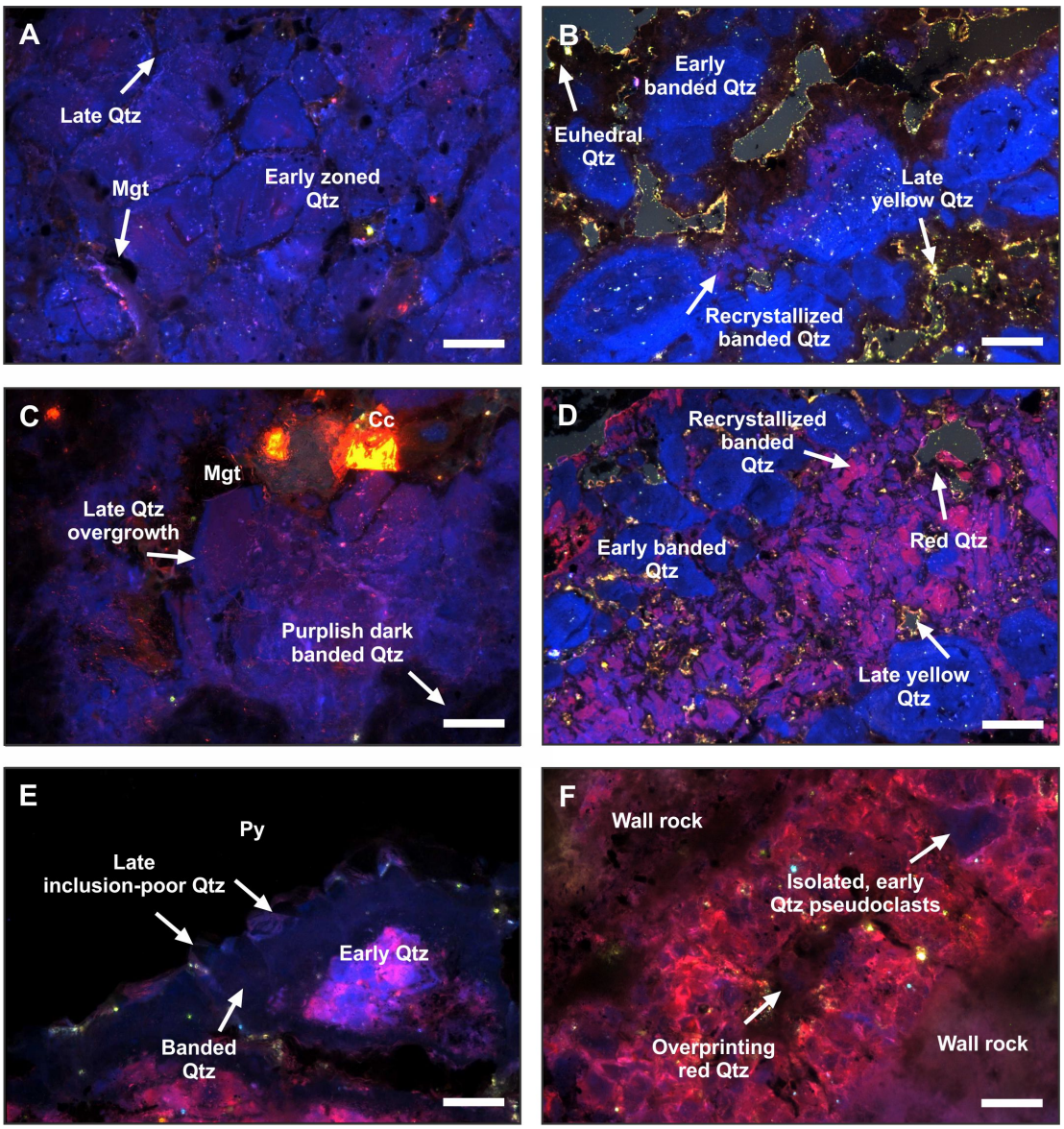

FIG. 3-4: Cathodoluminescence photomicrographs of quartz vein textures from porphyry deposits of the Maricunga belt, Chile. (A) CL image of quartz in an early A veinlet from the Cerro Casale deposit showing a bright blue CL with weakly developed oscillatory growth zoning and a minor late overprint by red quartz. Sample ALC-1 292.8 m. (B) Banded quartz vein from the Pancho deposit showing a bright blue CL with a pervasive late red overprint. Yellow quartz occurs as an overgrowth that overprints all earlier quartz types. Sample RP054. (C) Banded quartz vein from the Verde deposit exhibiting a blue CL. A late red overprint and purplish luminescence along the dark bands can be observed. Sample DD26 36-38 m. (D) Quartz microbreccia cutting a banded quartz vein at the Pancho deposit. Fragments of early blue- and pink-CL quartz are cemented by the late red quartz, with fine overgrowths of yellow quartz lining the margins of open space vugs. Sample RP054. (E) CL image showing the hybrid A-banded vein and D-vein intersection from Fig. 3-3E. Early A-vein quartz shows a bright blue to purplish luminescence and is overgrown by banded quartz that shows more homogeneous blue CL. The banded quartz is overgrown by a fine margin of late euhedral red to nonluminescent quartz that terminates against the pyrite. Sample CAV-2 203 m. (F) A-vein quartz from the Cavancha deposit, showing a distinct blue CL pseudoclast encapsulated in the bright blue to pink CL A-vein quartz. All quartz in this vein contains abundant brine and vapor inclusions, and has likely been subjected to pervasive CL alteration by later fluids. Sample CAV-2 203 m. Cc = calcite, Mgt = magnetite, Py = pyrite, Qtz = quartz. All scale bars are 200 μm.

vein shows bright blue to pink luminescence with distinct clasts or pseudoclasts showing a blue CL, which contain abundant brine inclusions. These features suggest the presence of relict blue CL quartz fragments that survived pervasive CL alteration by late hydrothermal fluids. The pink CL could be similar to the pink overprint observed at Pancho.

In the veins investigated from the Pancho deposit, all of the quartz types are overprinted by a late quartz that shows a bright yellow CL. This quartz occurs as thin (<2 µm) overgrowths on the margins of the earlier quartz crystals. Overgrowths of this latest quartz type are inclusion poor, and produce a CL emission that is reminiscent of ore-stage quartz in high sulfidation epithermal deposits (e.g., Holley, 2012).

3.6 Discussion

3.6.1 Petrographic Characteristics of Stockwork Veins

The microscopic investigations of the present study support the results of earlier studies, showing that individual stockwork veins in porphyry deposits are composed of multiple quartz generations that formed at different temperature and pressure conditions during different stages of the evolution of the investigated porphyry systems (Hedenquist et al., 1998; Penniston-Dorland, 2001; Rusk and Reed, 2002; Redmond et al., 2004; Rusk et al., 2006; Landtwing and Pettke, 2005; Landtwing et al., 2005, 2010; Pudack et al., 2009; Müller et al., 2010; Redmond and Einaudi, 2010; Marsh, 2012; Rusk., 2012). Integrated with observations at the macroscopic scale, including the occurrence of different crosscutting vein types and their spatial distribution at the deposit scale, the study of the relationships between multiple quartz generations at the scale of an individual vein is, therefore, critical to understanding the evolution of porphyry systems and the reasons for metal deposition.

The present study focused on a comparison of the CL properties and fluid inclusion characteristics of stockwork quartz veins from several world-class porphyry deposits that have been previously studied in detail. In these deposits, the early quartz veins, which are A veinlets according to the nomenclature of Gustafson and Hunt (1975), range

macroscopically from discontinuous and irregular to continuous and straight-walled. The vein morphology suggests that these veins were formed at the transition from ductile to brittle conditions, implying that the host rocks of these veins cooled from temperatures above approximately 400°C to temperatures below 400°C at the time of vein formation. Although multiple crosscutting generations of veinlets can be observed in individual deposits (e.g., A1 to A4 veins of Redmond and Einaudi, 2010) that differ in orientation and vein morphology, the quartz in these early veinlets has generally similar macroscopic and microscopic properties. The quartz is vitreous and composed of anhedral grains that form a mosaic texture of large interlocking grains. The anhedral quartz contains abundant fluid inclusions that were entrapped at high temperatures.

Under CL, the early quartz shows a blue luminescence. The veins from Butte in Montana represent the deepest veins from the porphyry environment investigated in the present study. Early quartz in the quartz-molybdenite veins from the deepest part of the deposit shows a somewhat mottled, homogeneous blue luminescence. Early vein quartz from the shallower gray sericite veins shows a similar bright blue luminescence, but exhibits well developed oscillatory growth zoning. The early quartz in the porphyry veins from Bingham Canyon shows a relatively homogeneous blue luminescence with weakly developed oscillatory growth zoning. The quartz appears to show progressively stronger zoning with decreasing depth within the deposit. The early quartz from the shallow porphyry deposits of the Maricunga belt shows similar CL properties when compared to the other vein quartz samples. The earliest banded quartz from the Pancho and Verde deposits at Refugio shows a bright blue luminescence, but lacks distinct growth zoning textures. At Verde, purplish luminescence occurs along the continuous vapor-rich bands. Early quartz in hybrid A-banded veins from Cavancha and Cerro Casale also shows bright blue to purplish luminescence with weakly developed oscillatory growth zoning.

The textural similarities between the different quartz veins investigated suggests that similar processes must have occurred during the early stages of the evolution of the magmatic-hydrothermal fluids in all investigated porphyry deposits. The comparable CL properties suggest that the quartz formed in a unique physicochemical environment.

Weis et al. (2012) proposed that creation of open space during the formation of quartz at high temperatures could be related to transient overpressuring of the hydrothermal fluids, resulting in hydraulic fracturing of the host rocks. Although this process explains the formation of early quartz veins, the limited observations of the present study suggest that the mechanisms of early quartz precipitation varied as a function of the depth of deposit formation. Within the deep parts of the Butte deposit, the early quartz generally lacks oscillatory growth zoning identifiable by optical CL microscopy, while similar blue quartz at Bingham Canyon, Far Southeast (see previous chapter), and Maricunga is characterized by pronounced oscillatory growth zoning.

In all deposits investigated in this study, the early quartz showing a blue luminescence is postdated and overprinted by a distinct quartz generation that is red brown under the optical CL microscope. The quartz occurs as distinct zones transecting early blue quartz, as an overgrowth on the margins of early quartz grains in veins with vuggy centerlines, or as distinct euhedral crystals. The red brown quartz shares irregular boundaries with the earlier blue quartz in all the deposits studied. The red-brown quartz can form a matrix surrounding pseudoclasts of blue quartz, with the intensity of the blue luminescence in the pseudoclasts varying as function of the intensity of the hydrothermal overprint as indicated by the degree of matrix development. Based on this textural observation and detailed fluid inclusion petrography described in the previous chapter, it is concluded that alteration of the preexisting quartz and associated quenching of the blue CL of the earlier quartz may have resulted in the development of the red-brown quartz. The late quartz undoubtedly represents a new precipitate only where the red-brown quartz forms a clear overgrowth on earlier quartz grains or occurs as euhedral crystals.

At Bingham Canyon, deposition of the late red-brown quartz appears to have been preceded by dissolution of the earlier formed quartz. This is particularly suggested by the observation that oscillatory zoning in the blue quartz is commonly truncated by the later red-brown quartz. The contact between the early blue quartz and the red-brown overgrowth is irregular to lobate. These textures are similar to those reported by Redmond et

al. (2004), Landtwing and Pettke (2005), Landtwing et al. (2005, 2010), and Redmond and Einaudi (2010). Similar dissolution textures have not been observed at the other deposits studied here.

In all deposits investigated, the late red-brown quartz only contains rare fluid inclusion. However, where present, the inclusion inventory of the late quartz is distinct from the inclusions entrapped in the early blue quartz. At all deposits, the inclusions indicate that the formation of the late quartz occurred at temperatures lower than those prevailing during early quartz depositions. At Butte and Far Southeast (see previous chapter), the red-brown quartz contains inclusions of a low-salinity liquid. In contrast, the late quartz at Bingham Canyon hosts rare brine and vapor inclusions. Rare low-salinity liquid inclusions were also observed in the late quartz contained in the A veins from Maricunga.

In all cases investigated, the red-brown quartz is texturally closely associated with the ore minerals and may have formed either shortly before or during sulfide deposition. Similar relationship has been previously documented using SEM-CL at Butte (Rusk and Reed, 2002; Rusk et al., 2006) and at Bingham Canyon (Redmond et al., 2004; Landtwing and Pettke, 2005; Landtwing et al., 2005, 2010; Redmond and Einaudi, 2010). At Far Southeast, the close textural association of late quartz with sulfide minerals has been previously described by Hedenquist et al. (1998). The occurrence of gold in the banded veins of the deposits in the Maricunga belt may also be related to a late overprint of the quartz veins. Muntean and Einaudi (2000) noted that gold grains in the banded veins at Verde occur within the veinlets or along the margins of the veins in the wall rock. Although some gold is found with the magnetite in the dark bands, most gold grains are associated with pyrite that fills fractures and clearly postdates the dark bands, implying that gold precipitated after the dark bands during the late stage of vein filling.

3.6.2 Constraints on the Pressure and Temperature Conditions of Stockwork Veins Formation

The present study examined porphyry veins from world-class deposits that formed at different crustal depths. Based on microthermometric data provided by previous workers, it is possible to reconstruct the pressure and temperature conditions during stockwork vein formation and the role that pressure plays during fluid evolution and ore deposition in the porphyry environment.

The porphyry deposit at Butte is associated with a deep intrusion. At the high ambient pressure conditions, the high-temperature magmatic-hydrothermal fluids degassed from a magmatic source formed a single-phase vapor-like fluid. Early quartz at Butte showing a blue CL contains abundant intermediate density fluid inclusions. Due to the large vertical gradient in the deposit, the density of the intermediate density fluid changes with depth, explaining the observed systematic variations in the size of the vapor bubble in the intermediate density fluid inclusions present in the early quartz at different levels within the deposit (referred to as B35 and B60 inclusions of Rusk, 2003; Rusk et al., 2004, 2008a).

Previous fluid inclusion investigations suggested that the intermediate density inclusions in the early blue luminescent quartz in quartz-molybdenite veins at Butte from moderate depth were entrapped at temperatures of approximately 500^{o} to 650^{o}C under fluctuating pressure conditions of 800 to 2000 bars (Rusk et al., 2008; Reed et al., 2013). This pressure range equates to a paleodepth of 3.2 to over 6.0 km at lithostatic pressure conditions (Fig. 3-5). True trapping temperature and pressures of intermediate density inclusions contained in the late gray sericite veins, which only occur at shallow levels within the deposit, were estimated to have been between 350 and 450^{o}C and 400 to 700 bars, which corresponds to a paleodepth of 1.6 to 2.5 km under lithostatic conditions (Rusk et al., 2008). The presence of rare brine and abundant vapor inclusions in early blue luminescent quartz in the gray sericite vein quartz examined by Rusk et al. (2008) and the present study indicates that pressures dropped at least locally below the solvus,

allowing the single-phase vapor-like fluid to unmix into a hypersaline liquid and a coexisting low-salinity vapor.

Late red-CL quartz that crosscuts and overgrows early blue quartz in both the quartz-molybdenite and gray sericite veins contains low-salinity liquid inclusions. This distinct quartz generation is texturally closely associated with the sulfide minerals. Secondary liquid inclusions forming trails cutting the early quartz homogenize at 200 to 330^{o}C (Rusk, 2003; Rusk et al., 2008a). Pressure estimates for the formation of this inclusion type are not reported in the literature. However the lack of evidence for boiling along secondary trails of liquid inclusions, and the occurrence of this inclusion type in gray sericite veins assumed to have formed at paleodepth of 1.6 to 2.5 km suggests that the liquid inclusions were trapped at pressures between 160 and 250 bars assuming hydrostatic pressure conditions (Fig. 3-6).

The Bingham Canyon porphyry deposit formed at an intermediate depth. Within the deep parts of the system, stockwork vein quartz contains intermediate density fluid inclusions, suggesting quartz formation from a single-phase vapor-like fluid (nomenclature see Driesner and Heinrich, 2007). These fluids were entrapped at temperatures >500°C and pressures exceeding 800 bars (Landtwing et al., 2010). Immediately below the ore shell, the single-phase vapor-like hydrothermal fluid intersected its solvus. Fluid unmixing at temperatures of 350-560^{o}C produced a 38-50 wt.% NaCl equiv. hypersaline liquid that coexisted with an immiscible vapor of distinctly lower salinity (Redmond, 2002). Both fluids were trapped in the early blue luminescent quartz at Bingham Canyon as brine and vapor inclusions, respectively. Fluid unmixing is thought to have occurred at pressures of 550-140 bar, which is consistent with fluctuations in pressure between lithostatic and hydrostatic conditions at an inferred paleodepth of 1.4 to 2.1 km (Fig. 3-5).

The early blue quartz in the stockwork veinlets at Bingham Canyon is also overprinted by a distinctly younger quartz generation that shows a red-brown CL color. Although the quartz is generally fluid inclusion poor, primary brine inclusions that have salinities of 38-45 wt.% NaCl equiv. and homogenization temperatures of 308-390^{o}C have

been recognized (Redmond, 2002; Redmond et al., 2004; Landtwing et al., 2005, 2010). This late quartz is intergrown with ore minerals in the veins at Bingham Canyon. Based on microthermometric measurements on coexisting brine and vapor inclusions in the late quartz, Redmond (2002) calculated a pressure of 250 bars, consistent with a paleodepth of 2.5 km at hydrostatic conditions (Fig. 3-6).

The formation of early blue stockwork quartz in the deposits of the Maricunga belt occurred at even lower pressures, as these deposits formed in association with shallow porphyry intrusions. Under the ambient pressure conditions, the hydrothermal fluids formed a hypersaline liquid coexisting with a lower salinity vapor. The early quartz veins from Cavancha, Cerro Casale, Pancho, and Verde contain both brine and vapor inclusions. Early quartz in these deposits formed at high temperatures of up to 675^{o}C and lithostatic pressure conditions corresponding to 0.5 to 1.5 km paleodepth (Fig. 3-5). Creation of open fracture networks resulted in flashing of the hypersaline liquid. Due to the pressure drop from lithostatic to vaporstatic conditions at these shallow depths, the hydrothermal fluids existed in the vapor plus salt coexistence field of the H_2O-NaCl system. The banded quartz veins at Pancho and Verde record formation of quartz veins under vaporstatic conditions. Homogenization of brine inclusions coexisting with vapor inclusions in banded veins from Verde occurred at 325 to 350^{o}C. The veins were estimated to have formed at pressures of 19 to 150 bars (Muntean and Einaudi, 2000). This pressure range is consistent with paleodepth of formation between 190 and 440 m at vaporstatic to hydrostatic pressure conditions (Fig. 3-5).

In summary, the previous microthermometric investigations established that the early blue vein quartz in porphyry deposits formed at high temperatures of approximately 675 to 450°C. Pressure conditions during quartz formation may have ranged from approximately 2000 bars in deep deposits such as Butte to 20 bars in the shallow deposits of the Maricunga belt. Pressure may have fluctuated subsequently. Lithostatic conditions during early quartz formation were probably maintained in deep deposits while such high pressures could only be maintained in deposits of intermediate and shallow depth prior to cooling of the host intrusion below the ductile to brittle transition. When open fracture

networks were established, the early quartz could have formed under hydrostatic conditions or even vaporstatic conditions as observed in the case of the deposits of the Maricunga belt.

The later red-brown quartz formed at distinctly lower temperatures of <350°C. During quartz formation, hydrostatic conditions were maintained. As mentioned above, deposition of the ore minerals occurred during or after the precipitation of the red-brown quartz. This suggests that sulfide minerals were formed at temperatures below ca. 350°C.

3.6.3 Implications to the Deposit Model

Combined with the review of existing literature, the findings of the present study allow the reconstruction of fluid evolution in a number of world-class porphyry deposits that formed at different crustal depths. The Butte deposit in Montana and the deep root of the Bingham Canyon deposit in Utah are examples of the deep porphyry environment. Deposits formed at intermediate depth included Bingham Canyon and Far Southeast in the Philippines (see previous chapter). Quartz veins from the deposits of the Maricunga belt in Chile were investigated to provide information on the fluid evolution in the shallow porphyry environment.

The study of porphyry veins from these different deposits highlighted commonalities between the different deposits. In particular, it is notable that stockwork veins in all deposits contain an early quartz generation that formed at high temperatures that is overprinted by later quartz that formed at distinctly lower temperatures. Both types of quartz can be distinguished by optical CL microscopy. The early quartz shows a bright blue luminescence while the later quartz is red-brown.

Formation of the early quartz generation at high temperatures appears to be generally associated with potassic alteration of the immediate host rocks although the nature and intensity of the potassic alteration may vary from deposit to deposit. The early high-temperature fluids are thought to be of magmatic origin, formed through active degassing

of a magma chamber at depth. At high ambient pressures, the hydrothermal fluids exsolve from the magma occurred as single-phase vapor-like fluids. At Butte and the deep roots of the Bingham Canyon deposit, these fluids formed early quartz containing intermediate density fluid inclusions. Temperatures of quartz formation suggest that the fluids already cooled by approximately 100-200°C during their fluid ascent prior to the formation of the first quartz.

During continued fluid ascent and related decompression, the single-phase vapor-like fluids of magmatic origin intersected the solvus H_2O-NaCl system (cf. Driesner and Heinrich, 2007). Condensation resulted in the formation of a hypersaline liquid and a co-existing low salinity vapor. The study by Redmond et al. (2004) and Landtwing et al. (2010) established that this processes of condensation of the high-temperature hydrothermal fluids occurred over a vertical distance of approximately 400 m immediately below the ore shell of the Bingham Canyon deposit. Above this transition zone, early quartz only contains brine and vapor inclusions, with no intermediate density fluid inclusions being present.

In contrast to Bingham, where the early high temperature quartz formed essentially at the transition from the single-phase field of the H_2O-NaCl system (cf. Driesner and Heinrich, 2007) to the two-phase liquid plus vapor field, early quartz formation at Far Southeast (see previous chapter) occurred at lower pressure conditions within the liquid plus vapor field of the H_2O-NaCl system (Hedenquist et al., 1998). The hypersaline liquid and vapor entrapped in the early quartz at Far Southeast could have derived from an ascending single-phase vapor-like fluids of magmatic origin that underwent phase separation below the Far Southeast deposit, which would be similar to situation at Bingham Canyon. Alternatively, the slightly lower pressure conditions could have allowed exsolution of hydrothermal fluids from a magma within the two-phase liquid plus vapor field of the H_2O-NaCl system (cf. Driesner and Heinrich, 2007), with no precursor single-phase fluid being produced.

The deposits of the Maricunga belt formed at even lower pressure conditions. In the case of these deposits, the early high-temperature magmatic-hydrothermal fluids were probably separated from the magma at lower pressure conditions and directly degassed from the magma within the liquid plus vapor field or even the vapor plus salt field of the H_2O-NaCl system (cf. Driesner and Heinrich, 2007). In the formed case, creation of open fracture networks would have caused a further decrease in pressure, allowing the hypersaline liquid to cross the coexistence boundary surface between the liquid and vapor and the vapor and salt fields of the H_2O-NaCl system (cf. Driesner and Heinrich, 2007). This resulted in the vaporization of the liquid, creating a large amount of vapor. Early banded veins are interpreted to have formed in association with this process of vapor streaming.

The formation of the later quartz, showing a red-brown CL color, occurred largely within preexisting veins. This relationship cannot be identified by hand specimen inspection and is difficult to identify even by standard optical petrography. The present study shows that optical CL investigations represent a powerful tool to visualize these textural relationships.

Based on isotopic evidence, Hedenquist et al. (1998) showed that the late quartz in the porphyry veins is also formed from a hydrothermal fluid of magmatic origin. This fluid simply evolved towards lower temperatures prior to the formation of the late quartz in a temperature interval that is centered on the critical point of pure water.

At Butte in Montana and Far Southeast in the Philippines (see previous chapter), the late quartz contains liquid inclusions, suggesting that the quartz formed from a hydrothermal liquid of low salinity. As discussed by Hedenquist et al. (1998), this liquid could have formed from the early single-phase vapor-like hydrothermal fluid through isochemical contraction accompanying cooling at elevated pressures. Such a process could be related to the inward cooling of the source magma chamber, causing active degassing to occur at progressively increasing pressure conditions. Due to the increase in transport distance associated with the retreating magma front and conductive cooling of the intrusion, the fluids could cool towards lower temperatures during their ascent.

At Butte and Far Southeast, the lower-temperature hydrothermal liquid caused extensive sericite-pyrite or chlorite-sericite alteration of the wall rocks. As the ore minerals formed either at the same time as the late quartz or precipitated shortly after, it is suggested that ore formation occurred at sericite-pyrite or chlorite-sericite stable conditions. Although this has already been documented by Hedenquist et al. (1998), this conclusion has not been widely accepted by subsequent workers, presumably because this paragenetic relationship is not obvious on the hand specimen scale as mentioned above.

The Bingham Canyon deposit appears to be an exception. The host rocks of the stockwork quartz veins show intense potassic alteration. A strong hydrothermal overprint by sericite has not been documented at this deposit. At the same time, the late quartz showing a red-brown luminescence contains hypersaline liquid and vapor inclusions, not low salinity inclusions as observed at the Butte and Far Southeast deposits. Although ore formation occurred at similar temperature conditions, the ore forming fluid was apparently a hypersaline liquid at Bingham Canyon. As both the early high-temperature quartz and the late low-temperature quartz formed from hypersaline liquids coexisting with vapor, the hydrothermal system at Bingham Canyon appears to have developed differently from those at Butte and Far Southeast. At Bingham Canyon, cooling of the host rocks across the ductile to brittle boundary, allowing a transition from lithostatic to hydrostatic conditions, coincided with a rapid cooling of the hydrothermal system to temperatures below 400°C and the precipitation of sulfide minerals.

3.6.4 Quartz as a Pathfinder Mineral in Porphyry Exploration

The investigation of porphyry vein quartz from several well-studied world-class porphyry deposits has shown that the CL behavior and fluid inclusion properties of porphyry quartz are unique. Early high-temperature quartz is characterized by blue CL and the presence of high-temperature fluid inclusion assemblages (high-temperature intermediate density inclusions, brine and vapor inclusions, or vapor inclusions only). Later low-temperature quartz associated with the ore minerals shows a red CL and contains

low-temperature fluid inclusion assemblages (low-temperature brine and vapor inclusions, liquid inclusions, or liquid and vapor inclusions).

Based on the unique CL and fluid inclusion properties identified in the present study, procedures could be developed to use quartz as a pathfinder mineral in porphyry exploration. The use of quartz as a pathfinder mineral could prove particularly useful during early stage exploration where identification of porphyry quartz and distinction from other types of quartz in, for instance, surface grab or float samples, regolith samples containing residual quartz fragments, and sands recovered from stream sediment surveys would be essential.

In addition to the identification of porphyry quartz and its distinction from quartz of other origins, the combined study of the CL properties and fluid inclusion inventory of quartz samples could provide a range of additional information on the environment of porphyry formation critical in mineral exploration. For instance, the petrographic study of fluid inclusions in quartz alone allows the depth of quartz vein formation to be bracketed, even without the need for detailed microthermometric investigations. Knowledge on the depth of vein formation provides first-order information on the expected style of mineralization (e.g., Murakami et al., 2010). In cases where limited geological information is available, the study of the CL properties and fluid inclusion inventory of quartz samples, combined with the current understanding of the zonality of porphyry deposits, could be used for vectoring towards the hydrothermal centre.

3.7 Conclusions

Quartz vein formation in the porphyry environment takes place over a wide range of temperature and pressure conditions in an evolving magmatic-hydrothermal system. Based on the study of vein samples from well-characterized world-class porphyry deposits, the present contribution shows that a similar progression of quartz deposition can be observed in different deposits. Based on optical CL microscopy and fluid inclusion pe-

trography, several distinct quartz generations were defined that form at different stages during the evolution of porphyry systems.

Porphyry quartz veins are texturally complex and typically composed of multiple quartz generations that formed at different times during the lifetime of the magmatic-hydrothermal system through reopening of the previously formed veins. As these complex relationships are not visible in hand specimen or drill core, reconstruction of the fluid evolution in porphyry systems has to be based on advanced analytical tools and methods such as the combination of optical CL microscopy and fluid inclusion petrography. It is particularly important to note that the results of the present study demonstrate that macroscopic observations cannot reliably establish paragenetic relationships between quartz and ore minerals and the relationships between ore minerals in the veins and the mineralogy of the alteration halo surrounding the veins.

Comparison of vein quartz from different world-class porphyry deposits not only allowed the establishment of unified model describing the evolution of the porphyry systems, but also highlighted differences between deposits that are related to different depths of the porphyry intrusions. The fluid inclusion investigations demonstrate that the phase behavior of the hydrothermal fluids varies systematically as function of the depth of porphyry formation. However, temperature is the principal control on ore deposition in the porphyry environment as base and precious metal deposition in the investigated deposits can always be linked to the cooling of the hydrothermal fluids across a narrow temperature range centered on the critical point of pure water.

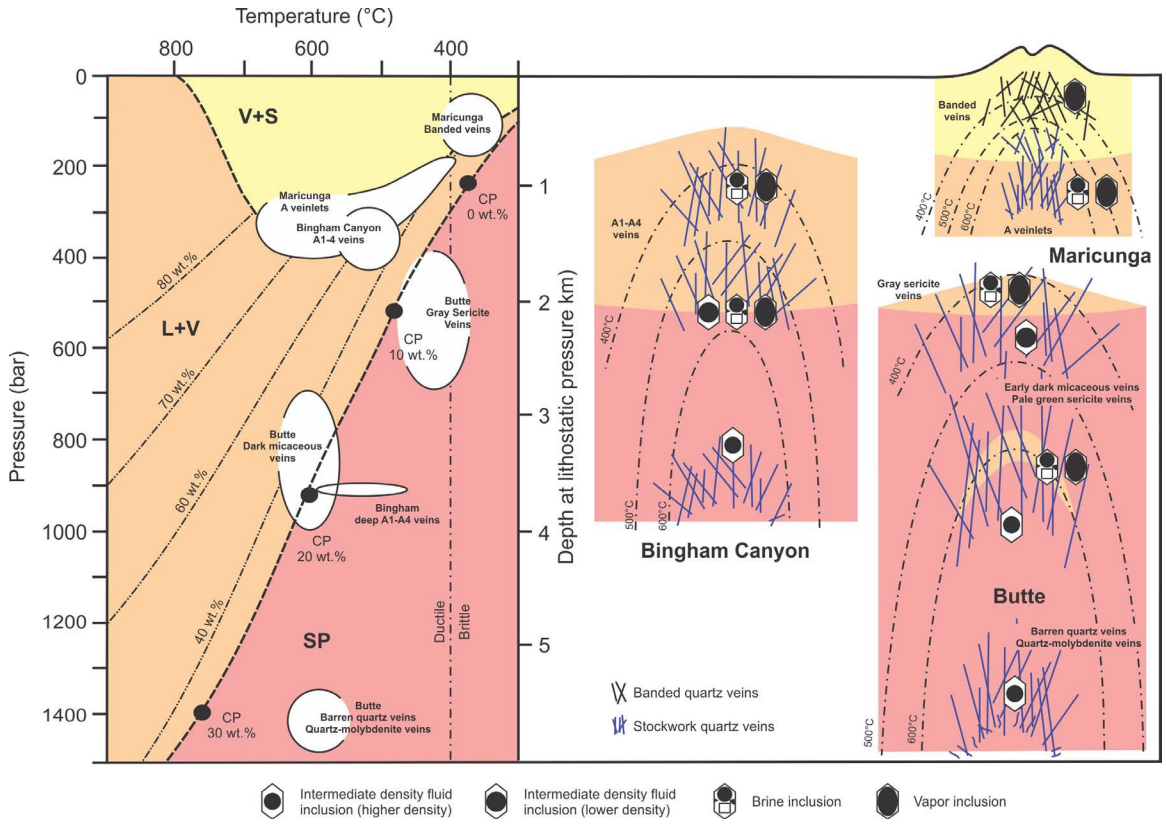

FIG. 3-5: Schematic diagram depicting the pressure-temperature relations during the formation of early blue quartz in the Butte, Bingham Canyon, and Maricunga porphyry deposits. The results of the fluid inclusion petrography are depicted schematically. The different colored regions in the diagram correspond to the phase regions in the H_2O-NaCl phase diagram. Depths are based on a 2.5 g/cm^3 lithostatic load. Isopleths of NaCl in the liquid are shown in the liquid plus vapor field by the dashed-double-dot lines. The vertical dot-dash line shows the approximate location of the brittle-ductile boundary at a strain rate of 10^{-14} s^{-1}. CP = critical point, SP = single-phase fluid, L=liquid, V= vapor, S= salt. Diagram adapted from Muntean and Einaudi (2001).

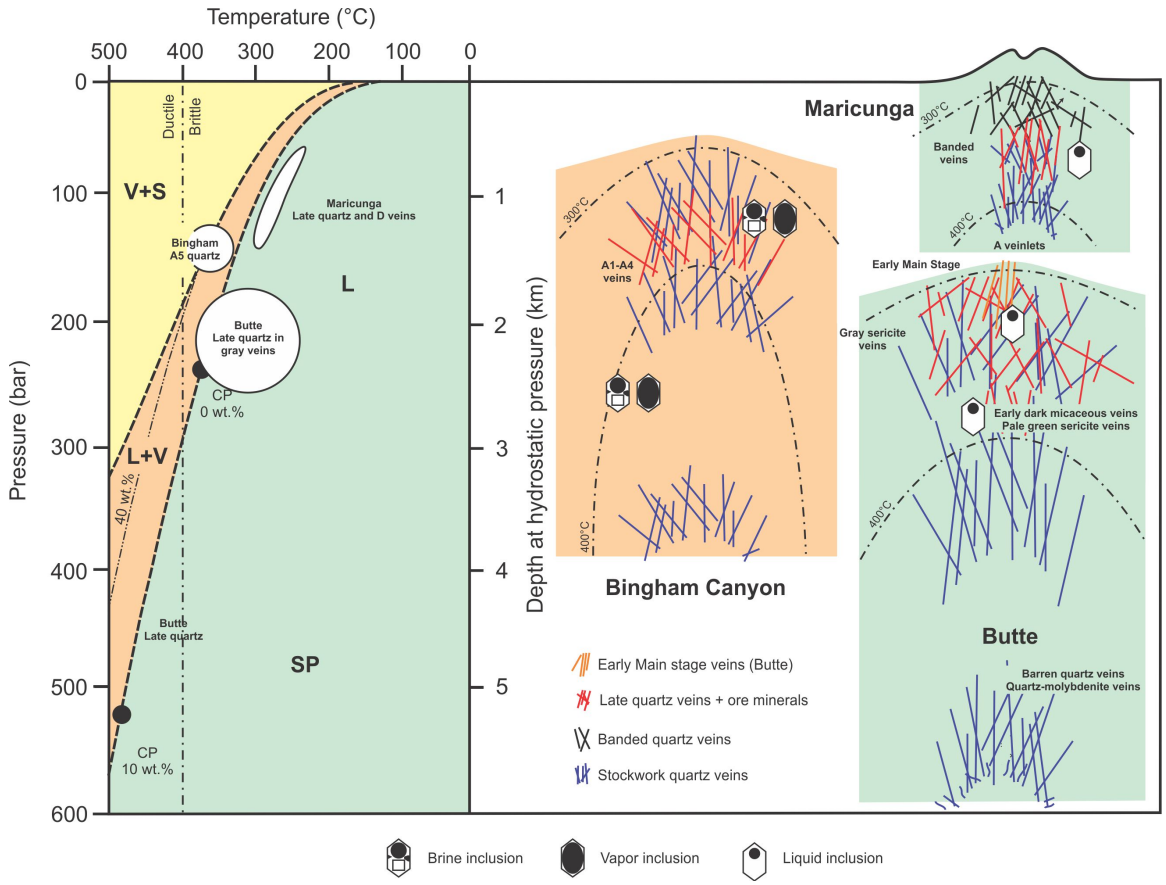

FIG. 3-6: Schematic diagram depicting the pressure-temperature relations during the formation of late red-brown quartz at the Butte, Bingham Canyon, and Maricunga porphyry deposits. Note that ore formation is thought to have occurred at similar conditions. The results of the fluid inclusion petrography are depicted schematically. The different colored regions in the diagram correspond to the phase regions in the H_2O-NaCl phase diagram. Depths are based on a 2.5 g/cm^3 lithostatic load. Isopleths of NaCl in the liquid are shown in the liquid plus vapor field by the dashed-double-dot lines. The vertical dot-dash line shows the approximate location of the brittle-ductile boundary at a strain rate of 10^{-14} s^{-1}. CP = critical point, SP = single-phase fluid, L=liquid, V= vapor, S= salt. Diagram adapted from Muntean and Einaudi (2001).

CHAPTER IV
FLUID INCLUSION AND CATHODOLUMINESCENCE INVESTIGATIONS ON STREAM SEDIMENT SAMPLES: A NEW INTEGRATED EXPLORATION TECHNIQUE FOR PORPHYRY DEPOSITS

4.1 Introduction

Porphyry deposits are significant source of metal ores, supplying most of the world's copper, 50% of the molybdenum, and 20% of the gold (Sillitoe, 2010). The deposits form in suprasubduction and post-subduction environments from hydrothermal fluids associated with the intrusion of felsic to intermediate calc-alkaline magmas enriched in chalcophile metals (Richards, 2009). Vein-hosted and disseminated metal-bearing ores in these deposits occur within well-defined zones characterized by distinct alteration mineral assemblages associated with dense stockworks of quartz veins (Lowell and Guilbert, 1970; Gustafson and Hunt, 1975; Titley and Beane, 1981; Seedorff et al., 2005).

The host rocks of porphyry deposit are intensely altered due to interaction with the magmatic-hydrothermal fluids. Common alteration mineral associations include a core of potassic alteration that is overprinted by sericitic and shallow argillic alteration. With increasing distance from the hydrothermal centre, propylitic alteration of the host rocks prevails (Seedorff et al., 2005). As the hydrothermal alteration halo can extend for several kilometers, alteration mapping is routinely conducted during early stage exploration for porphyry deposits (Seedorff et al., 2005). Alteration mapping can involve various techniques, ranging from remote sensing to field based mapping (Birnie and Francica, 1981; Abrams et al., 1983; Cudahy et al., 2000; Pour and Hashim, 2012). Based on the results of alteration mapping, exploration targets are selected for more detailed and costly investigations such as geophysical surveys or follow-up drilling.

Exploration for porphyry deposits is more challenging in areas of limited exposure, especially in areas where the bedrocks are covered by younger sedimentary rocks or are concealed below thick regolith. In these environments, regional surface-geochemical

surveys have proven to be powerful exploration tools, allowing detection of chemical anomalies associated with partially or entirely concealed porphyry deposits. In particular, BLEG (bulk cyanide leach extractable gold) analysis of the fine fraction of stream sediment samples has been used extensively in the exploration industry to identify metal anomalies associated with concealed deposits (Radford, 1996; Carlile et al., 1998; Leduc and Itard, 2003). Samples are initially taken at a density of one per several square kilometers, after which locations with favorable BLEG anomalies are sampled at a higher density to vector towards the source of the anomaly.

Although regional stream sediment surveys are a standard tool in mineral exploration today, inherent problems in data interpretation exist. In particular, problems may arise during exploration in geologically complex terranes as different deposit types can produce similar geochemical anomalies. In addition, prioritization between a typically large number of anomalies identified in regional surveys has to rely on the assumption that the magnitude of the anomaly correlates with an increased prospectivity of the area in which the sample was taken, which may not necessarily always be the case.

The present study demonstrates that stream sediment geochemical surveys can be supplemented by mineralogical investigations on the same sample materials to provide additional information on the source of an identified geochemical anomaly. It is shown that quartz can be used as a pathfinder mineral in porphyry exploration, as erosion of porphyry deposits liberates large amounts of quartz grains and this mineral is highly stable during weathering and transport in the sedimentary environment. A novel method is described that uses a combination of fluid inclusion petrography and optical CL microscopy to identify porphyry quartz grains in sand samples. Based on two case studies conducted in Haiti and Papua New Guinea, it is shown that the study of quartz in stream sediments can be integrated into real-life exploration programs, providing information critical in porphyry exploration.

4.2 Unique Characteristics of Porphyry Quartz

Reliable identification of porphyry quartz in stream sediments is only possible if certain mineral properties can be identified that are intrinsic to this type of quartz. Although previous studies have shown that the trace element content of quartz and the bulk geochemistry of fluid inclusions or inclusion leachates can be directly related to the quartz origin (Suttner and Leininger, 1972; Bottrell et al., 1988; Heynke et al., 1992; Monecke et al., 2002; Götze et al., 2004; Rusk, 2012), the analytical costs required to determine these mineral properties are prohibitive to allow their routine use to discriminate porphyry quartz grains from other types of quartz in stream sediment samples. For reasons of practicality, discrimination has to rely on petrographic methods that could be used to screen a large number of sand grains quickly. Based on literature review and investigation of quartz veins from a variety of porphyry deposits, including Butte in Montana, Bingham Canyon in Utah, Far Southeast in the Philippines, and the deposits of the Maricunga belt in Chile, it was decided that a combination of fluid inclusion petrography and optical CL microscopy could be used to distinguish porphyry quartz from other types of quartz present in stream sediments.

4.2.1 Fluid Inclusion Inventory of Porphyry Quartz

Previous studies on porphyry deposits have established that hydrothermal vein quartz in porphyry deposits contains a limited range of petrographically distinguishable fluid inclusion types and that the fluid inclusion inventory of porphyry quartz differs significantly from other types of hydrothermal quartz, as well as quartz contained in most common igneous or metamorphic rocks (e.g., Bodnar, 1995). Based on well-established conditions of porphyry formation (Seedorff et al., 2005) and known phase relationships in the H_2O-NaCl system (Driesner and Heinrich, 2007), it can be predicted which types of fluid inclusions can occur in hydrothermal vein quartz from porphyry deposits.

Quartz in stockwork veins formed in porphyry deposits associated with comparably deep intrusions entraps hydrothermal fluids within the single-phase field of the H_2O-

NaCl system (Fig. 4-1). Under those conditions, single-phase hydrothermal fluids, which typically contain between 5 to 7 wt.% NaCl (Redmond et al., 2004; Landtwing et al., 2005, 2010; Klemm et al., 2008; Rusk et al., 2008a; Pudack et al., 2009), have an intermediate density of approximately 0.40 to 0.73 g/cc (Rusk et al., 2008a; Pudack et al., 2009; Landtwing et al., 2010). When entrapped, these fluids form intermediate density fluid inclusions that commonly homogenize by critical or near critical behavior. Under laboratory conditions, intermediate density fluid inclusions consist of a vapor bubble and liquid. The proportion of vapor to liquid in these inclusions may vary, depending on the density of the entrapped single-phase fluid, which in turn depends on the temperature and pressure of entrapment. Intermediate density fluid inclusions are the dominant fluid inclusion type in quartz veins at the Butte porphyry deposit in Montana (Rusk, 2003; Rusk et al., 2004, 2008a; see previous chapter) and the deep roots of the Bingham porphyry deposit in Utah (Landtwing and Pettke, 2005; Landtwing et al., 2005, 2010; Redmond, 2002; Redmond et al., 2004; Redmond and Einaudi, 2010).

Vein quartz in porphyry deposits formed at intermediate to shallow emplacement depths entrap hydrothermal fluids under the pressure and temperature conditions of the two-phase field of the H_2O-NaCl system (Fig. 4-1). Under those conditions, a hypersaline liquid coexists with a low-salinity vapor. Porphyry vein quartz formed within the two-phase field typically contains abundant brine inclusions. At laboratory conditions, these negatively quartz crystal shaped inclusions contain medium to large vapor bubbles and a halite crystal, in addition to other daughter minerals and accidental phases such as chalcopyrite or hematite. Brine inclusions are the principal inclusion type encountered in quartz vein material from shallow depth within the Butte deposit in Montana (Rusk, 2003; Rusk et al., 2004, 2008a), intermediate to shallow depth at Bingham in Utah (Redmond et al., 2004; Landtwing et al., 2005, 2010), the Far Southeast porphyry in the Philippines (Hedenquist et al., 1998), as well as several deposits in the Maricunga belt in Chile (Muntean and Einaudi, 2001).

Vein quartz containing brine inclusions typically also hosts vapor inclusions, which formed by entrapment of the low-salinity vapor coexisting with the hypersaline

liquid within the two-phase field of the H_2O-NaCl system (Fig. 4-1). This inclusion type is abundant and ubiquitous in all above mentioned porphyry systems that formed at intermediate to shallow emplacement depths (Hedenquist et al., 1998; Rusk, 2003; Redmond et al., 2004; Rusk et al., 2004, 2008a; Landtwing et al., 2005, 2010). In addition, vapor inclusions can be entrapped in porphyry systems that form at shallow crustal depth within the vapor plus salt stability field of the H_2O-NaCl system. The most prominent examples of shallow porphyry deposits formed in the vapor plus salt stability field occur in the Maricunga belt in Chile, where quartz veins have a banded macroscopic appearance due to the presence of abundant trails of vapor inclusions (Muntean and Einaudi, 2000, 2001).

In most porphyry deposits, the fluid inclusion types described above homogenize at high temperatures (>400°C), indicating that the host quartz was formed at high temperatures. The veins are typically associated with potassic alteration of the surrounding rocks. The fluid inclusions homogenizing at these high temperatures are equant-shaped, while inclusions entrapped at lower temperatures are commonly more irregular in shape (Bodnar et al., 1985). Thus, even without carrying out microthermometric measurements, a first estimate of the entrapment conditions can be made. It is also important to note that the high-temperature fluid inclusions found in most porphyry quartz veins are not primary in nature and either occur along healed microfractures or as apparently randomly distributed groups of inclusions within the host quartz. Primary fluid inclusion assemblages aligned along growth bands in the quartz are comparatively rare.

A number of studies have shown that quartz veins carrying sulfide minerals typically also contain fluid inclusions that were entrapped at distinctly lower (<400° C) temperatures (Fig. 4-1). These inclusions form assemblages that overprint the earlier formed high-temperature quartz or occur within distinct late quartz crystals that are intergrown with the sulfide minerals (Hedenquist et al., 1998; Rusk and Reed, 2002; Redmond et al., 2004; Landtwing and Pettke, 2005; Landtwing et al., 2005, 2010; Rusk et al., 2006; Redmond and Einaudi, 2010). The late inclusions are irregular-shaped, low-salinity liquid inclusions that were entrapped at temperatures around the critical point of pure water. At

laboratory conditions, these inclusions contain a small vapor bubble in an inclusion volume that is mostly filled with liquid. These inclusions may coexist with vapor inclusions, implying that the hydrothermal liquid forming the liquid inclusions sometimes boiled during entrapment (Hedenquist et al., 1998). With the notable exception of Bingham Canyon, where this type of inclusion has only rarely been recognized in latest overprinting D vein quartz (Redmond et al., 2004; Landtwing et al., 2005, 2010), these late liquid inclusions occur in most porphyry deposits studied in detail and appear to be linked to chlorite-sericite or sericite-pyrite alteration of the host rocks (see previous chapter).

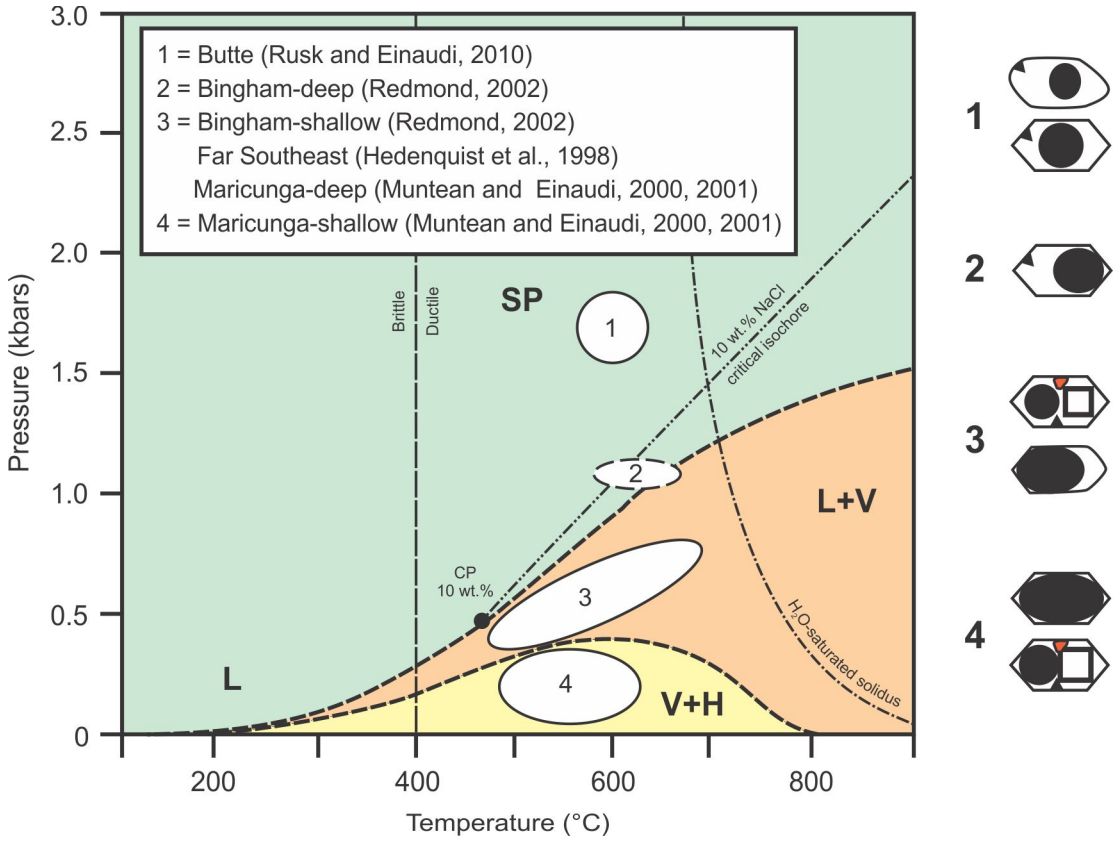

FIG. 4-1: Diagram depicting the microscopic appearance of fluid inclusions at room temperature that were entrapped in porphyry quartz at different pressure and temperature conditions. The different areas in the phase diagram show the areas in which hydrothermal fluids occur as a homogeneous single-phase fluid, as coexisting liquid and vapor, or vapor and halite. At pressures and temperatures below the critical point of pure water, hydrothermal fluids occur as a liquid. The phase diagram is given for a 10 wt.% NaCl solution. H = halite, L = liquid, SP = single-phase fluid, and V = vapor. Diagram modified from Bodnar (1995).

Quartz phenocrysts contained in the porphyritic host rocks may contain all fluid inclusion types described above, forming secondary fluid inclusion trails (e.g., Pudack et al., 2009). Primary melt inclusions may or may not occur in the same crystals.

4.2.2 Cathodoluminescence Characteristics of Porphyry Quartz

In combination with fluid inclusion petrography, optical CL investigations can be used to confidently distinguish porphyry vein quartz from other types of quartz. Although textural relationships in quartz veins from porphyry deposits are complex, as the veins are generally composed of more than one type of quartz (Hedenquist et al., 1998; Penniston-Dorland, 2001; Rusk and Reed, 2002; Redmond et al., 2004; Rusk et al., 2006; Landtwing and Pettke, 2005; Landtwing et al., 2005, 2010; Pudack et al., 2009; Müller et al., 2010; Redmond and Einaudi, 2010; Marsh, 2012; Rusk, 2013), porphyry quartz generally shows a surprisingly consistent CL behavior with no significant differences occurring in different deposits (see previous chapter).

Early quartz contained in stockwork veins hosting fluid inclusions entrapped at high temperatures is typified by a bright CL emission. Color CL investigations show that the quartz exhibits a short-lived light blue CL color. During continued electron bombardment, the short-lived CL turns into a darker blue (see previous chapter). In many deposits, including Bingham Canyon in Utah and Far Southeast in the Philippines, the quartz shows well-developed oscillatory growth zoning under CL (see previous chapter). The different CL zones show variations in the abundances of trace elements such as Ti and Al (Landtwing and Pettke, 2005; Landtwing et al., 2005; Müller et al., 2010; Rusk et al., 2006; Rusk, 2012). In some deposits, including Butte in Montana, oscillatory zoning of the early high-temperature quartz is rare, although the quartz also shows the dark blue CL color characteristic for porphyry vein quartz (see previous chapter).

The late quartz type that is intergrown with the sulfide minerals in most porphyry deposits exhibits a dull CL response (Penniston-Dorland, 2001; Rusk and Reed, 2002; Redmond et al., 2004; Landtwing and Pettke, 2005; Landtwing et al., 2005; Rusk et al.,

2006; Rusk, 2012). Based on optical CL investigations, it can be shown that this late quartz has a short-lived bright blue CL that changes over time to a red or dark brown color. The luminescence response can be observed as an overprint on the earlier formed blue quartz (this study). In addition, quartz showing a red or dark brown CL occurs as late overgrowths on the earlier blue quartz or as fracture fillings in small veinlets. Correlation with the fluid inclusion observations suggests that newly formed red to brown quartz is typically inclusion poor. Due to its inclusion-poor nature, the quartz forming the late-stage red overgrowth or infilling late crosscutting fractures is difficult to identify using fluid inclusion petrography alone.

Quartz phenocrysts contained in the host rocks of porphyry deposits is also typically characterized by a long-lived dark blue to red-blue CL color (Watt et al., 1997; Götze et al., 2001; Peppard et al., 2001; Müller et al., 2005). However, a short-lived CL signal similar to that observed for porphyry vein quartz has not been observed for unaltered quartz phenocrysts in the host rock (Götze et al., 2001).

4.2.3 Criteria to Identify Porphyry Quartz in Stream Sediments

The above review shows that porphyry quartz has characteristic fluid inclusion inventories and CL properties. As a consequence, it should be possible to identify porphyry quartz in stream sediment samples through a combination of both techniques. Based on literature review, a ranking scheme has been developed that assigns levels of confidence in the positive identification of porphyry quartz (Fig. 4-2).

The developed ranking scheme is primarily based on the fluid inclusion characteristics of the quartz grains, with the CL properties of the quartz grains only being a secondary criterion. The ranking scheme takes into account that the analysis of quartz grains can occur in two fundamentally different exploration scenarios. Firstly, exploration could take place in areas of known porphyry outcrops. If vein samples from these outcrops have

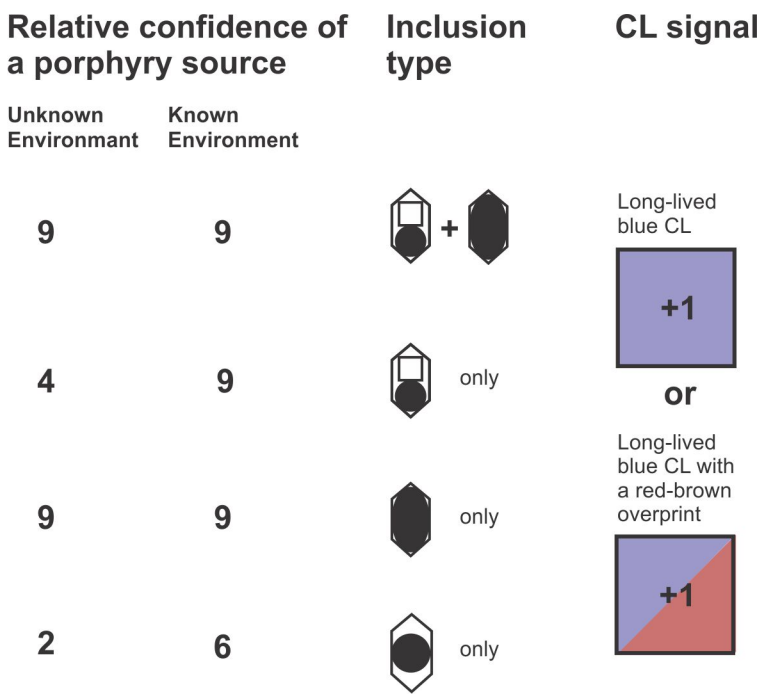

FIG. 4-2: Diagram establishing relative confidence in correct identification of porphyry quartz based on fluid inclusion characteristics and cathodoluminescence behavior.

been studied, a higher confidence can be assigned to certain types of fluid inclusions in the sand grains. In cases where the quartz study would be implemented into large regional surveys, lower confidence levels would be assigned to some inclusion types. This distinction accounts for the fact that quartz grains may be of more geologically diverse origins and that correctly distinguishing between porphyry grains and other types of hydrothermal quartz would be important (Fig. 4-2).

The occurrence of brine inclusions coexisting with vapor inclusions is regarded to be strong evidence for a porphyry source of the quartz grains. This inclusion type is abundant and ubiquitous in intermediate depth porphyry deposits, where hydrothermal fluids occur in the two-phase liquid plus vapor field of the H_2O-NaCl system (Driesner and Heinrich, 2007). The occurrence of a stable blue CL emission or a combination of a stable blue CL and a red-brown overprint would be taken as an additional favorable indication.

Quartz grains containing only brine inclusions would be indicative of a porphyry source if exploration were carried out in areas of known porphyry veins. In such cases, it could be assumed that coexisting vapor has not been trapped or that vapor has been removed under open system conditions prior to quartz formation due to its high buoyancy. If microthermometric investigations would be performed such brine inclusions would likely be characterized by homogenization through halite dissolution. In regional exploration where little is known about the geological source of the sand grains, these inclusions would be assigned a lower confidence level. Brine inclusions could form in deep environments, where the first fluids to be exsolved from intrusions could be highly saline (Cline and Bodnar, 1991). As magmatic quartz grains are commonly blue in CL color (Götze et al., 2001), distinction between quartz from deep granitic intrusions and porphyry quartz would not be readily possible by CL.

A high importance is also assigned to quartz grains containing vapor inclusions only. The occurrence of vapor inclusions only is restricted to shallow magmatic-hydrothermal systems where the hydrothermal fluids occur in the vapor plus salt field of the H_2O-NaCl system (Driesner and Heinrich, 2007), such as shallow porphyries and perhaps certain high-sulfidation deposits associated with porphyritic intrusions. The same confidence is assigned to grains containing only vapor inclusions in both exploration scenarios. A stable blue CL of quartz grains containing vapor inclusions only confirms that the quartz is derived from such a system.

Coexistence of vapor inclusions with liquid inclusions in the same grains would be taken as a negative indication of a porphyry source. Such quartz grains could be derived from a wide range of hydrothermal systems where boiling occurs at lower temperatures, including low sulfidation epithermal systems (cf. Bodnar et al., 1985). Such quartz grains would not be counted in stream sediment surveys.

Similarly, the occurrence of liquid inclusions is not a strong indicator that quartz grains formed in the porphyry environment. Many different types of quartz can contain

liquid inclusions, including quartz formed in low-grade metamorphic environments or hydrothermal quartz formed in epithermal deposits (cf. Bodnar et al., 1985). Although the presence of liquid inclusions in late quartz in porphyry veins is important from a genetic point of view (see previous chapter), it would likely not be possible to identify this type of quartz in stream sediments without textural context such as intergrowth with sulfide minerals or the early quartz that is blue under the CL microscope. For this reason, only quartz grains are registered that contain liquid inclusions in addition to brine and vapor inclusions as these grains are unequivocally derived from porphyry quartz that has been overprinted at lower temperatures by a mineralizing liquid.

The presence of intermediate density fluid inclusions in transported quartz grains contained in stream sediments is regarded as being a moderately strong indicator for the occurrence of a porphyry source in the catchment areas. A higher level of importance is assigned to these inclusions in exploration scenarios where the study of vein samples has already established the occurrence of quartz veins formed at higher pressure conditions. In regional surveys, less importance is assigned to intermediate density fluid inclusions. Petrographically similar inclusion types could occur, for instance, in the pegmatitic phases of deep, unmineralized intrusions (Götze et al., 2004). In addition, orogenic gold deposits can have similar inclusion types as documented at the Muruntau deposit in Uzbekistan (Graupner et al., 2001) and the El Sid deposit in Egypt (Harraz, 2000), although intermediate density inclusions in those deposits typically contain higher CO_2 contents. Combination of the fluid inclusion investigations with CL microscopy increases the confidence in the correct identification of grains containing intermediate density fluid inclusions as porphyry grains (Fig. 4-2).

It is important to note that recognition of intermediate density fluid inclusions is not trivial as the vapor to liquid ratio under room conditions can vary, depending on the pressure at which these inclusions were entrapped. Under many circumstances, intermediate density fluid inclusions may be difficult to distinguish petrographically from liquid or even vapor inclusions. Although microthermometric investigations could be used to

assist in the positive identification of intermediate density fluid inclusion, the use of these techniques would be cost prohibitive in an exploration context.

The difficulty of confidently recognizing intermediate density inclusions in stream sediments represents a major limitation of the approach used in this contribution. The methodology developed here for the identification of porphyry grains in stream sediments will not be effective in the search for porphyry deposits formed in deeper environments where hydrothermal fluids occur in the single-phase region of the H_2O-NaCl system (cf. Driesner and Heinrich, 2007). Identification of deep porphyry systems such as Butte in Montana (Rusk et al., 2008a) using regional stream sediments would probably not be possible.

4.3 Development of an Analytical Protocol for the Study of Stream Sediments

Following the establishment of the unique fluid inclusion and CL properties of porphyry quartz, an analytical protocol was developed to identify porphyry quartz grains in stream sediment samples. Method development was based on the assumption that a large number of stream sediment samples would ultimately need to be processed under routine conditions, requiring the analytical protocol to be fairly simple. At the same time, it was assumed that the typical sample material would be a coarse reject from BLEG analysis as the investigation of the quartz would likely be performed as a follow-up of the geochemical analysis of stream sediments.

4.3.1 Sample Preparation

Initial investigations on the coarse rejects of BLEG samples showed that the sediment samples to be analyzed have a wide grain size range. As fluid inclusion petrography and optical CL microscopy cannot be readily performed on small grains (<250 μm), it was decided that the sediment samples need to be sieved to remove small grains. In addition, the samples needed to be sieved to remove large particles (>500 μm) as a statistically significant number of sand grains (i.e., a minimum of approximately 400 grains)

need to me screened in a standard grain mount for petrographic analysis. Systematic tests showed that the selected grain size range is optimal for the microscopic investigations. No systematic errors were introduced by limiting inspection of sand grains to this grain size range.

The initial investigations also demonstrated that the coarse rejects of BLEG samples are typically not mature and contain a high proportion of rock fragments and a diverse range of mineral grains. As the present study focuses entirely on quartz grains, a method of sample preparation was devised to enrich quartz in the samples prior to the petrographic analysis. Using density separation, the amount of quartz in each sample could be increased significantly. Although pure quartz separates could not be readily obtained, this step of enriching quartz in the samples proved to be critical to optimize time spent on the microscopic analysis of each sample mount.

Based on this framework, the following protocol was developed and implemented for the preparation of the stream sediment samples. Initially, each sediment sample (ca. 500 g) was sieved using a 500 µm mesh to remove granule and larger grains, followed by sieving using a 250 µm mesh. The sand fraction obtained this way was split into subsamples of approximately 100 g weight using a riffle splitter. One subsample was carefully washed to ensure that all dust was removed and used for further treatment.

After drying, the sand sample was split again using a riffle splitter. Two 15 g splits were transferred to 250 ml separatory funnels for density separation. Using lithium metatungstate, a variable density heavy liquid solution, rock and mineral grains having a density below 2.62 g/cc and above 2.73 g/cc were removed (quartz has a density of 2.68 g/cc). After density separation, the two sample splits were recombined and thoroughly washed to recover all lithium metatungstate.

The obtained sand sample was subsequently used to prepare a grain mount. For each sample, between 0.3 and 6 grams of sand (depending on the yield of the density separations) was mixed with epoxy and placed into a 35 mm plastic mold. The mold was

then backfilled with epoxy. The molds were cured for a minimum of 4 hours in a vacuum vessel to remove as many bubbles from the epoxy as possible. This proved to be an important sample preparation step, as automated grain counting (see below) cannot reliably distinguish between sand grains and bubbles in the epoxy. The obtained grain mounts were then prepared as single polished, 60 µm thick sections, mounted on a regular thin section glass slide using UV-cured epoxy to avoid reheating and melting of the grain mounts.

4.3.2 Validation of the Sample Preparation Procedure

The effectiveness of the developed method was tested on a representative stream sediment sample. The weight of the sample was recorded after each sample preparation step and grain mounts were prepared before and after the density separation. Automated mineralogical analysis using QEMSCAN^{TM} technology was performed on these mounts to determine relative mineral abundances before and after each sample preparation step.

Automated mineralogical analysis showed that the unprocessed sample contained 28.6 modal% quartz. The first step of density separation using lithium metatungstate with a density of 2.62 g/cc isolated the bulk of the K-feldspar from the sand samples. Quartz only formed 13.4 modal% of the light fraction, mostly occurring within rock fragments and as intergrowths with lower density minerals (Fig. 4-3A). In the fraction having a density above 2.62 g/cc, quartz constituted 46.7 modal%. Plagioclase formed 13.4 modal% (Fig. 4-3B). The heavy mineral fraction produced by the second density separation step using lithium metatungstate at a density of 2.73 g/cc contained only 6.0 modal% quartz, mostly as a component in rock fragments, as intergrowths with higher density minerals, and as rare isolated quartz grains (Fig. 4-3C). A large amount of chlorite, augite, and calcite was concentrated in the heavy mineral fraction. Following both steps of density separation, the sample having a density between 2.62 and 2.73 g/cc contained a total of 49.0 modal% quartz, in addition to 17.6 modal% white mica (illite or muscovite) and 15.5 modal% plagioclase (Fig. 4-3D). The experiment demonstrates that the density separation was successful, resulting in a significant increase in the relative amount of quartz.

Removal of the majority of calcite grains during the second step of density separation proved to be important prior to the optical CL investigations. Quartz is difficult to image in the presence of calcite as calcite has a bright red-orange CL signal, whereas the CL of quartz is not as intense. A similar outcome might be achieved by treating the sand samples in a dilute HCl solution following the first density separation. However, this preparation method was not tested in the present study in an attempt to keep chemical treatment of the samples to a minimum.

4.3.3 Automated Grain Counting

To allow quantification of porphyry quartz grains in the grain mounts, a method of automated grain counting had to be developed. Although the number of grains in a given mount can be easily determined using QEMSCAN^{TM} technology, a simpler method was adopted for the present study to minimize analytical costs on a per sample basis (backscatter electron imaging of an entire grain mount at 20 μm resolution takes about 15 min instrumentation time on a QEMSCAN^{TM} scanning electron microscope).

Systematic experiments showed that the following procedure can be used effectively to quantify the number of grains in a given polished grain mount. Initially, the grain mount is scanned at high resolution (2400 dots per inch for large grain size fractions and up to 4800 dots per inch for small grain size fractions) using a standard document scanner. The image is converted into black-and-white and then analyzed using the freeware program ImageJ with the plugin CellCounter, which was originally developed for image analysis of biological sample materials. If the grain mounts have been prepared at a low sample-to-epoxy ratio, yielding an overall low grain density in the mount with few individual grains overlapping in clusters, the program ImageJ can reliably determine the number of grains present.

Preventing grain overlap in the mounts is extremely difficult in practice, and so adjustable watershed segmentation is applied to the scanned images prior to counting, in order to methodically differentiate touching and overlapping grains. Following a tech-

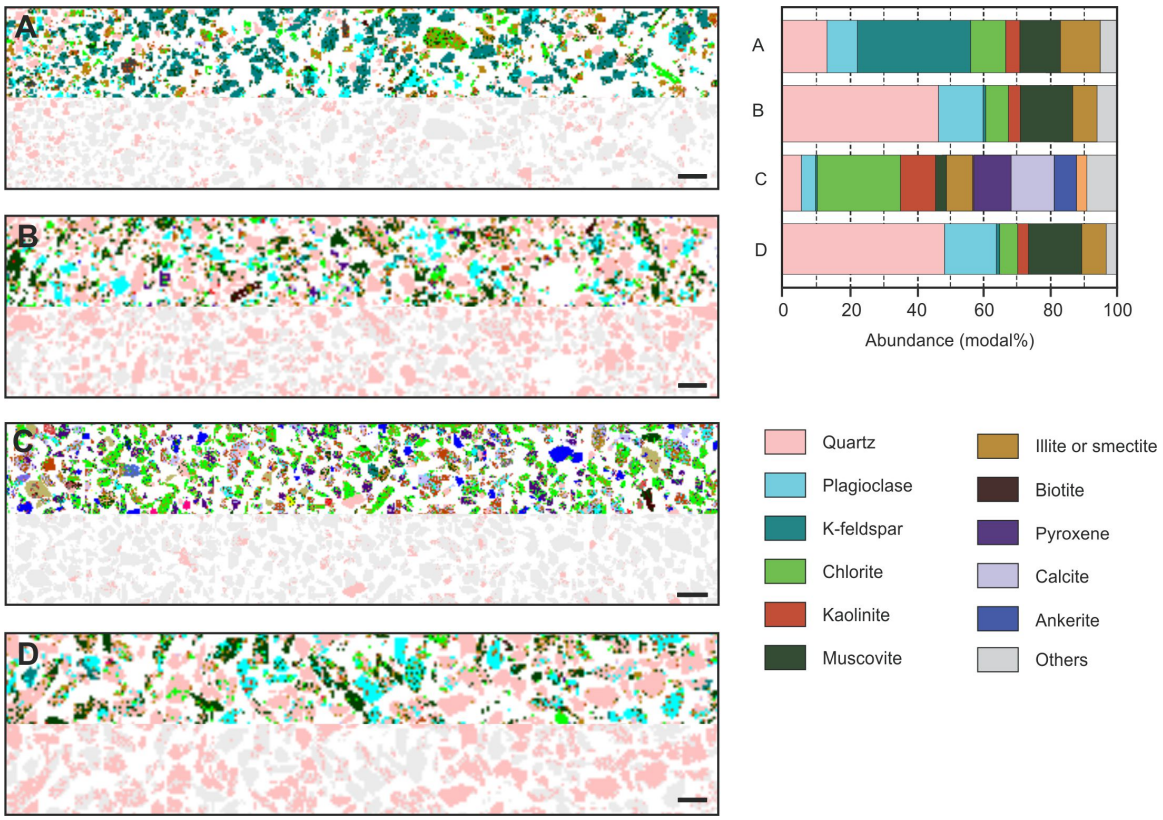

FIG. 4-3: False color image of the grain mounts from sample 66311showing the distribution of quartz grains and other minerals. (A) Mineral distribution of the <2.62 g/cc fraction after the first step of density mineral separation. (B) Mineral distribution of the >2.62 g/cc fraction after the first step of density separation, illustrating enrichment of quartz grains. (C) Mineral distribution of the >2.73 g/cc fraction after the second step of density separation. (D) Mineral distribution of the <2.73 g/cc fraction after the second step of mineral separation. The upper part of the images shows the distribution of all minerals in the respective samples. The lower parts of the images highlight only the distribution of quartz versus other minerals for the same field of view. Scale bars are 500 µm.

nique described by Sime and Ferguson (2003) using an adjustable watershed segmentation plugin developed by Michael Schmid (pers. communication, 2012), ImageJ is used to automatically count the total number of grains in each grain mount. The automated counting technique requires a minimal amount of operator time as the analyses can be performed in approximately one minute per grain mount. Systematic experiments on a series of grain mounts of different size fractions showed that the number of grains identified this way is typically within 5% of the number of grains, as established by manual grain counting.

4.3.4 Microscopic Investigations

To identify porphyry quartz grains, the grain mounts were screened using an Olympus BX51 optical microscope. Based on fluid inclusions petrography using the criteria outlined above, quartz grains interpreted to have been derived from an eroding porphyry deposit were identified and marked on the grain mount, as well as on the digital image of the mount using CellCounter.

Subsequent to the identification of porphyry grains using fluid inclusion petrography, the grain mounts were carbon coated for the CL investigations. Each marked quartz grains was then inspected using a HC5-LM hot cathode CL microscope by Lumic Special Microscopes, Germany, which represents a modified Olympus BXFM-S optical microscope. The microscope was operated at 14 kV and with a current density of ca. 10 μA mm^{-2} (Neuser, 1995). CL images of the quartz grains were captured using a high sensitivity, double-stage Peltier cooled Kappa DX40C CCD camera, with acquisition times ranging from 5 to 10 seconds.

4.4 Case Study at the Vert de Gris Porphyry, Haiti

To test whether the fluid inclusion and CL analysis of quartz grains in stream sediments can be used successfully as an exploration tool, a case study was conducted at the Vert de Gris property in Haiti. A total of 14 vein quartz samples were collected from a known porphyry prospect. In addition, eight stream sediment samples were taken as part of an exploration program within the catchment area.

4.4.1 Geological Setting

The Vert de Gris porphyry Cu-Mo prospect is located approximately 7.5 km southwest of the city of Jean-Rabel in Haiti. The porphyry forms part of the northwestern extension of the Terre Neuve massif, a series of northwest-trending early Paleocene intrusive centers.

The regional setting of the Vert de Gris property has been described by Jones (1918). These authors showed that basement rocks in the area, referred to as the Sierra Group, consist of a series of shales, sandstones, and conglomerates. These are unconformably overlain by a thick sequence of undifferentiated early Tertiary massive to banked limestones that are exposed as a large belt along the south side of the Northern Range. Igneous units in the region cover a broad range of compositions, and include an earliest series of equigranular (locally porphyritic) syenite and granite intrusions that intrude the sedimentary rocks of the Sierra Group, occupying large areas and belts that parallel the axis of the Northern Range. Younger intrusions in the area are composed of quartz diorite. Andesite flows and breccias represent the youngest rocks in the area.

Within the Vert de Gris area, the massive to banked limestone units are cut by a series of intrusions. These include, from oldest to youngest, porphyritic hornblende-biotite tonalite, porphyritic dacite, rhyodacite, and quartz diorite intrusions and intrusive breccias. Dikes of hornblende andesite porphyry also occur (Cheilletz et al., 1978; Nelson et al., 2011). The age of intrusion is interpreted as 67.3 ± 4 Ma (Rb/Sr whole rock isochron age from Cheilletz et al., 1978).

The mineralized zones consisting of bornite, chalcopyrite, and minor molybdenite are centered on the intrusions and are hosted in part within the rhyodacite breccias. Zones of elevated base metal grade are associated with potassic alteration consisting of apatite, K-feldspar, and secondary biotite dated at 57.7 ± 5 Ma (four K/Ar age dates from biotite separates from Cheilletz et al., 1978). Later stage zones of phyllic alteration and a larger scale propylitic alteration halo have also been recognized. A series of tightly clustered crackle and intrusive breccias are present in the south-central part of the prospect area that may relate to quartz veining and mineralization.

4.4.2 Characteristics of Vein Samples

In most quartz vein samples, two distinct generations of quartz occur. Texturally early quartz contains brine and vapor inclusions that were entrapped at high temperatures

(Fig. 4-4A). The quartz shows a short-lived light blue CL that changes to a blue CL emission over time. The quartz grains exhibit well-developed oscillatory zoning (Fig. 4-4B). Early quartz in a single quartz vein sample containing molybdenite hosts abundant intermediate density fluid inclusions (Fig. 4-4C) that show decrepitation textures (Fig. 4-4D; Jim Reynolds, pers. communication). The early quartz in this sample is also characterized by a stable blue CL, but oscillatory growth zoning is only weakly developed (Fig. 4-4F).

Texturally late quartz in the veins is typified by the presence of low-salinity liquid inclusions (Fig. 4-4E). The late quartz is difficult to identify by optical microscopy, but can be readily visualized by optical CL microscopy. The quartz shows a stable red-brown CL. It occurs as an overgrowth on the earlier blue quartz grains, as fracture fill cutting the earlier blue quartz crystals, and as a matrix surrounding pseudoclasts of blue quartz (Fig. 4-4G). Early quartz in the pervasively overprinted areas typically exhibits a purplish CL, suggesting that the formation of the late quartz resulted in the alteration of the CL signal of the earlier quartz generation (Fig. 4-4H). The late red-brown quartz is intergrown with sulfide grains that fill irregular vugs within the quartz veins. The late quartz overprint is most strongly developed in veins associated with pervasive sericitic alteration and in veins containing abundant Cu sulfides.

4.4.3 Characteristics of Stream Sediment Samples

Porphyry sand grains identified in the stream sediment samples from the Vert de Gris area typically contain brine inclusions. These inclusions are usually arranged in clusters and secondary trails, but also occur as isolated inclusions within the quartz (Fig. 4-5A-C). The brine inclusions vary from 2 to 20 μm in size and are negative crystal shaped or irregular. The sizes of the vapor bubbles and halite crystals vary widely between individual sand grains. In some cases, hematite and anhydrite form daughter minerals in the brine inclusions (Fig. 4-5C). An unidentified opaque daughter mineral may also be present.

Some of the porphyry quartz grains host secondary trails and clusters of equant shaped vapor inclusions. The equant vapor inclusions range from <1 to 10 μm in size.

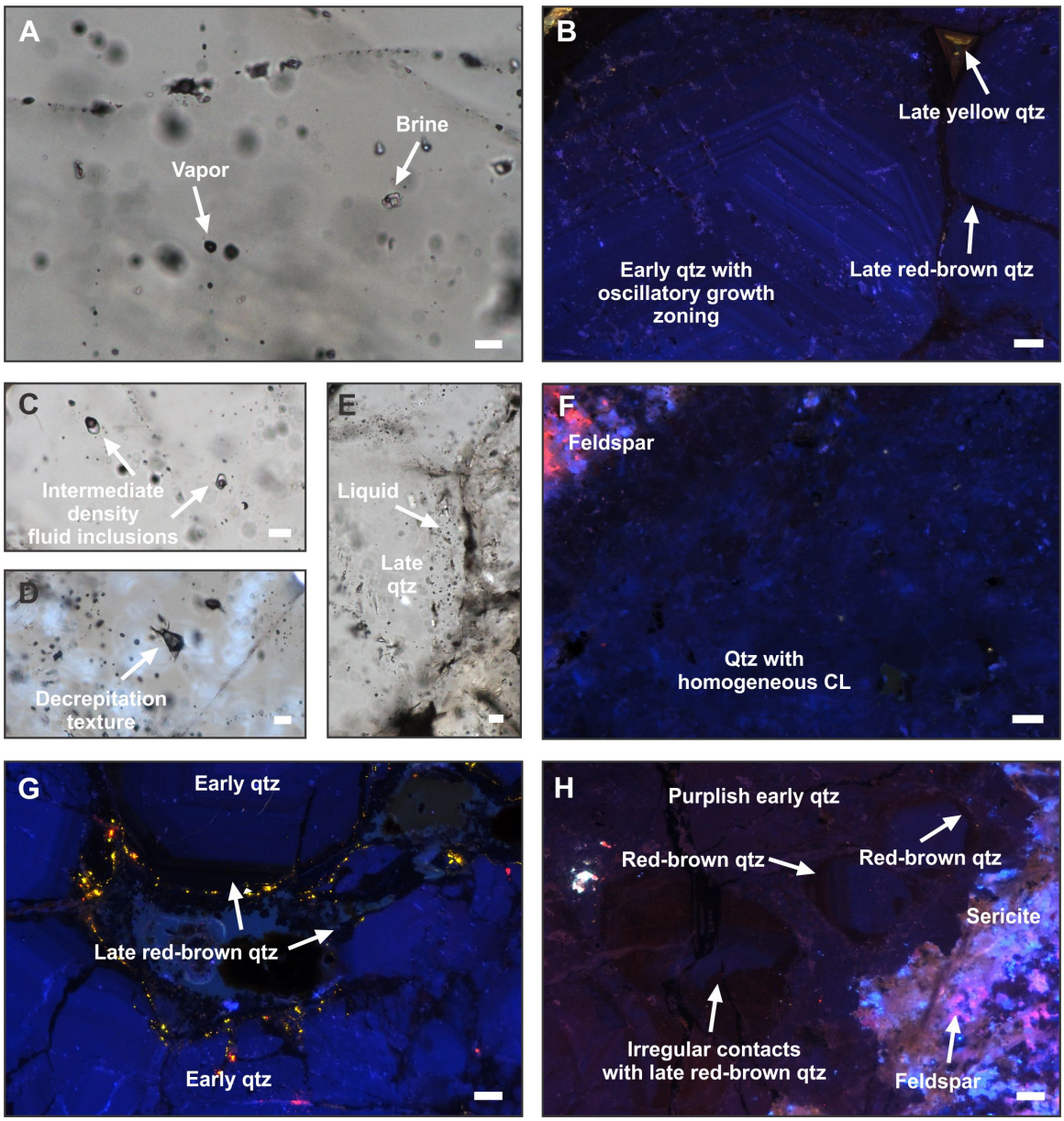

FIG. 4-4: Plane light and CL images showing fluid inclusion assemblages and CL textures encountered during petrography of quartz veins from the Vert de Gris porphyry prospect in Haiti. (A) Secondary brine inclusions and abundant vapor inclusions. Sample 101026-4. (B) Quartz showing a bright luminescence and well-developed oscillatory growth zoning. Sample 101020-1. (C) Intermediate density fluid inclusions. Sample 101027-1. (D) Intermediate density fluid inclusions with decrepitation texture resulting from thermal overprint of the vein. Sample 101021-1. (E) Plane light image of liquid inclusions associate with late quartz. Sample 101021-6. (F) Early quartz showing homogenous blue luminescence. Sample 06112010-2. (G) Late red-brown to non-luminescent quartz occurring as overgrowths and fracture fill after early quartz. Sample 101020-1. (H) Early quartz tinted purple in association with late red-CL quartz. Sample 101021-6. Qtz = quartz. Scale bars for fluid inclusion images are 10 µm. Scale bars for CL images are 100 µm.

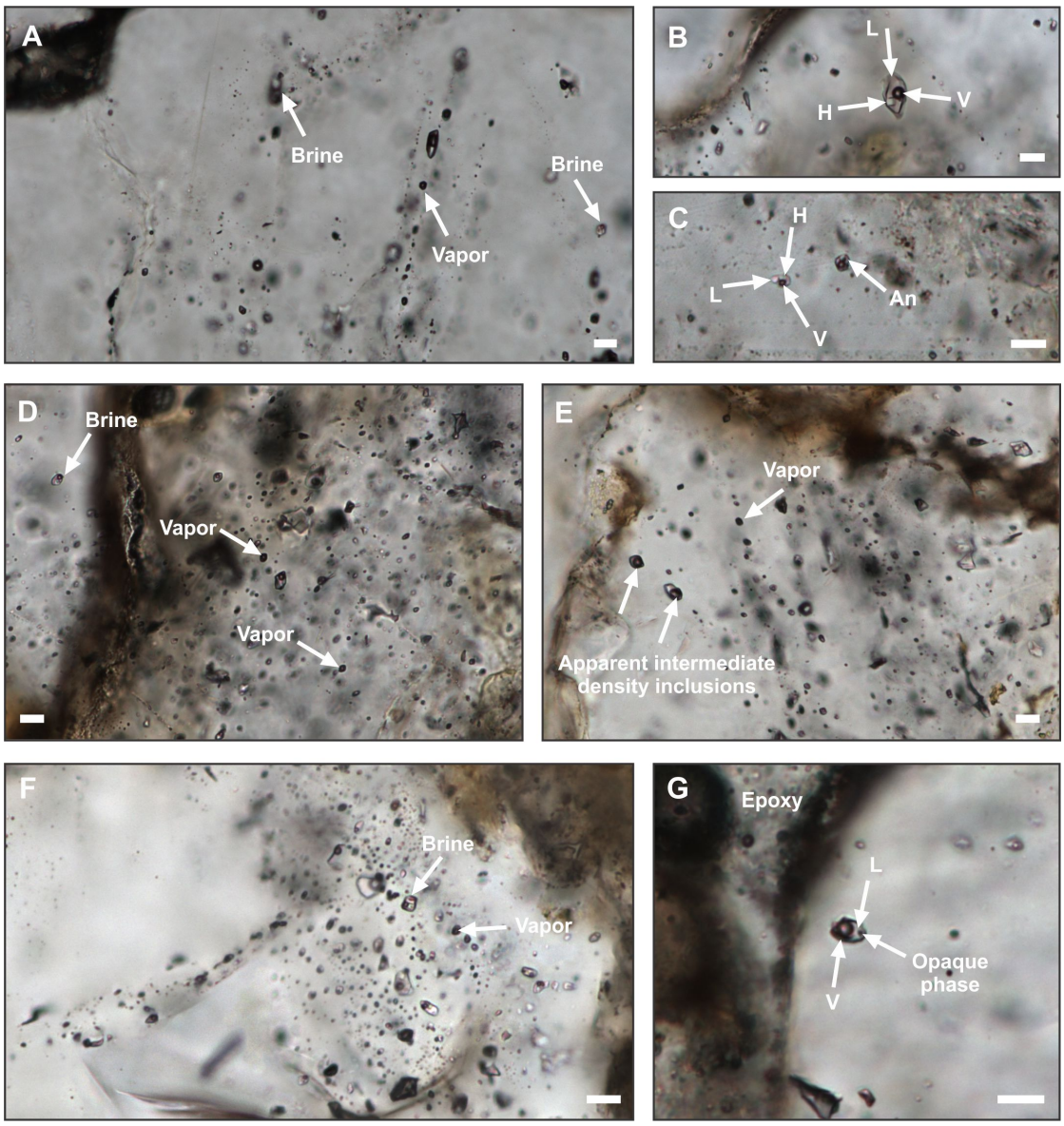

FIG. 4-5: Fluid inclusion characteristics of sand grains from the Vert de Gris porphyry property in Haiti. (A) Secondary assemblage of brine inclusions. Sample NHB-01587, grain MtH87-2_3. (B) Isolated brine inclusion. Sample NHB-01585, grain MtH85-2_12. (C) Rare secondary brine inclusions containing an anhydrite daughter mineral in addition to halite. Sample NHB-01593, grain MtH93-2_3. (D) Clusters of equant-shaped vapor inclusions. The same quartz grain also contains fewer brine inclusions. Sample NHB-01591, grain MtH95-1_29. (E) Secondary trails of equant-shaped vapor and apparent intermediate density inclusions. Sample NHB-01595, grain MtH95-1_36. (F) Rare secondary assemblage of cogenetic brine and vapor inclusions in a single quartz grain. Sample NHB-01595, grain MtH95-2_80. (G) Isolated rectangular-shaped apparent intermediate density fluid inclusion containing a small, unidentified opaque daughter mineral. Sample NHB-01585, grain MtH85-2_26. H = halite. All scale bars are 10 μm.

The vapor inclusions typically occur in the same grains as the brine inclusions (Fig. 4-5D,E) although some sand grains also host vapor inclusions only. In a single grain, a secondary trail of cogenetic brine and vapor inclusions was identified (Fig. 4-5F).

Occasionally, sand grains were identified that contain liquid or apparent intermediate density inclusions that are irregular to rectangular in shape and range from 2 to 15 μm in size (Fig. 4-5E,G). These inclusions sometimes contain a small, unidentified opaque daughter mineral. As pointed out above, microthermometric investigations were not performed on these inclusions to test whether they homogenize by critical or near critical behavior.

All grains showing the fluid inclusion types described above were subsequently examined by optical CL microscopy to provide independent verification that the quartz was correctly identified. Of the grains identified by fluid inclusion petrography, approximately 96% exhibited a blue CL that resembled that of early porphyry vein quartz (Fig. 4-6A,B). The remaining 4% of the grains examined either emitted a dull red CL characteristic of the late quartz in porphyry veins or formed small wedges of quartz within the grain mounts with no exposure on the polished surface, prohibiting CL investigations. In rare cases, feldspar grains containing porphyry-type inclusions were misidentified as quartz grains due to the lack of visible cleavage planes.

Most grains identified as porphyry quartz exhibit a short-lived bright blue CL that faded to the stable blue or red-brown colors mentioned above during prolonged exposure to the electron beam (Fig. 4-6C,D). The quartz grains having a stable blue CL typically show a homogeneous luminescence behavior although grains exhibiting weak growth zoning have also been encountered (Fig. 4-6E). The blue quartz can also be intergrown with the red-brown quartz. The red-brown quartz forms a distinct overgrowth on the blue quartz or occurs along fractures transecting the earlier quartz (Fig. 4-6A). A large number of quartz grains were also intergrown with or enclosed by feldspar grains showing a bright pink or light blue luminescence. These grains may represent hydrothermally altered quartz phenocrysts or are derived from thin veins surrounded by wall rocks (Fig. 4-

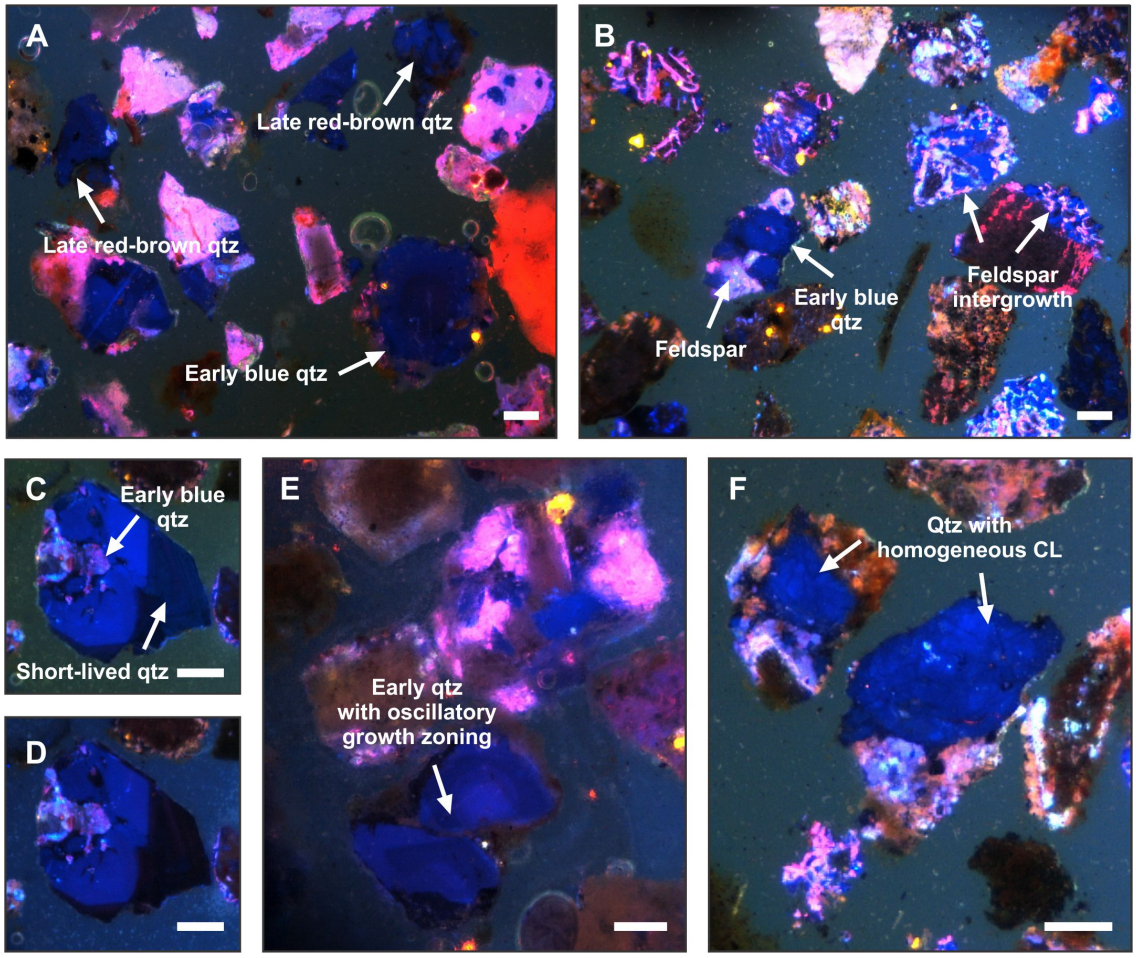

FIG. 4-6: Cathodoluminescence characteristics of sand grains from the Vert de Gris porphyry property in Haiti. (A) Quartz grains with bright blue CL overgrown and crosscut by fractures containing red-brown CL quartz. Sample NHB-01595, grains MtH95-2_77 to 80. (B) Quartz grains with bright blue CL that are intergrown with feldspars showing light blue and bright pink CL. Sample NHB-01593, grain MtH95-2_2. (C) Initial exposure of a quartz grain with a large short-lived blue overgrowth. Well-developed oscillatory growth zoning is faintly visible within the short-lived-blue overgrowth rim. Sample NHB-01593, grain MtH95-2_26. (D) The short-lived blue luminescence fades to a purplish to red-brown luminescence with prolonged exposure to the electron beam, and growth zoning becomes obscured. Sample NHB-01593, grain MtH95-2_26. (E) Blue quartz grains with faintly visible oscillatory growth zoning. Sample NHB-01585, grain MtH95-2_31. (F) Quartz grains exhibiting a homogenous blue luminescence. Sample NHB-01593, grains MtH95-2_14 and MtH95-2_15. Qtz = quartz. All scale bars are 100 µm.

6B). Similarly, grains containing porphyry-type fluid inclusions and exhibiting a homogenous dark blue luminescence could represent magmatic quartz that was affected by hydrothermal alteration (Fig. 4-6F).

4.4.4 Dispersion Characteristics

Using the ranking scheme described above (Fig. 4-2), each grain was assigned a numerical value reflecting confidence in the identification as a porphyry quartz grain. For each sample, the number of grains that potentially could be porphyry grains were recorded, in addition to the number of grains that are definitely porphyry quartz grains (Table 4-1). In addition, the percentage of grains in the grain mounts was recorded. Using the mass fractions recorded during sample preparation, this number was recalculated to derive the concentration of porphyry quartz grains in the bulk BLEG sample (Table 4-1).

At the Vert de Gris porphyry prospect, the lowest concentration of identified porphyry quartz grains occurs in the sample NHB01587 at the southern margin of the target area (Fig. 4-7). This sample contained only 0.2% porphyry quartz grains in the grain mount. Only seven grains were confidently identified as being derived from a porphyry source. Other samples located along the margins of the target area show similarly low concentrations of porphyry grains, ranging from 0.4 to 0.7% (samples NHB001585, NHB001589, and NHB001597). However, these samples contain a significant number of confidently identified porphyry grains.

The concentration of porphyry quartz grains increases downstream of a series of porphyry outcrops that were sampled for their stockwork quartz veins. The stream sediment (sample NHB001591) taken at this location contained 1.7% porphyry quartz grains in the grain mount. The highest concentration of porphyry grains was encountered in sample NHB001595, collected near the center of the target area. This sample contained 5.0% porphyry quartz grains. An additional sample collected adjacent to and at approximately the same elevation contained comparatively lower concentrations of 0.5% porphyry quartz grains (sample NHB01593).

Table 4-1: Summary of stream sediment survey from the Vert de Gris porphyry property in Haiti. All data are for the 250-500 µm and 2.62 to 2.73 g/cc fraction of the BLEG samples.

Sample	Number of grains (ranking <10)	Number of grains (ranking >10)	Porphyry grains in mount	Porphyry grains in bulk BLEG sample
NHB01585	5	29	0.66%	30‰
NHB01587	1	7	0.24%	17‰
NHB01589	0	17	0.60%	14‰
NHB01591	7	29	1.71%	147‰
NHB01593	7	17	0.53%	24‰
NHB01595	22	56	5.04%	374‰
NHB01597	5	21	0.44%	11‰
NHB01599	13	19	1.03%	7‰

The final sample NHB001599 was collected approximately 3.5 km downstream of the intrusive center, and contained significant concentrations of porphyry quartz grains at 1.0% despite its distance from the outcrop areas containing porphyry veins. This finding may indicate that porphyry quartz grains can be distributed far down the drainage pattern. Alternatively, a hitherto undiscovered target could be located between the main intrusive window and the sample location.

4.5 Case Study at Hides Creek, Papua New Guinea

A second case study was conducted at the Hides Creek porphyry project in Papua New Guinea. At this location, three vein quartz samples were collected from the limited outcrops available. In addition, eight stream sediment samples were taken to study the dispersion behavior of porphyry quartz.

4.5.1 Geological Setting

The Hides Creek porphyry prospect is located in the southeastern Morobe district within the Eastern Fold Belt of the New Guinea Orogenic Province (Corbett, 2005). The Morobe district contains several precious metal deposits that have been associated with volcanic activity, including the 5.8 Moz Au Hidden Valley carbonate-base metal deposit located approximately 40 km northeast of Hides Creek, and the 40 Moz Au and 15

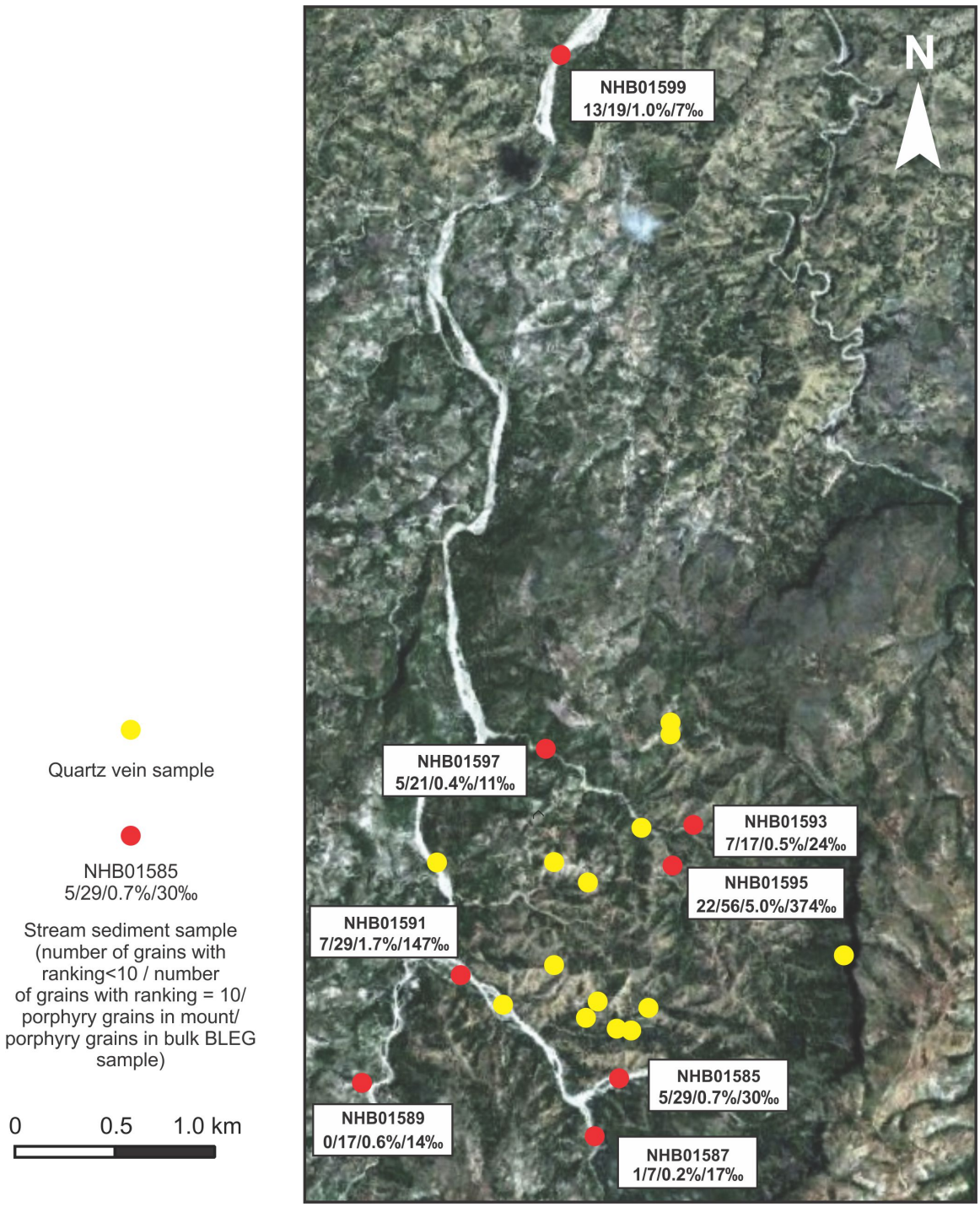

FIG. 4-7: Map of the Vert de Gris porphyry property in Haiti. The map shows the location of stream sediment and vein samples.

million tons Cu Wafi high sulfidation epithermal Au and associated Golpu porphyry Cu-Au deposit at a distance of about 80 km to the north (Singer et al., 2008; Noku et al., 2011). The district is centered on the Wau Basin, between the Neogene sediment-filled Aure Deformation Zone to the west and the overthrust gabbroic to basaltic Papuan ultramafic rocks and underlying Kaindi metamorphic rocks of the Mesozoic Owen Stanley Thrust Belt to the east (Corbett, 2005).

Basement rocks within the Morobe district include blue-grey graphitic slates and phyllites, chloritic and sericitic schists, and minor quartzite and marble occurrences of the Cretaceous Owen Stanley metasedimentary package (Fisher, 1944; Sillitoe et al., 1984). These units are intruded by the mid-Miocene Morobe granodiorite batholith, and host several significant deposits associated with episodic Pliocene dacitic to andesitic quartz-biotite porphyry magmatism that includes the Edie Porphyry (Fisher, 1944, 1945; Page and McDougall, 1972; Corbett, 2005). Older units in the district are overlain by a Pliocene sequence that includes the Bulolo volcanic rocks, consisting of several hundred meters of poorly bedded felsic ignimbrite believed to be the eruptive equivalent of the Edie Porphyry, and the Otibanda Formation, a 700 m-thick sequence composed of shales, mudstones, sandstones, and poorly sorted conglomerates, with minor intercalations of reworked tuff and ignimbrite in the basal strata (Fisher, 1944; Carswell, 1990; Corbett, 2005). The Namie Breccia described by Sillitoe et al. (1984), unconformably overlies the Owen Stanley metasedimentary package and locally occurs as diatremes associated with mineralized intrusive centers. The breccia contains clasts derived from the Owen Stanley metasedimentary package, the Edie Porphyry, the Morobe Granodiorite, and the Bulolo Ignimbrite.

4.5.2 Characteristics of Vein Samples

The three vein samples from the Hides Creek property are characteristic porphyry stockwork veins. The quartz veins consist mostly of anhedral grains that form an interlocking mosaic texture. The wall rock surrounding the veins has been affected by potassic alteration characterized by the presence of secondary biotite. Pyrite in the veins appears

to be paragenetically late and may have formed after the quartz. Where pyrite is present, a weak sericitic overprint of the host rocks can be observed. CL and fluid inclusion petrography revealed that the quartz and pyrite were overprinted by a later event that recrystallized the majority of the quartz in the veins. Calcite is present and appears to occur late in the paragenesis, probably even postdating the recrystallization of the quartz.

Equant-shaped brine and vapor inclusions are the dominant inclusion types in the earliest anhedral quartz identified in the three vein samples. The early quartz and its fluid inclusion signature are best observed in the vein sample 06112010-1 and in early veinlets of sample 06112010-3. Brine inclusions in these samples typically contain an unidentified opaque daughter mineral in addition to the halite crystal. Both brine and vapor inclusions form irregular clusters and secondary trails cutting the anhedral quartz crystals. Secondary trails rarely contain cogenetic assemblages of brine and vapor inclusions (Fig. 4-8A). Primary assemblages of brine inclusions were identified in alignment with oscillatory growth zones visible using optical CL microscopy or occur within clusters of rutile hairs hosted by the quartz (Fig. 4-8B). This confirms that the anhedral vein quartz precipitated from a hypersaline liquid.

In all quartz veins, liquid inclusions have also been encountered in the quartz (Fig. 4-8C). The liquid inclusions form secondary trails crosscutting the anhedral quartz grains, occur as isolated inclusions within texturally late quartz overgrowths, or are found in small euhedral quartz crystals that are generally inclusion poor. In some cases, these isolated liquid inclusions contain small daughter minerals. As these isolated inclusions do not define distinct fluid inclusion assemblages, it is difficult to determine whether these liquid inclusions are primary. Euhedral quartz crystals hosting these inclusions share grain boundaries with pyrite. This late quartz is interpreted to have formed shortly before or during pyrite precipitation.

The early quartz in the three samples is characterized by a short-lived bright blue CL (Fig. 4-8F). During continued electron bombardment, the anhedral quartz grains change to a stable blue CL (Fig. 4-8G). Well-developed growth zoning is common in

veins consisting primarily of early quartz. In many cases, only the cores of these crystals exhibit a stable blue CL, while the rims exhibit a short-lived blue CL that quickly fades towards a red-brown color (Fig. 4-8G). These red-brown rims are in contact with pyrite grains and contain the isolated liquid inclusions. Based on the CL microscopy and fluid inclusion petrography, formation of quartz overgrowths and crystallization of the euhedral quartz containing liquid inclusions that display a red-brown luminescence occurred after the precipitation of the blue quartz containing primary brine inclusions.

The anhedral quartz in the veins occasionally hosts rare clusters and secondary trails of irregularly shaped intermediate density fluid inclusions that contain approximately 50-60 vol.% vapor and a small opaque daughter mineral (Fig. 4-8C,D). Quartz dominated by sub-rounded intermediate density inclusions constitutes the bulk of the vein quartz in sample 06112010-2, and forms a distinct vein in sample 06112010-3 that crosscuts the earlier vein containing pyrite and quartz that hosts brine and vapor inclusions.

Under CL, the quartz in the veins hosting intermediate density inclusions appears to have been extensively recrystallized. It exhibits a homogenous short-lived blue luminescence that fades to a stable blue color. In the late crosscutting vein in sample 06112010-3, narrow domains at the edges of modified grains preserve isolated brine and vapor inclusions, implying that quartz in these veins recrystallized from the earlier quartz types (Fig. 4-8D). Blue quartz with strong oscillatory growth zoning is only rarely observed in quartz grains adjacent to pyrite in sample 06112010-2, in which the earlier vein quartz is almost entirely recrystallized (Fig. 4-8E). This zoned quartz contains preserved brine inclusion clusters. The oscillatory growth zoning is crosscut by secondary trails of intermediate density inclusions (Fig. 4-8C). The textural evidence suggests that early quartz was locally preserved adjacent to pyrite crystals, as these areas were more resistant to the late overprint. Carbonate grains present in the veins are texturally associated with the modified quartz, and show a bright orange luminescence with rare zoning (Fig. 4-8H).

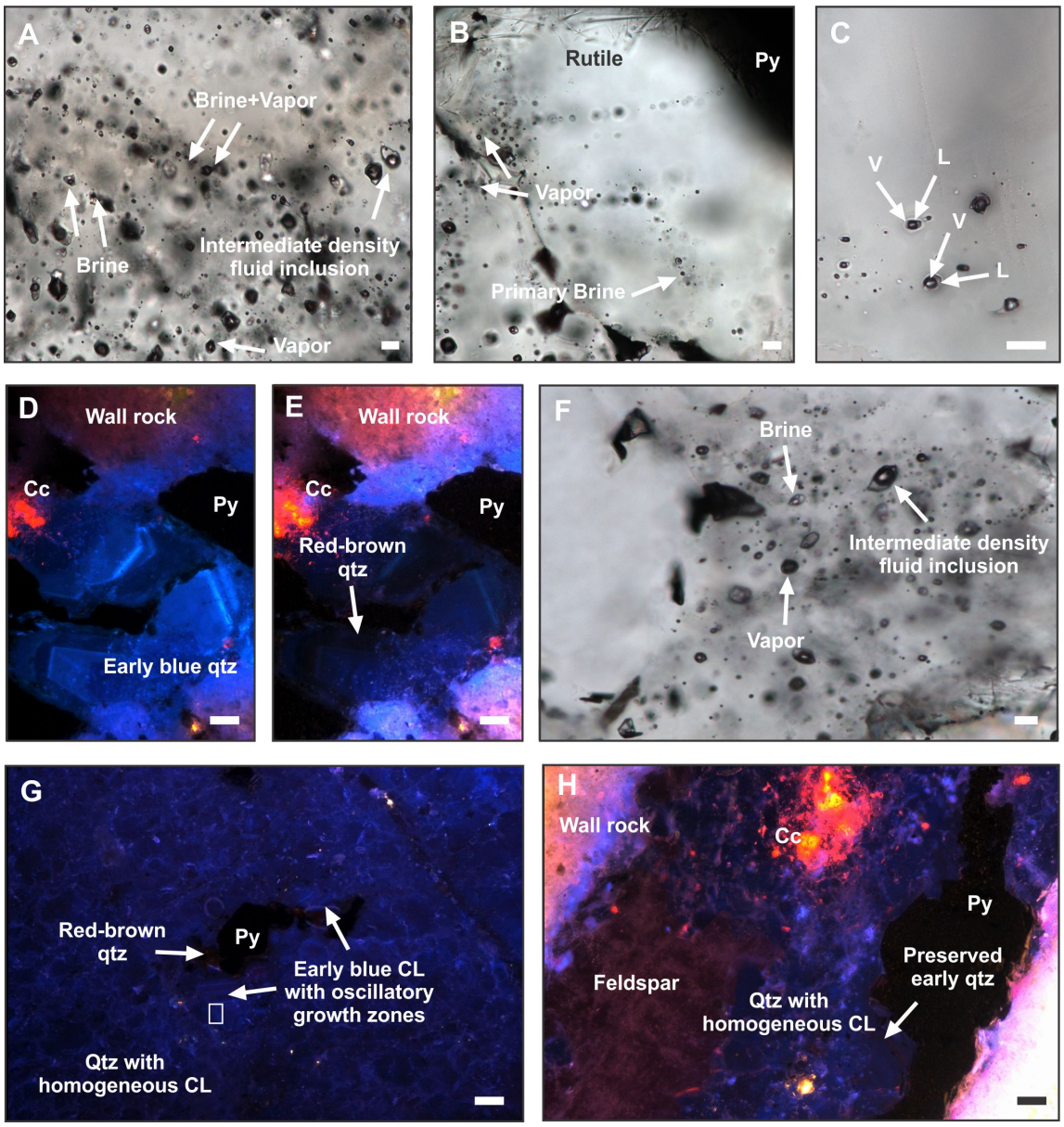

FIG. 4-8: Plane light and CL images showing fluid inclusion assemblages and CL textures encountered during petrography of quartz veins from the Hides Creek porphyry property in Papua New Guinea. (A) Plane light image of typical secondary brine and abundant vapor inclusions. One of the trails consists of cogenetic brine and vapor inclusions. A trail of intermediate density inclusions also occurs. Sample 06112010-1. (B) Primary brine inclusions trapped along growth zones in early quartz. Sample 06112010-3. (C) Trail of intermediate density inclusions in early quartz. Sample 06112010-2. The viewing area shown in the image is marked in plate E. Primary growth zoning is faintly visible at high angle to the trail. (D) Early short-lived bright blue quartz with well-developed growth zoning. The image was taken at 8 seconds of exposure to the electron beam. Sample 06112010-3. (E) The quartz shows a stable blue luminescence. The image was taken after 30 seconds exposure to the electron beam. Sample 06112010-3. (F) Quartz with intermediate density inclusions as well as brine and vapor inclusions. Sample 06112010-3. (G) Quartz exhibiting homogenous short-lived blue luminescence. In some areas, especially close to pyrite, patches of early blue quartz showing oscillatory growth zoning occur. Sample 06112010-2. (H) Vein showing homogenous blue CL. Sample 06112010-3. Cc = calcite, L = liquid, Qtz = quartz, V = vapor. Plane light photomicrograph scale bars are 10 µm. CL photomicrograph scale bars are 100 µm.

4.5.3 Characteristics of Stream Sediment Samples

In comparison to the samples of the first case study from the Vert de Gris property in Haiti, porphyry quartz grains were much less abundant in the stream sediment samples collected at Hides Creek. The vast majority of porphyry sand grains identified contained apparent intermediate density fluid inclusions that form irregular clusters in the quartz grains or occur along distinct secondary trails (Fig. 4-9A,B). The apparent intermediate density fluid inclusions in the sand grains range from 2 to 15 μm in size and vary from irregular to slightly rounded or equant in shape.

In addition to grains hosting apparent intermediate density fluid inclusions, porphyry quartz containing secondary trails and clusters of brine inclusions (Fig. 4-9C) are also present in intermediate abundances in the stream sediments. The size and shape of the brine inclusions entrapped in the quartz grains vary from <2 to 15 μm and from negative crystal to irregular-shaped, respectively. Similarly, the sizes of the vapor bubble and halite crystal are also variable. Brine inclusions rarely contain hematite and/or an unidentified opaque daughter mineral in addition to halite (Fig. 4-9D,E). A single grain from sample 66317 contained a primary assemblage of brine inclusions (Fig. 4-9H). The vapor inclusions in the quartz grains range from <1 to 10 μm in size and are typically equant-shaped. The vapor inclusions generally occur in the same textural context as the brine inclusions (Fig. 4-9F,G).

Many quartz grains in the samples from Hides Creek contain wispy secondary trails of liquid inclusions (Fig. 4-9I). The wispy nature of the fluid inclusion trails may suggest that these quartz grains are of metamorphic origin.

The porphyry grains identified exhibit a short-lived bright blue luminescence under the optical CL microscope. In the case of the quartz grains hosting apparent intermediate density inclusions, this short-lived CL signal changed to stable blue color during continuous electron bombardment (Fig. 4-10A). The stable blue CL is typically homogenous, although grains exhibiting blue luminescence with variably developed oscillatory

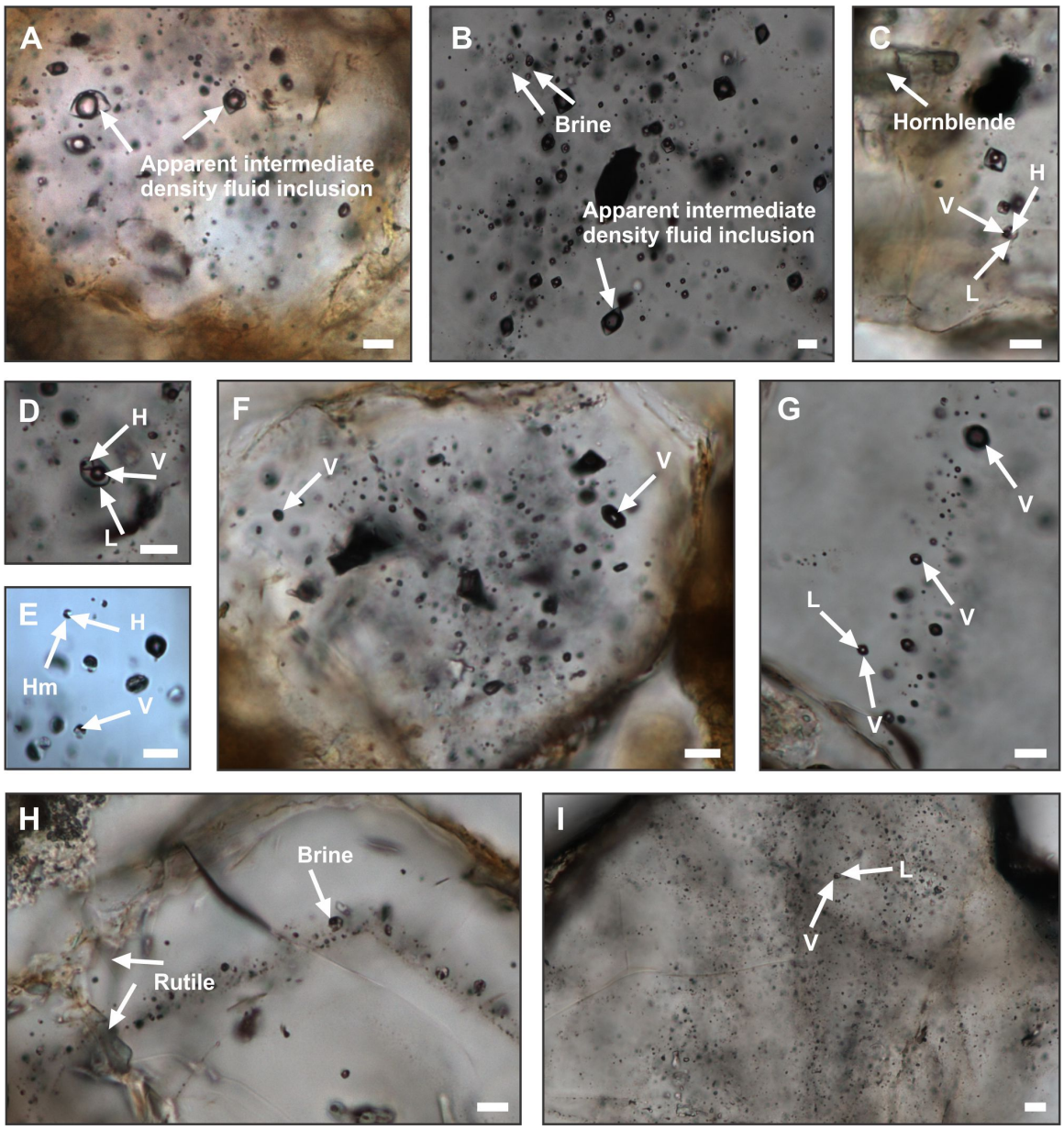

FIG. 4-9: Fluid inclusion characteristics of sand grains from the Hides Creek porphyry property in Papua New Guinea. (A) Cluster of irregularly shaped intermediate density inclusions. Sample 66315, grain HH10. (B) Abundant secondary trails of rectangular-shaped intermediate density inclusions and trails of brine inclusions. Sample 66315, grain HH5. (C) Secondary trail of brine inclusions in a quartz grain intergrown with hornblende. Sample 66317, grain J2. (D) Negative crystal shaped brine inclusion containing an unidentified opaque daughter mineral. Sample 66315, grain HH6. (E) Small brine inclusions with rounded shapes that contain hematite daughter minerals in addition to halite. Sample 66315, grain GG11.2. (F) Irregular cluster of equant-shaped vapor inclusions within a small quartz grain. Sample 66314, grain CC1. (G) Secondary trail of equant-shaped vapor inclusions. Sample 66315, grain FF14. (H) Rare assemblage of primary brine inclusions. Small rutile inclusions are present. Sample 66317, grain K1. (I) Metamorphic quartz grain containing wispy secondary trails of small, irregular shaped liquid inclusions. Sample 66315, metamorphic grain GG. H = halite, L = liquid, V = vapor. All scale bars are 10 μm.

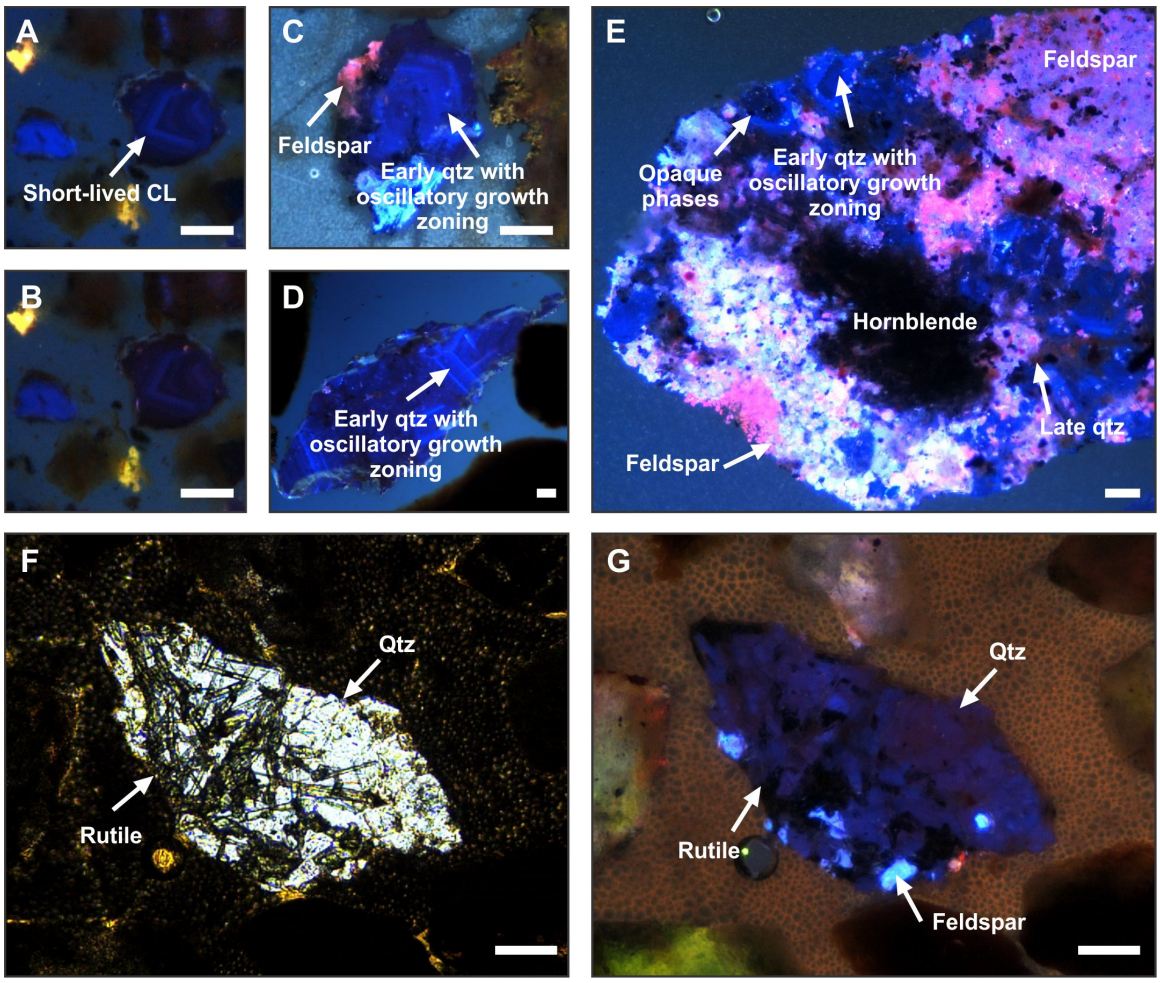

FIG. 4-10: Cathodoluminescence characteristics of sand grains from the Hides Creek porphyry property in Papua New Guinea. (A) Quartz crystal within a rock fragment showing a short-lived bright blue luminescence. Sample 66315, grain FF18. (B) Same quartz grain after continued exposure to the electron beam. The bright blue luminescence has faded to a dull red-brown color. Sample 66315, grain FF18. (C) Bright blue luminescent quartz grain with well developed oscillatory growth zoning. The grain is intergrown with feldspar. Sample 66317, grain K1. (D) Quartz grain showing bright blue luminescence with well developed oscillatory growth zoning. Sample 66315, grain HH6. (E) Rock fragment consisting of quartz (bright blue and dull red), feldspar (pink and light blue), hornblende (non luminescent), and opaque phases (black). Early blue quartz shows variably developed oscillatory growth zoning, and is crosscut by dull red CL quartz filling microfractures. The luminescence of this rock fragment resembles that of veins and wall rock selvages from Bingham Canyon in Utah. Sample 66317, grain J2. (F) Plane light photomicrograph of a quartz grain containing abundant rutile inclusions. The epoxy surrounding the grain is burned due to prolonged exposure to the electron beam. Sample 66317, grain K5. (G) Cathodoluminescence image of the same grain. The quartz exhibits a short-lived blue luminescence and is intergrown with feldspar. Sample 66317, grain K5. All scale bars are 100 µm.

growth zoning are fairly common (Fig. 4-10A,B). Grains containing brine and/or vapor inclusions showed a similar short-lived bright blue CL. The grains have a stable blue CL and commonly show weakly- to strongly-developed oscillatory growth zoning (Fig. 4-10C). Overprinting of the early quartz by later red-brown quartz was only rarely observed. Grains crosscut or overgrown by late red-brown CL quartz were only observed in abundance in samples 66312, 66315, and 66317 (Fig. 4-10D-E). Quartz grains with encapsulated rutile and opaque phases were also identified in sample 66317 (Fig. 4-10F,G).

4.5.4 Dispersion Characteristics

The same procedure described above was used to rank the significance of the sand grains from Hides Creek (Fig. 4-11). The samples collected within the prospect area generally show low percentages of porphyry quartz grains (Fig. 4-11). The highest concentrations of porphyry quartz were encountered in two samples within less than ~1.5 km from the target area. These samples (66315 and 66317) contained 0.6% and 0.2% porphyry quartz and correlate with high BLEG values of 31 and 36.8 ppb Au, respectively. Both samples contain a number of unequivocal porphyry grains.

Samples 66314 and 66316 contained no porphyry quartz grains, despite their close proximity to the target area and high BLEG values of 40.6 and 71 ppb Au, respectively. Follow up field work showed that the sample 66316 was taken close to an outcrop of a quartz vein interpreted to be a low-sulfidation epithermal vein. This suggests that the method developed here can be effectively used to discriminate between geochemical anomalies caused by different styles of mineralization.

4.6 Discussion

4.6.1 Interpretation of Case Studies

The case studies conducted at Vert de Gris in Haiti and the Hides Creek property in Papua New Guinea demonstrate that porphyry-derived quartz grains can be successfully identified in stream sediment samples at low concentrations using the microscopic

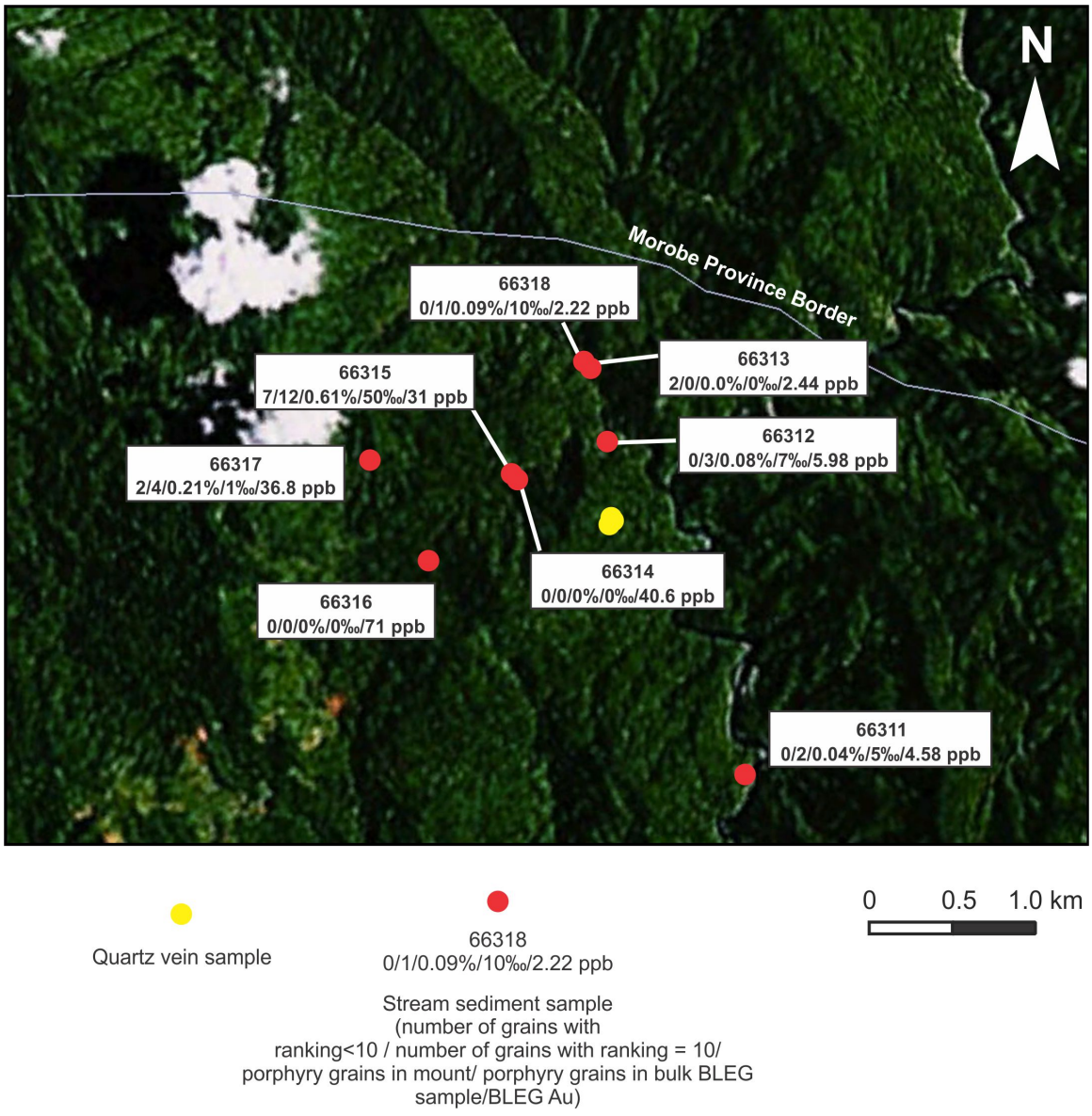

FIG. 4-11: Map of the Hides Creek porphyry property in Papua New Guinea. The map shows the location of stream sediment and vein samples.

Table 4-2: Summary of stream sediment surveys from the Hides Creek porphyry prospect in Papua New Guinea. All data are for the 250-500 μm and 2.62 to 2.73 g/cc fraction of the BLEG samples.

Sample	Number of grains (ranking <10)	Number of grains (ranking >10)	Porphyry grains in mount	Porphyry grains in bulk BLEG sample
66311	0	2	0.04%	5‰
66312	0	3	0.08%	7‰
66313	2	0	0.00%	0‰
66314	0	0	0.00%	0‰
66315	7	12	0.61%	50‰
66316	0	0	0.00%	0‰
66317	2	4	0.21%	1‰
66318	0	1	0.09%	10‰

methods described above and that quantification of the abundance of these grains is possible. As porphyry quartz grains were dispersed up to five kilometers away from the inferred source, quartz can be used as a pathfinder mineral to locate eroding porphyries within the sampled catchment areas.

In addition to the exploration implications, it is important to note that the combination of information gathered from the stream sediments and limited outcrop sampling provides some additional information on the mineralization potential at the two porphyry properties studied.

Early quartz in the veins from the Vert de Gris, Haiti porphyry deposit predominantly contained abundant equant-shaped brine and vapor inclusions. The quartz shows a long-lived stable blue CL emission, with many grains being characterized by oscillatory growth zoning. This fluid inclusion and CL signature of the early vein, therefore, resembles that of quartz veins examined from porphyry deposit formed at intermediate to shallow emplacement depths. Similar fluid inclusion properties and luminescence behavior have been encountered in A-vein quartz from the Bingham Canyon deposit in Utah; Far Southeast in the Philippines; Cavancha, Cerro Casale, and Verde in the Maricunga belt; as well as the shallow levels of the Butte porphyry deposit (see previous chapter). Only one sample from Vert de Gris, a quartz-molybdenite vein, contained intermediate density

fluid inclusions. This fluid inclusion signature resembles that of quartz veins from Butte in Montana (Rusk, 2003; Rusk et al., 2004, 2008a) and the deep roots of the Bingham Canyon ore body (Landtwing et al., 2005, 2010; Redmond et al, 2002, 2004; Redmond and Einaudi, 2010).

The stream sediment samples from the Vert de Gris area consisted of approximately equal amounts of quartz grains hosting brine and vapor inclusions and grains containing apparent intermediate density fluid inclusions. Based on the investigations of the vein samples, it is assumed that the sand grains hosting brine and vapor inclusions and those containing apparent intermediate density fluid inclusions are derived from the erosion of porphyry zones formed at different times and different depths. It is envisaged here that a stockwork of quartz-molybdenite veins occurs within the catchment area that is associated with an earlier intrusion. Veining associated with a later intrusion may have occurred at lower pressure conditions, allowing quartz formation in the two-phase field of the H_2O-NaCl system (cf. Driesner and Heinrich, 2007). This interpretation of multiple periods of vein formation is supported by the presence of early quartz veins containing intermediate density fluid inclusions that show decrepitation textures, which could indicate that the veins have been overprinted by a later thermal event. Porphyry-style mineralization associated with a younger intrusion could have yielded the quartz grains containing brine and vapor inclusions, which typically do not show decrepitation textures. If this is indeed the case, the fluid inclusion signature of the sands would suggest the presence of a zone of quartz veins in the catchment area that formed at intermediate crustal depth, which could be favorable in terms of exploration.

The early blue quartz from the vein samples at the Vert de Gris area is variably overprinted by a later quartz generation that exhibits a dull red to black luminescence, as in the other systems examined during this study (see previous chapter). The red luminescence response is restricted to late quartz overgrowths and healed fractures transecting veins consisting primarily of early blue quartz. Overprinting is pervasive and widespread in the veins at Vert de Gris. In the vein samples, this type of quartz is intergrown with the sulfide minerals. The presence of late quartz in the vein samples is encouraging from an

exploration standpoint, as this quartz forms as part of the mineralizing event in porphyry deposits.

Quartz in early veins from Hides Creek contained several primary assemblages of brine inclusions, and showed a short-lived light blue and a long-lived blue luminescence. Primary inclusion assemblages were aligned with oscillatory growth zoning, confirming that earliest quartz formed from a hypersaline liquid. Quartz in these veins is crosscut by abundant secondary assemblages of brine and vapor inclusions. Several of the secondary assemblages were cogenetic. The fluid inclusion and CL properties of the quartz are similar to early, high-temperature quartz examined from other deposits that formed at intermediate to shallow emplacement depths (see previous chapter).

The early blue quartz at Hides Creek is variably overprinted by a later quartz generation that exhibits a short-lived bright blue luminescence that fades to red or brown. This luminescence behavior is similar to the other systems examined during this study (see previous chapter). The red-brown luminescence response is restricted to late quartz overgrowths and healed fractures transecting early blue quartz. However, the late quartz with red luminescence in the Hides Creek veins is either weakly developed or poorly preserved. It is most clearly observed in the quartz-pyrite veins in sample 06112010-3. The fluid inclusion evidence suggests that the quartz formed from a low-salinity liquid. The lack of pervasive overprinting by late quartz in the vein samples from Hides Creek is somewhat discouraging from an exploration standpoint, as this quartz type typically is present in abundance in porphyry deposits. However, a larger number of vein samples would need to be examined to affirm the overall low abundance of this important quartz type.

Vein samples from Hides Creek show evidence for an unusual late overprint by high-temperature hydrothermal fluids. The quartz veins were partially to pervasively recrystallized during the overprint. Based on the occurrence of intermediate density fluid inclusions, it appears likely that this overprint was caused by a single-phase hydrothermal fluid. The fact that the earlier quartz hosting brine and vapor inclusions is overprinted by

a later fluid that occurs in the single-phase field of the H_2O-NaCl system, as well as the occurrence of cogenetic brine and vapor inclusions in the early quartz suggests that vein formation at Hides Creek occurred at a fairly deep crustal level at conditions close to the solvus of the H_2O-NaCl system (cf. Driesner and Heinrich, 2007). At Bingham Canyon, an approximately 400 m thick transition zone is observed below the ore body, in which quartz veins contain brine and vapor inclusions as well as intermediate density inclusions (Redmond et al., 2004; Landtwing et al., 2005, 2010).

Overprinted and recrystallized veins at Hides Creek show a homogenous long-lived blue luminescence with only few of the grains exhibiting oscillatory growth zoning. The late crosscutting quartz vein in sample 06112010-3 that is composed of quartz hosting mostly intermediate density fluid inclusions exhibits a similar CL and fluid inclusion signature, but with rare domains between the recrystallized quartz grains that contained preserved brine and vapor inclusions from the early quartz. The homogenous blue luminescence observed in samples from both prospects is similar to that described by Sprunt et al. (1978) in metamorphosed quartzite from the Bergell Alps, Switzerland, and the Johnson Springs Formation, California. The quartzite in the study exhibited luminescence that could be correlated with metamorphic grade, in which blue luminescence corresponded to amphibolite-facies metamorphism. In the case of the latest quartz veins at Hides Creek, the inferred conditions of recrystallization are broadly similar. Rusk (2012) also proposed that the CL textures of quartz can be annealed at higher temperatures. The results of the combined fluid inclusion and CL investigations are consistent with the homogeneous blue CL in the quartz from Hides Creek being caused by a high-temperature overprint.

In contrast to the limited number of outcrop samples available, the vast majority of porphyry-derived quartz grains contained in the stream sediments from the Hides Creek property contain apparent intermediate density fluid inclusions. Only few grains hosting brine and vapor inclusions were identified. This confirms the above conclusion that the porphyry veins at Hides Creek formed under conditions close to the solvus of the H_2O-NaCl system, probably comparable to the zone immediately underlying the ore zone

at Bingham Canyon in Utah (Redmond et al., 2004; Landtwing et al., 2005, 2010). If this would be the case, the study of the stream sediment samples implies a fairly deep level of erosion within the region. Unless a potential ore zone at Hides Creek was formed at a deep level like Butte in Montana, it would have to be assumed that most of the ore zone has already been eroded.

4.6.2 Optimization of Analytical Procedure and Areas for Future Improvements

Integration of the method proposed in the present contribution into real-life exploration programs will undoubtedly require further streamlining of the analytical procedure to reduce personnel time and cost for consumables.

Under routine conditions, it appears feasible that the second step of heavy mineral separation removing minerals having a density exceeding 2.72 g/cc could be replaced or supplemented by magnetic separation using a Frantz magnetic separator to further enhance the amount of quartz recovered. It is also important to note that further systematic tests may be required to optimize the sample preparation procedure for stream sediments of different mineralogical composition, which could be the case if different rock types are exposed in the sampled catchment area.

Future method developments should focus on implementing procedures to better characterize the fluid inclusion assemblages contained in the porphyry quartz grains identified. The analysis of daughter minerals contained in the fluid inclusions or direct chemical analysis of the fluid inclusions by laser ablation inductively coupled-plasma mass spectrometry could provide insights into whether the entrapped hydrothermal fluids were metal-bearing or not. Comparison to the signature of known barren and fertile porphyry systems may then permit first-order constraints on the mineralization potential of the eroding source of the porphyry grains.

4.6.3 Implementation in Mineral Exploration Programs

It is envisaged here that the method described in the present contribution can be effectively implemented in regional exploration programs that aim to identify concealed porphyry targets through stream sediment surveys.

In regional geochemical surveys, several hundred to thousand stream sediment samples are typically collected across large land packages at an average sample density of one sample per several square kilometers (Radford, 1996; Carlile et al., 1998; Leduc and Itard, 2003). Following geochemical analysis of these samples, for instance using the BLEG technique, infill samples are collected to increase sample coverage in areas regarded to be favorable. Based on the results of the geochemical analyses of these infill samples, targets are delineated that will be followed up by groundwork or other types of surveys, typically involving geophysical techniques.

In large regional exploration programs, it is crucial to objectively prioritize targets for follow-up work. It is suggested that the porphyry quartz content of the stream sediments could be used as an additional ranking criteria for identifying favorable geochemical anomalies for follow up work. In analogy to the present study, the fluid inclusion and CL investigations would be conducted on the rejects of stream sediment samples already analyzed geochemically. As only samples returning anomalous geochemical results would be of interest, only a small subset of the total number of regional stream sediment samples would need to be analyzed using the methods described in the present contribution. Selecting only a small subset of samples will be beneficial as the integrated microscopic analysis of the stream sediments is time consuming, and therefore, would undoubtedly be more costly than routine geochemical analysis.

Measuring the abundance of porphyry grains in stream sediments will provide an important ranking criterion for samples with anomalous geochemical characteristics. The case study at Hides Creek, where known porphyry showings are located in the sampled catchment area, showed that a broad correlation exists between the BLEG value of a give

sample and the number of porphyry quartz grains identified. However, at least one sample exhibited a significant BLEG anomaly, but lacked the occurrence of porphyry quartz grains. As mentioned above, this apparent discrepancy was explained by follow-up field work that documented outcropping epithermal gold veins close to the sampling location. This example shows that combined fluid inclusion and CL investigations can distinguish between different types of BLEG anomalies, which could prove to be highly useful in exploration. In addition to the numerical value for the abundance of porphyry quartz grains, the calculated level of confidence as discussed above could be used to further rank the significance of geochemical anomalies.

4.7 Conclusions

The present study demonstrates that porphyry quartz is typified by fluid inclusion and CL properties that distinguish this type of quartz from quartz formed in other geological environments. As a consequence, porphyry quartz can be used as a pathfinder mineral in exploration for porphyry deposits. The two dispersion studies conducted in Haiti and Papua New Guinea illustrate that transported porphyry quartz grains can be identified in stream sediment samples following a procedure that enriches quartz with respect to other minerals and rock fragments contained in the sands. Information derived from the study of this pathfinder mineral can be used to rank stream sediment geochemical anomalies, providing a new objective tool that can be used to prioritize targets for more costly follow-up investigations.

The test studies show that the newly developed method can be incorporated into real-life exploration programs. It is suggested that application may be most beneficial in large regional surveys where prioritization between large numbers of identified geochemical anomalies is required. Future research should concentrate on minimizing cost associated with sample preparation and analytical approaches to better constrain the mineralization potential of the eroding porphyry source based on the study of sand grains.

CHAPTER V
CONCLUSIONS

5.1 Introduction

The principle aims of the present study were to (1) establish the characteristics of porphyry quartz through integrated fluid inclusion petrography and optical CL microscopy; (2) compare and contrast the fluid inclusion and CL characteristics of vein quartz from four porphyry deposits previously established to have formed at different depths; (3) refine the model of porphyry deposit formation in the light of these findings; and (4) develop a method for rapidly screening quartz grains in stream sediments using combined fluid inclusion petrography and CL microscopy to confidently identify grains derived from porphyry deposits formed at intermediate depth.

The following section summarizes key observations and interpretations that are based on the laboratory investigations carried out for this research. Recommendations for future work are made that could further improve understanding of the processes involved in the formation of porphyry ore deposits and enhance the analytical protocol and applicability of the exploration method developed over the course of this project.

5.2 Main Findings

The main scientific findings of the present research are:

1) The present study confirms the key finding of Hedenquist et al. (1998) and subsequent workers including Penniston-Dorland (2001), Rusk and Reed (2002), Redmond et al. (2004), Landtwing et al. (2005, 2010), Rusk et al. (2006, 2008b), Klemm et al. (2007, 2008), Pudack et al. (2009), Müller et al. (2010), Redmond and Einaudi (2010), and Marsh (2012) that quartz veins in porphyry deposits consist of multiple quartz generations. As these quartz generations formed at different times during the evolu-

tion of the magmatic-hydrothermal systems, the analysis of quartz can be used to reconstruct fluid evolution in the porphyry environment.

2) In all deposits studied, the earliest quartz generation recognized formed at high temperatures (>400°C) and lithostatic pressure conditions. Vein opening under these conditions must have occurred through hydraulic fracturing, with the open space created being transient in nature. This early quartz type is characterized by a short-lived bright blue CL emission that changes to a long-lived blue CL during continuous electron bombardment. The quartz may show oscillatory growth zoning. In all deposits investigated, early quartz precipitation is associated with potassic alteration of the wall rocks. At Far Southeast, early quartz showing a blue CL emission is characterized by high Ti concentrations.

3) At Far Southeast, a second generation of quartz was recognized that has a short-lived bright blue CL that changes to a stable red-brown CL emission during continued exposure to the electron beam. This quartz generation appears to have formed at intermediate temperatures and possibly under hydrostatic pressure conditions. The quartz has elevated Al and K concentrations. Limited data suggests that the irregularly shaped brine inclusions of this quartz generation homogenizing through disappearance of the salt crystal. Identification of this quartz generation and its petrographic characteristics represents one of the key findings of the present study. Although not yet identified as a separate quartz generation in other deposits, literature review suggests that fluid inclusions with similar homogenization behavior are common in other porphyry deposits (Reynolds and Beane, 1985).

4) In all deposits investigated, the latest quartz generation is typified by short-lived bright blue CL and a stable red-brown CL emission. This quartz generation general lacks fluid inclusions. The evidence suggests that this quartz was formed at low temperatures (<400°C) at hydrostatic or vaporstatic pressure conditions. At Far Southeast, this late quartz generation has low abundances of key trace elements such as Ti, Al, and K. The late quartz occurring in the investigated porphyry deposits is typically in

close textural association with hypogene sulfide minerals and may have formed immediately before or during sulfide deposition. This suggests that hypogene mineralization in the porphyry environment formed late in the paragenesis at temperatures below ~400°C. The late quartz generation is associated with chlorite-sericite or sericite-pyrite alteration at porphyry deposits such as Butte in Montana and Far Southeast in the Philippines, where the ore-forming fluid was a low-salinity liquid. Bingham Canyon in Utah appears to be an exception as late quartz formation occurred under biotite stable conditions from a hypersaline liquid.

5) The porphyry deposits investigated in this study were emplaced at different crustal depth, which impacts the phase behavior of the hydrothermal fluids (single-phase fluid, two phase hypersaline liquid plus vapor, or vapor plus salt). Despite these differences in the fluid properties, it is remarkable that similar textural and paragenetic relationships can be observed in the quartz veins and that the overall evolution of the hydrothermal systems is comparable across all deposits (two main stages in all deposits with the possibility of a third stage as observed at Far Southeast; hypogene mineralization associated with the formation of low-temperature quartz). This suggests that precipitation of the hypogene sulfide minerals is primarily related to the temperature dependent solubility of the metal complexes, with the phase behavior of the hydrothermal fluids only being of secondary importance.

6) The observed two-stage evolution of porphyry systems (or perhaps three stages as suggested by the study at Far Southeast) has significant implications to the understanding of the link between the porphyry and epithermal environments. The results of the present study confirm the findings of Hedenquist et al. (1998). These authors demonstrated that acid-type alteration in the epithermal environment and hypogene epithermal mineralization do not occur from the same fluids at the same time.

7) The present study shows that quartz as a mineral is susceptible to hydrothermal alteration. A series of alteration processes is recognized in the case of the vein quartz, ranging from the modification and quenching of the CL signal of preexisting quartz

through changes in the trace element abundances to structural reorganization resulting in the formation of subgrains or wholesale recrystallization. It is shown that fluid inclusions can be inherited from unaltered quartz to its intensely altered equivalents without notable changes to their petrographic appearance. Formation of multiple quartz generations within a single vein resulted in complex overprinting and alteration textures. The complex textural relationships are difficult to interpret without the aid of integrated fluid inclusion petrography, CL microscopy, and electron microprobe mapping.

8) The findings of this research also highlight the fact that identification of multiple quartz generations in a given vein and correct interpretation of textural and paragenetic relationships is not possible at the hand-specimen scale and difficult to achieve through standard optical microscopy. This casts doubt on genetic models of porphyry formation that are only based on macroscopic observations.

The present study has the following exploration implications:

1) The present study shows that exploration strategies can be built on the fact that early quartz in porphyry deposits formed at intermediate depths always has a distinct fluid inclusion inventory (brine and coexisting vapor inclusions) and is typified by a blue CL color. It is shown that quartz grains that originated from an eroding porphyry can be confidently identified in stream sediments through combined fluid inclusion petrography and CL microscopy. A methodology to identify these grains has been developed that can be incorporated into BLEG exploration programs. The analytical steps, which include grain size separation, quartz enrichment through heavy liquid separation, and preparation of thick sections, have been optimized for routine application. Overall, the time and cost involved on a per sample basis is comparable to the analysis of till samples in diamond exploration.

2) Dispersion studies conducted at Vert de Gris in Haiti and Hides Creek in Papua New Guinea show that porphyry quartz grains can be traced up to several kilometers

downstream of the source. The abundance of porphyry grains increases systematically towards the eroding porphyry. This suggests that quantification of the number of porphyry grains in stream sediments can be effectively used for vectoring purposes.

3) The high numbers of porphyry grains in the stream sediments correlate with the occurrence of high BLEG Au values. In the case of the Hides Creek property in Papua New Guinea, one high BLEG Au value did not correlate with the occurrence of porphyry quartz in the stream sediment. Based on observations in the field, it is likely that the BLEG Au anomaly resulted from a nearby epithermal showing. This indicates that the developed method can potentially be used to differentiate between different sources of Au causing BLEG anomalies in regional surveys.

4) It is demonstrated that fluid inclusion petrography on surface grab samples can be used to predict the crustal level at which the source pluton was emplaced and the erosion level of the source porphyry. At Hides Creek, the porphyry body was probably deeply emplaced where hydrothermal fluids occur as single-phase fluids. The level of erosion is deep and a potential ore body may already have been eroded, producing significant BLEG anomalies in the drainage pattern. The conclusions drawn from the fluid inclusion work are unique and highlight the importance of fluid inclusion petrography during early stage exploration.

5) At Vert de Gris in Haiti, brine and vapor inclusions were the predominant fluid inclusions encountered in surface grab samples. This suggests that the porphyry veins were formed at an intermediate crustal level and that the erosion progressed to intermediate depths. The fluid inclusion and CL signature of the porphyry quartz from Vert de Gris is comparable to Bingham Canyon in Utah and Far Southeast in the Philippines (cf. Hedenquist et al., 1998; Redmond et al., 2004; Landtwing et al., 2005, 2010). The results of the stream-sediment analysis indicate partial erosion of the orebody. Significant follow-up work is recommended, as the ore zone may be exposed at surface, if present, which is favorable for open pit mining.

6) The case studies at Hides Creek and Vert de Gris highlight that the cost added for quartz analysis of BLEG samples is minimal when compared to the wealth of information that can be gained from it. The technique can be most effectively implemented into early stage regional exploration to prioritize BLEG anomalies for follow-up work.

5.3 Recommendations for Future Work

Based on the results of the present study, the following recommendations for research are made:

1) Careful analysis of quartz veins from Far Southeast has shown that three distinct types of quartz occur in the veins. The first quartz generation formed at high temperatures (potassic alteration) under lithostatic conditions. The second quartz generation also formed at intermediate temperatures, but likely following a shift to hydrostatic conditions. The third quartz generation is closely associated with ore minerals and precipitated at distinctly lower temperatures (chlorite-sericite alteration) and hydrostatic pressure conditions. Although the second generation of quartz is difficult to recognize without the help of integrated fluid inclusion petrography, CL microscopy, and microprobe mapping, formation of this quartz generation could be an important part of the evolution of the magmatic-hydrothermal system. In the other porphyry deposits investigated, quartz generations equivalent to the first and third quartz generations at Far Southeast were also recognized. Future work on the samples should focus on establishing whether the second type of quartz is also present in other porphyry deposits.

2) Spatially resolved oxygen isotopic research should be conducted on the vein quartz from Far Southeast to test whether the different generations of quartz can also be distinguished isotopically. It would also be critical to determine whether alteration of quartz can reset its isotopic signature. This would have important implications for the use of oxygen isotope research on hydrothermal quartz veins.

3) The geochemical investigations on the vein quartz should be expanded to other porphyry deposits to better understand commonalities and differences in the geochemistry of the different quartz generations across a range of deposits. Future research should also apply LA-ICP-MS investigations on quartz to broaden the spectrum of elements that can be analyzed.

The following recommendations for future work to improve the application of fluid inclusion petrography and CL microscopy in the study of stream sediments are made:

1) Future studies seeking to apply the methodology developed during for this research should attempt to enhance the characterization of porphyry-derived quartz grains identified in the fluvial setting. The method outlined in the present thesis is sufficient to identify deposits formed at intermediate crustal depths that formed in the two-phase field of the H_2O-NaCl system, where hypersaline liquids coexist with vapor. Murakami et al. (2010) suggested that a more rigorous characterization of the density of hypersaline liquid and coexisting vapor inclusions can be used to predict the Au/Cu ratio of a potential mineralized porphyry system.

2) Future research on sand grains could involve a more detailed characterization of daughter minerals contained in brine inclusions. Identification of chalcopyrite daughter crystals in inclusions contained in fluvial quartz grains may have significant implications in real life exploration.

3) It is recommended to test the viability of LA-ICP-MS investigations on fluid inclusions contained in fluvial quartz grains. This technique could be used to quantitatively determine the Cu content of individual fluid inclusions. Analysis of barren and mineralized systems should be conducted to establish threshold Cu concentrations in different types of fluid inclusions that can be used to differentiate between barren and mineralized systems. Although routine implementation of LA-ICP-MS analysis of fluid inclusions into real-world exploration programs may not be feasible at present,

methodology development will progress in coming years, making this technique more accessible and reliable to use in exploration programs.

4) Multiple feldspar grains in the sand samples were misidentified as quartz grains during the initial fluid inclusion petrography, based on their fluid inclusion content and lack of obvious cleavages. These feldspar grains were quickly identified during follow-up CL investigations and were excluded from the dataset presented in the exploration maps. While these grains are largely irrelevant to the present study, their initial identification based on the presence of porphyry-type inclusions indicates that the method of identifying transported porphyry quartz grains in the fluvial setting could be extended to feldspar as well. At the same time, the use of other CL active minerals as pathfinder phases should be tested. It is possible that minerals such as apatite can also be used as pathfinders in the porphyry environment.

5) Attempts should be made to extend the developed methodology of analyzing stream sediments to other deposit types, especially deposits that occur in the same geological setting as porphyry deposits. In particular, it is recommended to conduct systematic investigations on barren and mineralized lithocaps to test whether quartz formed or altered in the high-sulfidation environment could be confidently identified using the same methodology. If this would be the case, the methodology developed in the present study could be integrated into larger regional exploration programs for multiple deposit types.

REFERENCES CITED

Abrams, M.J., Brown, D., Lepley, L., and Sadowski, R., 1983, Remote sensing for porphyry copper deposits in southern Arizona: Economic Geology, v. 78, p. 591–604.

Arancibia, O.N., and Clark, A.H., 1996, Early magnetite-amphibole-plagioclase alteration-mineralization in the Island copper porphyry copper-gold-molybdenum deposit, British Columbia: Economic Geology, v. 91, p.402–438.

Arribas, A., Jr., Hedenquist, J.W., Itaya, T., Okada, T., Concepción, R.A., and Garcia, J.S., Jr., 1995, Contemporaneous for-mation of adjacent porphyry and epithermal Cu-Au deposits over 300 ka in northern Luzon, Philippines: Geology, v. 23, p. 337–340.

Birnie, R.W., and Francica, J.R., 1981, Remote detection of geobotanical anomalies related to porphyry copper mineralization: Economic Geology, v. 76, p. 637–647.

Bodnar, R.J., 1995, Fluid-inclusion evidence for a magmatic source for metals in porphyry copper deposits, *in* Thompson, J.F.H., Magmas, fluids, and ore deposits: Mineralogical Association of Canada Short Course Series, v. 23, p. 139–152.

Bodnar, R.J., Reynolds, T.J., and Kuehn, C.A., 1985, Fluid inclusion systematics in epithermal systems, in Berger, B.R., and Bethke, P.M., eds., Geology and geochemistry of epithermal systems: Reviews in Economic Geology, v. 2, p. 73–98.

Bottrell, S.H., Yardley, B., and Buckley, F., 1988, A modified crush-leach method for the analysis of fluid inclusion electrolytes: Bullétin de Minéralogie, v. 111, p. 279–290.

Brimhall, G.H., Jr., 1977, Early fracture-controlled disseminated mineralization at Butte, Montana: Economic Geology, v. 72, p. 37–59.

Brimhall, G.H., Jr., 1979, Lithologic determination of mass transfer mechanism of multiple-stage porphyry copper mineralization at Butte, Montana: vein formation by hypogene leaching and enrichment of potassium-silicate protore: Economic Geology, v. 74, p. 556–589.

Brown, A.J., and Rayment, B., 1991, Refugio gold project, Chile: Mining Magazine, v. 165, p. 306–312.

Carlile, J.C., Davey, G.R., Kadir, I., Langmead, R.P., and Rafferty, W.J., 1998, Discovery and exploration of the Gosowong epithermal gold deposit, Halmahera, Indonesia: Journal of Geochemical Exploration, v. 60, p. 207–227.

Carswell, J.T., 1990, Wau gold deposits, *in* Hughes, F.E. ed., Geology of the mineral deposits of Australia and Papua New Guinea, Australasian Institute of Mining and Metallurgy Monograph 14, p. 1763–1767.

Cheilletz, A., Kachrillo, J.J., Sonet, J., and Zimmerman, J.L., 1978, Pétrographie et géochronology de deux complexes intrusifs à porphyre cuprifères d'Haïiti. Contribution à la connaissance de la province cuprifère laramienne de l'arc insulaire de Grande Antilles: Bulletin Société Géologique de France, Serie 7, v. 20, p. 907–914.

Chang, Z., Hedenquist, J.W., White, N.C., Cooke, D.R., Roach, M., Deyell, C.L., Garcia, J., Jr., Gemmell, J.B., McKnight, S., and Cuison, A.L., 2011, Exploration tools for linked porphyry and epithermal deposits: Example from the Mankayan intrusion-

centered Cu-Au district, Luzon, Philippines: Economic Geology, v. 106, p. 1365–1398.
Clark, A.H., 1993, Are outsize porphyry copper deposits either anatomically or environmentally distinctive ? *in* Whiting, B.H., Hodgson, C.J., and Mason, R., eds., Giant ore deposits. Society of Economic Geologists Special Publication, no. 2, p. 213–283.
Claveria, R.J.R., 2001, Mineral paragenesis of the Lepanto copper and gold and the Victoria gold deposits, Mankayan mineral district, Philippines: Resource Geology, v. 51, p. 97–106.
Cline, J.S., and Bodnar, R.J., 1991, Can economic porphyry copper mineralization be generated by a typical calc-alkaline melt? Journal of Geophysical Research, v. 96, p. 8113–8126.
Concepción, R.A., and Cinco, J.C., Jr., 1989, Geology of Lepanto Far Southeast gold-rich porphyry copper deposit, Mankayan, Benguet, Philippines: International Geological Congress, 28th, Washington, D.C., 9–19 July 1989, Proceedings, p. 319–320.
Cooke, D.R., Hollings, P., and Walshe, J.L., 2005, Giant porphyry deposits: Characteristics, distribution, and tectonic controls: Economic Geology, v. 100, p. 801–818.
Corbett, G., 2005, The geology and mineral potential of Papua New Guinea, *in* Williamson, A., and Hancock, G., eds., Port Moresby, Papua New Guinea Department of Mining, 152 p.
Cudahy, T.J., Okada, K., Yamato, Y., Maekawa, M., Hackwell, J.A., and Huntington, J.F., 2000, Mapping skarn and porphyry alteration mineralogy at Yerington, Nevada, using airborne hyperspectral TIR SEBASS data: CSIRO Exploration and Mining Exploration and Mining Report 734R, 78 p.
Czehura, S., 2006, Butte: A world class ore deposit: Mining Engineering, v. 58, p. 14–19.
Donovan, J.J., Lowers, H.A., and Rusk, B.G., 2011, Improved electron probe microanalysis of trace elements in quartz: American Mineralogist, v. 96, p. 274–282.
Driesner, T., and Heinrich, C.A., 2007, The system H_2O-NaCl. Part I: Correlation formulae for phase relations in temperature-pressure-composition space from 0 to 1000°C, 0 to 5000 bar, and 0 to 1 X_{NaCl}: Geochimica et Cosmochimica Acta, v. 71, p. 4880–4901.
Einaudi, M.T., 1977, Environment of ore deposition at Cerro de Pasco, Peru: Economic Geology, v. 72, p. 893–924.
Einaudi, M.T., 1982, General features and origin of skarns associated with porphyry copper plutons, southwestern North America, *in* Titley, S.R , ed., Advances in geology of the porphyry copper deposits, southwestern North America: Tucson, The University of Arizona Press, p. 185–209.
Fisher, N.H., 1944, Outline of the geology of the Morobe goldfield: Proceedings of the Royal Society of Queensland, v. 55, p. 51–58.
Fisher, N.H., 1945, The fineness of gold, with special reference to the Morobe gold field, New Guinea: Economic Geology, v. 40, p. 449–495.
Fisher, A.J., Hayes, W., and Stoneham, A.M., 1990, Theory of the structure of the self-trapped exciton in quartz: Journal of Physics: Condensed Matter, v. 2, p. 6707–6720.
Flores, R., 1993, Geología del pórfido aurífero Verde, proyecto Refugio, Tercera Región, Chile: Revista Geológica de Chile, v. 20, p. 57–69.

Fournier, R.O., 1999, Hydrothermal processes related to movement of fluid from plastic into brittle rock in the magmatic-epithermal environment: Economic Geology, v. 94, p. 1193–1211.
Furrer, C., 2006, Fluid evolution and metal zonation at the Bingham porphyry Cu-Au-Mo deposit, Utah: Constraints from microthermometry and LA-ICPMS analysis of fluid inclusions: Unpublished M.Sc. thesis, Zurich, Switzerland, ETH Zurich, 96 p.
Garcia, J.S., Jr., 1991, Geology and mineralization characteristics of the Mankayan mineral district, Philippines. Geological Survey of Japan Report, v. 277, p. 21–30.
Götze, J., Plötze, M., and Habermann, D., 2001, Origin, spectral characteristics and practical applications of the cathodoluminescence (CL) of quartz – a review: Mineralogy and Petrology, v. 71, p. 225–250.
Götze, J., Plötze, M., Graupner, T., Hallbauer, D. K., and Bray, C. J., 2004, Trace element incorporation into quartz: A combined study by ICP-MS, electron spin resonance, cathodoluminescence, capillary ion analysis, and gas chromatography: Geochimica et Cosmochimica Acta, v. 68, p. 3741–3759.
Griggs, D.T., and Blacic, J.D., 1965, Quartz: Anomalous weakness of synthetic crystals: Science, v. 147, p. 292–295.\
Gruen, G., Heinrich, C.A., and Schroeder, K., 2010, The Bingham Canyon porphyry Cu-Mo-Au deposit. II. Vein geometry and ore shell formation by pressure-driven rock extension: Economic Geology, v. 105, p. 69–90.
Gustafson, L.B., and Hunt, J.P., 1975, The porphyry copper deposit at El Salvador, Chile: Economic Geology, v. 70, p. 857–912.
Gustafson, L.B., and Quiroga, J.G., 1995, Patterns of mineralization and alteration below the porphyry copper orebody at El Salvador, Chile: Economic Geology, v. 90, p. 2–16.
Graupner, T., Kempe, U., Spooner, E.T.C., Bray, C.J., Kremenetsky, A.A., and Irmer, G., 2001, Microthermometric, laser Raman spectroscopic, and volatile-ion chromatographic analysis of hydrothermal fluids in the Paleozoic Muruntau Au-bearing quartz vein ore field, Uzbekistan: Economic Geology, v. 96, p. 1–23.
Harraz, H.Z., 2000, A genetic model for a mesothermal Au deposit: Evidence from fluid inclusions and stable isotopic studies at El Sid Gold Mine, Eastern Desert, Egypt: Journal of African Earth Sciences, v. 30, p. 267–282.
Hedenquist, J.W., and Taran, Y.A., 2013, Modeling the formation of advanced argillic lithocaps: Volcanic vapor condensation above porphyry intrusions: Economic Geology, v. 108, p. 1523–1540.
Hedenquist, J.W., Arribas, A., Jr., and Reynolds, T.J., 1998, Evolution of an intrusion-centered hydrothermal system: Far Southeast-Lepanto porphyry and epithermal Cu-Au deposits, Philippines: Economic Geology, v. 93, p. 373–404.
Heinrich, C.A., 2007, Fluid-fluid interactions in magmatic-hydrothermal ore formation: Reviews in Mineralogy and Geochemistry, v. 65, p. 363–387.
Heinrich, C.A., Halter, W., Landtwing, M.R., and Pettke, T., 2005, The formation of economic porphyry copper (-gold) deposits: Constraints from microanalysis of fluid and melt inclusions: Geological Society, London, Special Publication, v. 248, p. 247–263.

Heynke, U., Leeder, O., and Schulz, H., 1992, On distinguishing quartz of hydrothermal or metamorphogenic origin in different monomineralic veins in the eastern part of Germany: Mineralogy and Petrology, v. 46, p. 315–329.

Holley, E.A., 2012, The Veladero high-sulfidation epithermal Au-Ag deposit, Argentina: volcanic stratigraphy, alteration, mineralization, and quartz paragenesis: Unpublished Ph.D. thesis, Golden, Colorado, Colorado School of Mines, 218 p.

Houston, R.A., and Dilles, J.H., 2013, Structural geologic evolution of the Butte district, Montana: Economic Geology, v. 108, p. 1397–1424.

Imai, A., 2000, Mineral paragenesis, fluid Inclusions and sulfur isotope systematics of the Lepanto Far Southeast porphyry Cu-Au deposit, Mankayan, Philippines: Resource Geology, v. 50, p. 151–168.

Imai, A., Concepcíon, R.A., Cinco, J.C., Jr, and Garcia, J.S., Jr., 1994, Magmatic hydrothermal system of the Lepanto-Far Southeast (FSE) porphyry Cu-Au deposit, Mankayan, Philippines: Mineral paragenesis, fluid inclusions, and sulfur isotope systematics: Resource Geology, v. 44, p. 266–267.

James, A., Smith, W., and Welsh, J., 1961, General geology and structure of the Bingham district, Utah, *in* Cook, B.R., ed.,Geology of the Bingham mining district and northern Ouquirrh Mountains, Guidebook to the Geology of Utah, no. 16, p. 49–69.

Jones, W.F., 1918, A geological reconnaissance in Haiti: A contribution to Antillean geology: The Journal of Geology, v. 26, p. 728–752.

Kempe, U., Götze, J., Enchbat, D., Monecke, T., and Poutivtsev, M., 2012, Quartz regeneration and its use as a repository of genetic information, *in* Götze, J., and Möckel, R., eds., Quartz: Deposits, mineralogy and analytics. Berlin, Springer, p. 331–335.

Klemm, L.M., Pettke, T., and Heinrich, C.A., 2007, Hydrothermal evolution of the El Teniente deposit, Chile: Porphyry Cu-Mo ore deposition from low-salinity magmatic fluids: Economic Geology, v. 102, p. 1021–1045.

Klemm, L.M., Pettke, T., and Heinrich, C.A., 2008, Fluid and source magma evolution of the Questa porphyry Mo deposit, New Mexico, USA: Mineralium Deposita, v. 43, p. 533–552.

Landtwing, M.R., 2004, Fluid evolution and ore mineral precipitation at the Bingham porphyry Cu-Au-Mo deposit, Utah, deduced from cathodoluminescence imaging and LA-ICPMS microanalysis of fluid inclusions: Unpublished Ph.D. thesis, Zurich, Switzerland, ETH Zurich, 260 p.

Landtwing, M.R., and Pettke, T., 2005, Relationships between SEM-cathodoluminescence response and trace-element composition of hydrothermal vein quartz: American Mineralogist, v. 90, p. 122–131.

Landtwing, M.R., Pettke, T., Halter, W.E., Heinrich, C.A., Redmond, P.B., Einaudi, M.T., and Kunze, K., 2005, Copper deposition during quartz dissolution by cooling magmatic-hydrothermal fluids: The Bingham porphyry: Earth and Planetary Science Letters, v. 235, p. 229–243.

Landtwing, M.R., Furrer, C., Redmond, P.B., Pettke, T., Guillong, M., and Heinrich, C.A., 2010, The Bingham Canyon porphyry Cu-Mo-Au deposit. III. Zoned copper-gold ore deposition by magmatic vapor expansion: Economic Geology, v. 105, p. 91–118.

Lang, I.M., and Cheney, E.S., 1971, Sulfur isotopic reconnaissance of Butte, Montana: Economic Geology, v. 66, p. 63–74.
Lanier, G., John, E.C., Swensen, A.J., Reid, J., Bard, C.E., Caddey, S.W., and Wilson, J.C., 1978, General geology of the Bingham mine, Bingham Canyon, Utah: Economic Geology, v. 73, p. 1228–1241.
Leduc, C., and Itard, Y., 2003, Low sampling density exploration geochemistry for gold in arid and tropical climates: Comparison between conventional geochemistry and BLEG: Geochemistry: Exploration, Environment, Analysis, v. 3, p. 121–131.
Lowell, J.D., and Guilbert, J.M., 1970, Lateral and vertical alteration-mineralization zoning in porphyry ore deposits: Economic Geology, v. 65, p. 373–408.
Lund, K., Aleinikoff, J.N., Kunk, M.J., Unruh, D.M., Zeihen, G.D., Hodges, W.C., Du Bray, E.A., and O'Neill, J.M., 2002, SHRIMP U-Pb and $^{40}Ar/^{39}Ar$ age constraints for relating plutonism and mineralization in the Boulder Batholith region, Montana: Economic Geology, v. 97, p. 241–267.
Mancano, D.P., and Campbell, A.R., 1995, Microthermometry of enargite-hosted fluid inclusions from the Lepanto, Philippines, high-sulfidation Cu-Au deposit: Geochimica et Cosmochimica Acta, v. 59, p. 3909–3916.
Marfunin, A.S., 1979, Spectroscopy, luminescence and radiation centers in minerals: Berlin, Springer, 352 p.
Marsh, E., 2012, Preliminary fluid inclusion paragenesis using scanning electron microscope-cathodoluminescence on samples from the Pebble porphyry Cu-Au-Mo deposit, SW Alaska: SEG 2012 Conference: Integrated Exploration and Ore Deposits, Lima, Peru 23–26 September 2012, Conference CD, Poster 62.
Meyer, C., 1965, An early potassic type of wall-rock alteration at Butte, Montana: American Mineralogist, v. 50, p. 1717–1722.
Meyer, C., Shea, E.P., Goddard, C.C., Jr., 1968, Ore deposits at Butte, Montana, *in* Ridge, J.D., ed., Ore deposits of the United States, 1933-1967, The Graton-Sales volume, New York, The American Institute of Mining, Metallurgical, and Petroleum Engineers, p. 1373–1416.
Monecke, T., Kempe, U., and Götze, J., 2002, Genetic significance of the trace element content in metamorphic and hydrothermal quartz: A reconnaissance study: Earth and Planetary Science Letters, v. 202, p. 709–724
Müller, A., Breiter, K., Seltmann, R., and Pécskay, Z., 2005, Quartz and feldspar zoning in the eastern Erzgebirge volcano-plutonic complex (Germany, Czech Republic): Evidence of multiple magma mixing: Lithos, v. 80, p. 201–227.
Müller, A., Herrington, R., Armstrong, R., Seltmann, R., Kirwin, D.J., Stenina, N.G., and Kronz, A., 2010, Trace elements and cathodoluminescence of quartz in stockwork veins of Mongolian porphyry-style deposits: Mineralium Deposita, v. 45, p. 707–727.
Muntean, J.L., and Einaudi, M.T., 2000, Porphyry gold deposits of the Refugio district, Maricunga belt, northern Chile: Economic Geology, v. 95, p. 1445–1472.
Muntean, J.L., and Einaudi, M.T., 2001, Porphyry-epithermal transition: Maricunga belt, northern Chile: Economic Geology, v. 96, p. 743–772.
Murakami, H., Seo, J.H., and Heinrich, C.A., 2010, The relation between Cu/Au ratio and formation depth of porphyry-style Cu-Au±Mo deposits: Mineralium Deposita, v. 45, p. 11–21.

Nelson, C.E., Proenza, J.A., Lewis, J.F., and López-Kramer, J., 2011, The metallogenic evolution of the Greater Antilles: Geologica Acta, v. 9, p. 229–264.
Neuser, R.D., 1995, A new high-intensity cathodoluminescence microscope and its application to weakly luminescing minerals: Bochumer Geologische und Geotechnische Arbeiten, v. 44, p. 116–118.
Noku, S.K., Akasaka, M., and Matsueda, H., 2011, The Crater Mountain deposit, Papua New Guinea: Porphyry-related Au-Te system: Resource Geology, v. 61, p. 63–75.
Page, R.W., and McDougall, I., 1972, Ages of mineralization of gold and porphyry copper deposits in the New Guinea Highlands: Economic Geology, v. 67, p. 1034–1048.
Parry, W.T., Wilson, P.N., Moser, D., and Heizler, M.T., 2001, U-Pb dating of zircon and $^{40}Ar/^{39}Ar$ dating of biotite at Bingham, Utah: Economic Geology, v. 96, p. 1671–1683.
Peppard, B.T., Steele, I.M., Davis, A.M., Wallace, P.J., and Anderson, A.T., 2001, Zoned quartz phenocrysts from the rhyolitic Bishop Tuff: American Mineralogist, v. 86, p. 1034–1052.
Penniston-Dorland, S.C., 2001, Illumination of vein quartz textures in a porphyry copper ore deposit using scanned cathodoluminescence: Grasberg Igneous Complex, Irian Jaya, Indonesia: American Mineralogist, v. 86, p. 652–666.
Pour, A.B., and Hashim, M., 2012, The application of ASTER remote sensing data to porphyry copper and epithermal gold deposits: Ore Geology Reviews, v. 44, p. 1–9.
Pudack, C., Halter, W.E., Heinrich, C.A., and Pettke, T., 2009, Evolution of magmatic vapor to gold-rich epithermal liquid: The porphyry to epithermal transition at Nevados de Famatina, northwest Argentina: Economic Geology, v. 104, p. 449–477.
Radford, N., 1996, BLEG sampling in gold exploration: An Australian view: Explore, v. 92, p. 8–10.
Redmond, P.B., and Einaudi, M.T., 2010, The Bingham Canyon porphyry Cu-Mo-Au deposit. I. Sequence of intrusions, vein formation, and sulfide deposition: Economic Geology, v. 105, p. 43–68.
Redmond, P.B., 2002, Magmatic-hydrothermal fluids and copper-gold ore formation at Bingham Canyon, Utah: Unpublished Ph.D. thesis, Stanford University, 228 p.
Redmond, P.B., Landtwing, M.R., and Einaudi, M.T., 2001, Cycles of porphyry dike emplacement, veining, alteration and mineralization in the Bingham porphyry Cu-Au-Mo deposit, Utah, *in* Piestrzynski, A.,, et al., eds., Mineral deposits at the beginning of the 21st century, Proceedings of the joint sixth biennial SGA-SEG meeting, Krakow, Poland, 26-29 August, 2001, p. 473–476.
Redmond, P.B., Einaudi, M.T., Inan, E.E., Landtwing, M.R., and Heinrich, C.A., 2004, Copper deposition by fluid cooling in intrusion-centered systems: New insights from the Bingham porphyry ore deposit, Utah: Geology, v. 32, p. 217–220.
Reed, M.H., Rusk, B., and Palandri, J., 2013, The Butte magmatic-hydrothermal system: One fluid yields all alteration and veins: Economic Geology, v. 108, p. 1379–1396.
Reynolds, T.J., and Beane, R.E., 1985, Evolution of hydrothermal fluid characteristics at the Santa Rita, New Mexico, porphyry copper deposit: Economic Geology, v. 80, p. 1328–1347.

Richards, J.P., 2009, Postsubduction porphyry Cu-Au and epithermal Au deposits: Products of remelting of subduction-modified lithosphere: Geology, v. 37, p. 247–250.
Roberts, S.A., 1975, Early hydrothermal alteration and mineralization in the Butte district, Montana: Unpublished Ph.D. thesis, Cambridge, Harvard University, 157 p.
Rusk, B.G., 2003, Cathodoluminescence quartz textures and fluid inclusions in veins of the porphyry copper-molybdenum deposit in Butte, Montana: Constraints on the physical and chemical evolution of the hydrothermal system: Unpublished Ph.D. thesis, Eugene, University of Oregon, 285 p.
Rusk, B., 2012, Cathodoluminescent textures and trace elements in hydrothermal quartz. *in* Götze, J., and Möckel, R., eds., Quartz: Deposits, mineralogy and analytics. Berlin, Springer, p. 307–329.
Rusk, B., and Reed, M., 2002, Scanning electron microscope-cathodoluminescence analysis of quartz reveals complex growth histories in veins from the Butte porphyry copper deposit, Montana: Geology, v. 30, p. 727–730.
Rusk, B.G., Reed, M.H., Dilles, J.H., Klemm, L., and Heinrich, C.A., 2004, Compositions of magmatic hydrothermal fluids determined by LA_ICP_MS of fluid inclusions from the porphyry copper-molybdenum deposit at Butte, MT: Chemical Geology, v. 210, p. 173–199.
Rusk, B.G., Reed, M.H., Dilles, J.H., and Kent, A.J.R., 2006, Intensity of quartz cathodoluminescence and trace-element content in quartz from the porphyry copper deposit at Butte, Montana: American Mineralogist, v. 91, p. 1300–1312.
Rusk, B.G., Reed, M.H., and Dilles, J.H., 2008a, Fluid inclusion evidence for magmatic-hydrothermal fluid evolution in the porphyry copper-molybdenum deposit at Butte, Montana: Economic Geology, v. 103, p. 307–334.
Rusk, B.G., Lowers, H.A., and Reed, M.H., 2008b, Trace elements in hydrothermal quartz: Relationships to cathodoluminescent textures and insights into vein formation: Geology, v. 36, p. 547–550.
Rusk, B.G., Miller, B.J., and Reed, M.H., 2008c, Fluid-inclusion evidence for the formation of Main Stage polymetallic base-metal veins, Butte, Montana, USA, *in* Spencer, J.E., and Titley, S.R., eds., Ores and orogenesis: Circum-Pacific tectonics, geologic evolution, and ore deposits: Arizona Geological Society Digest, v. 22, p. 573–581.
Seedorff, E., Dilles, J.H., Proffett, J.M., Jr., Einaudi, M.T., Zurcher, L., Stavast, W.J.A., Johnson, D.A., and Barton, M.D., 2005, Porphyry deposits: Characteristics and origin of hypogene features, *in* Hedenquist, J.W., Thompson, J.F.H., Goldfarb, R.J., and Richards, J.P., eds., Economic Geology 100th Anniversary Volume, Society of Economic Geologists, p. 251–298.
Seo, J.H., Guillong, M., and Heinrich, C.A., 2012, Separation of molybdenum and copper in porphyry deposits: The roles of sulfur, redox, and pH in ore mineral deposition at Bingham Canyon: Economic Geology, v. 107, p. 333–356.
Shinohara, H., and Hedenquist, J.W., 1997, Constraints on magma degassing beneath the Far Southeast porphyry Cu–Au deposit, Philippines: Journal of Petrology, v. 38, p. 1741–1752.
Siegel, G.H., Jr., and Marrone, M.J., 1981, Photoluminescence in as-drawn and irradiated silica optical fibers: An assessment of the role of non-bridging oxygen defect centers: Journal of Non-Crystalline Solids, v. 45, p. 235–247.

Sillitoe, R.H., 2010, Porphyry copper systems: Economic Geology, v. 105, p. 3–41.
Sillitoe, R.H., and Hedenquist, J.W., 2003, Linkages between volcanotectonic settings, ore-fluid compositions, and epithermal precious metal deposits, *in* Simmons, S.F., and Graham, I., eds., Volcanic, geothermal, and ore-forming fluids: Rulers and witness of processes within the Earth: Society of Economic Geologists Special Publication, no. 10, p. 315–343.
Sillitoe, R.H., Baker, E.M., and Brook, W.A., 1984, Gold deposits and hydrothermal eruption breccias associated with a maar volcano at Wau, Papua New Guinea: Economic Geology, v. 79, p. 638–655.
Sime, L.C., and Ferguson, R.I., 2003, Information on grain sizes in gravel-bed rivers by automated image analysis: Journal of Sedimentary Research, v. 73, p. 630–636.
Singer, D.A., Berger, V.I., and Moring, B.C., 2008, Porphyry copper deposits of the world: Database and grade and tonnage models, 2008: U.S. Geological Survey Open-File Report 2008-1155, 45 p.
Skewes, M.A., and Stern, C.R., 1996, Late Miocene mineralized breccias in the Andes of central Chile: Sr- and Nd-isotopic evidence for multiple magmatic sources, *in* Camus, F., Sillitoe, R.M., and Petersen, R., eds., Andean Copper Deposits: New discoveries, mineralization, styles and metallogeny: Society of Economic Geologists Special Publication, no. 5, p. 33–41.
Sprunt, E.S., Dengler, L.A., and Sloan, D., 1978, Effects of metamorphism on quartz cathodoluminescence: Geology, v. 6, p. 305–308.
Stevens-Kalceff, M.A., 2009, Cathodoluminescence microcharacterization of point defects in α-quartz: Mineralogical Magazine, v. 73, p. 585–605.
Stoffregen, R., 1987, Genesis of acid-sulfate alteration and Au-Cu-Ag mineralization at Summitville, Colorado: Economic Geology, v. 82, p. 1575–1591.
Suttner, L.J., and Leininger, R.K., 1972, Comparison of the trace element content of plutonic, volcanic, and metamorphic quartz from Southwestern Montana: Geological Society of America Bulletin, v. 83, p. 1855–1862.
Tilling. R.I., 1973, Boulder Batholith, Montana: A product of two contemporaneous but chemically distinct magma series: Geological Society of America Bulletin, v. 84, p. 3879–3900.
Tilling, R.I., Klepper, M.R., and Obradovich, J.D., 1968, K-Ar ages and time span of emplacement of the Boulder Batholith, Montana: American Journal of Science, v. 266, p. 671–689.
Titley, S.R., 1982, The style and progress of mineralization and alteration in porphyry copper systems, American Southwest, *in* Titley, S.R., ed., Advances in geology of the porphyry copper deposits, southwestern North America: Tucson, The University of Arizona Press, p. 93–116.
Titley, S.R., and Beane, R.E., 1981, Porphyry copper deposits, *in* Skinner, B.J., ed., Economic Geology 75th Anniversary Volume, Society of Economic Geologists, p. 214–269.
Wark, D.A., and Watson, E.B., 2006, TitaniQ: A titanium-in-quartz geothermometer: Contributions to Mineralogy and Petrology, v. 152, p. 743–754.
Watt, G.R., Wright, P., Galloway, S., and McLean, C., 1997, Cathodoluminescence and trace element zoning in quartz phenocrysts and xenocrysts: Geochimica et Cosmochimica Acta, v. 61, p. 4337–4348.

Weis, P., Driesner, T., and Heinrich, C.A., 2012, Porphyry-copper ore shells form at stable pressure temperature fronts within dynamic fluid plumes: Science, v. 338, p. 1613–1616.

Williams-Jones, A.E., and Heinrich, C.A., 2005, Vapor transport of metals and the formation of magmatic-hydrothermal ore deposits: Economic Geology, v. 100, p. 1287–1312.